2017

Chemical Synthesis: New Methods for O-Glycosylation and the Preparation of Organic Thin Films

Rashanique Deondria Quarels
Louisiana State University and Agricultural and Mechanical College

CHEMICAL SYNTHESIS: NEW METHODS FOR *O*-GLYCOSYLATION AND THE PREPARATION OF ORGANIC THIN FILMS

A Dissertation

Submitted to the Graduate Faculty of the
Louisiana State University and
Agricultural and Mechanical College
in partial fulfillment of the
requirements for the degree of
Doctor of Philosophy

in

The Department of Chemistry

by
Rashanique Deondria Quarels
B.S., Southern University and Agricultural & Mechanical College, 2012
May 2017

This degree is dedicated to my mother Danielle and my father Richard. Thank you for always believing in me even when I did not believe in myself. Your love and guidance have truly been appreciated. This degree is also dedicated to my grandmother Delores. I will never be able to thank you enough for your help raising Imani. Your sacrifice has truly been appreciated and has allowed me to finish this journey successfully. Finally, this degree is dedicated to my daughter Imani. You have brought so much purpose to my life. I push myself to succeed because I know you are watching. I would also like to thank my family and close friends for listening to my late-night venting sessions or babysitting while I go to work. Your sacrifices were not in vain.

TABLE OF CONTENTS

LIST OF TABLES

LIST OF FIGURES

LIST OF SCHEMES

LIST OF ABBREVIATIONS

ABBREVIATION:	NAME:
AFM	Atomic Force Microscopy
AIBN	Azobisisobutyronitrile
BNAH	Benzyl nicotinamide
BnBr	Benzyl bromide
CH_2Cl_2	Dichloromethane
CH_3CN	Acetonitrile
CS_2	Carbon disulfide
DBU	1,8-Diazabicycloundec-7-ene
DCC	*N*,*N*'-Dicyclohexylcarbodiimide
DMAP	4-Dimethylaminopyridine
DMF	*N*,*N*-Dimethylformamide
Et_2O	Diethyl ether
FG	Functional group
H_2SO_4	Sulfuric acid
HBr	Hydrobromic acid
HOAc	Acetic acid
IR	Infrared spectroscopy
IRRAS	Infrared Reflection-Absorption Spectroscopy
MEMCl	2-Methoxyethoxymethyl chloride
MeOH	Methanol
MLCT	Metal-to-ligand charge transfer

MUA	Mercaptoundecanoic acid
NaH	Sodium hydride
NaOMe	Sodium methoxide
NBDT	*p*-Nitrobenzenediazonium tetrafluoroborate
$Na_2S{\cdot}9H_2O$	Sodium sulfide nonahydrate
NMR	Nuclear magnetic resonance spectroscopy
Phth-CCH	10-Undecynoic phthalimide ester
Phth-CH_3	10-Undecanoic phthalimide ester
Phth-NHBoc	*N-Tert*-butoxycarbonylamino undecanoic phthalimide ester
Phth-OH	10-hydroxydecanoic phthalimide ester
Phth-OMEM	10-((2-methoxyethoxy)methoxy)decanoic phthalimide ester
SAM	Self-assembled monolayer
SET	Single-electron transfer
TCAI	Trichloroacetimidate
THF	Tetrahydrofuran
TLC	Thin layer chromatography
TOF SIMS	Time-of-flight secondary ion mass spectrometry
TSG	Template-stripped gold
XPS	X-ray photoelectron spectroscopy

ABSTRACT

This dissertation focuses on the diverse use of chemical synthesis. Herein, I will discuss the use of synthetic organic chemistry for the modification surfaces and the synthesis of small molecules. Chapter One is an introduction to the realm of surface chemistry. I have highlighted some key methods for surface modification. Additionally, methods to characterize the as-formed thin films are also outlined.

In Chapter Two, I discuss the use of visible-light photoredox catalysis in the nanoscale lithography of Au(111) surfaces. Blue LED irradiation of solutions of NBDT in the presence of $Ru(bpy)_3^{2+}$ results in the formation of *p*-nitrophenyl radicals that graft onto Au. Further reaction of the grafted arenes with aryl radicals results in oligomerization to polyphenylene structures with resulting film thicknesses that are dependent on both the initial concentration of diazonium salt and the duration of the grafting procedure. Grafting onto Au(111) coated with SiO_2 mesospheres (d = 500 nm) prior to mesospheres removal results in the production of nanopatterned surfaces wherein each nanopore represents the former location of a mesosphere.

Chapter Three focuses on the a novel use of visible light photoredox catalysis for organic thin film formation with nanoscale lithography of Au(111) surfaces. Irradiation of solutions of phthalimide esters with blue LEDs in the presence of the $Ru(bpy)_3Cl_2$ results in the formation of carbon centered radicals that form organic thin films. We propose that a series of additional reactions of the grafted aliphatic chains with alkyl radicals results in oligomerization and the formation of multilayers.

Chapter Four is a brief discussion of the significance of oligosaccharide synthesis. The development of efficient and stereoselective methods for glycosylation is a synthetic challenge. Thioglycosides are inert to many glycosylation methods and are bench top stable. Their stability

to common carbohydrate protecting group manipulations makes thioglycosides ideal glycosyl donors or acceptors. Traditionally, the activation of thioglycosides requires heavy metals, halogen electrophiles, or stoichiometric thiophilic reagents. In contrast, our method discussed in Chapter 5 requires catalytic Bronsted acid for the remote activation of a thioglycoside donor. Under these conditions, *O*-glycosylation formation and release of a tetrahydrothiophene aglycon is swift and high yielding.

CHAPTER 1: A BRIEF OVERVIEW OF SURFACE MODIFICATION

1.1 Introduction to Surface Modification

The interdisciplinary nature of surface science has sparked many new applications for surface chemistry. Since the 1990s, surface modification has become a major topic in materials science, medicine, and biotechnology. The goal of surface modification is to attach molecules with specific functionality to surfaces. The resulting thin films provide a barrier between a solid phase and a liquid or gaseous phase. The chemical manipulation of surfaces using thin films permits the development of specialized interfaces in which surfaces have controlled thickness and functionality. The utility of modified surfaces is most prevalent in the areas of corrosion-resistant surfaces[2,3], anti-fouling resists[4], biosensors[2,5], medical devices[5], and optical and electronic devices[6]. Thus, the ability to tailor the physical, mechanical, and chemical properties of a surface has made surface modification a topic of immense importance in a variety of scientific disciplines including materials science and surface chemistry.

1.2 Selected Applications of Surface Modification

1.2.1 Resists and Inhibitors

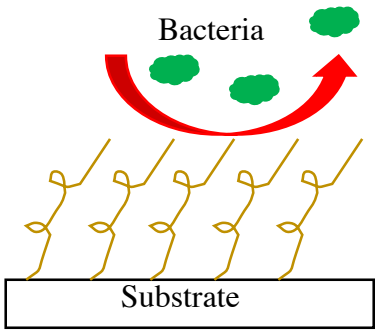

Figure 1.1 Thin Film used in Anti-Fouling

The most straightforward use of surface modification is for the protection of surfaces from harmful environmental conditions (*e.g.* anti-fouling and corrosion resists). For example, the paint on a car is attractive to the buyer, but it also serves as protective barrier against corrosion. Another example of this is the coating of precious metals with zinc. The exposed zinc forms a nonporous layer that inhibits the corrosion of the metal underneath.[7] Additionally, surface modification (Figure 1.1) has been used for the development of surfaces that are resistant to fouling by attachment of protein and even bacteria.

1.2.2 Biosensors

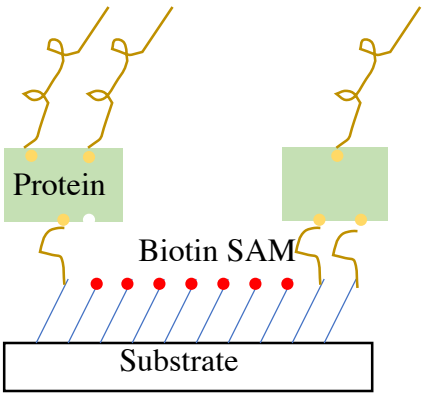

Figure 1.2 Thin Film used a Biosensor

Biomedical coatings can reduce adhesion within biological matrixes. Covalently linked organic thin films with a reactive terminal group can act as biosensors.[8,9] Reactive terminal groups on the thiol self-assembled monolayer (SAM) enhance their selectivity for analytes containing compatible functional groups. This method of surface modification also allows for additional reactions to occur at the interface if the analyte has terminal ends that can be further functionalized. This is particularly true if the analyte has an affinity for a molecule or readily couples to another functional group. For example, an alkyl thiol surface-assembled monolayer (SAM) can be further functionalized with a molecule of biotin (Figure 1.2). The resulting biotin SAM can then be used to detect proteins in solution such as Streptavidin.[47] Organic thin film

biosensors have also been developed for the detection of nucleic acids[10,11], glucose oxidase[14,15], and dopamine[12,13].

1.2.3 Electronic Devices

Thin films are also utilized in the realm of electronics. As previously mentioned, thin films protect against moisture and corrosion, but can also increase dielectric strength between conductors by the use of electronic coating. The capabilities, speed, and size of electronics has vastly changed over the last 30 years. The functionality of electronic devices is often attributed to the development of patterned surfaces.[16] Thins films play a part in many electronics including television, computers, and streaming devices such as Roku. Nanostructures on surfaces are used for data storage and information processing.[16,17] Many transistors, molecular junctions, inkjets, and environmental analysis tools now have coated interfaces.[18]

1.3 Methods for Surface Modification

1.3.1 Self-Assembled Monolayers

The first manuscript on surface self-assembly was published by Zisman and coworkers in 1946. These investigators observed the absorption of a surfactant onto a clean metal surface to form a monolayer.[19] SAMs are comprised of ordered molecules that attach to a surface to form a thin film. The surfactant molecule or thiol precursor for self-assembly has three major components: (1) the headgroup, (2) the backbone, and (3) the terminal end group, see Figure 1.3 for an example. The headgroup reacts directly with the surface of the substrate to form a new bond. The backbone promotes self-assembly of the molecules on the surface, while the terminal end gives the SAM its functionality and also, along with the headgroup and backbone, contribute to the SAMs overall chemical, physical, and mechanical properties. The ability to tailor the

headgroup and terminal end allows tuning of wetting, adhesion, lubrication, corrosion, and growth properties, as well as, ordering on the surface.[20] SAMs are a popular topic of research due to their ease of preparation, tunability of properties, formation of more complex structures, and their enhancement of the optical and electronic properties of metals.[20]

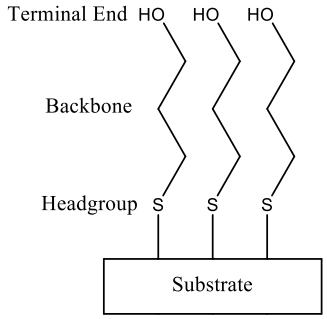

Figure 1.3 A Self-Assembled Monolayer

SAMs are mostly commonly prepared by the deposition of thiols. The formation of thiol SAMs can be accomplished by immersing the substrate (metals, carbon, etc.) in a millimolar solution of thiol. The immersion time is dependent on the surface substrate and concentration of the thiol. Thiols SAMs have been studied extensively since Whitesides and Nuzzo discovered the first example of thiol self-assembly on gold surfaces.[21] Transition metals exhibit a high affinity for thiols. More specifically, thiols spontaneously attach to gold surfaces forming self-assembled monolayers;[28] thus the gold-thiol system has been used as a model system for self-assembly. A variety of sulfur-based molecules have been evaluated for their binding affinity to gold. These species include xanthates[24], alkyl sulfides[22], disulfides[3], thiophenols[23], thiophenes[26], thioureas[25], and several other sulfur-containing molecules.[20]

1.3.2 Electrografting

The electrochemical reaction involving an electron transfer from an electrode to the surface substrate or an organic molecule that leads to an interaction between the surface and

molecule is termed electrografting. This method has been used on a variety of surface substrates including carbon (diamonds, nanotubes, nanowires), metals (Au, Fe, Ag, Pt), and metal oxides (ITO).[18] Covalent bond formation between the surface and organic layer is referred to as chemisorption, while weak interactions between the surface and the thin film are called physisorption.

Oxidative electrografting is achieved through a single electron transfer from an organic molecule to an anode to form a radical cation or a radical that covalently bonds to a surface. Amines, carboxylic acids, alcohols, and Grignard reagents have all been electrografted onto various surfaces using the oxidative method. Successful reductive electrografting has been achieved with vinylic compounds such as *N*-succinimidyl acrylate and acrylonitrile. Alkenes have been successfully electrografted onto the Fe, Ni, Au, carbon nanotubes, and many other surfaces.[18] It is also important to emphasize that further modification of the electrografted layers, similar to that seen with the deposition of thiols, is possible if the layers possess a terminal functional group. A general scheme of the functionalization of an organic thin film is illustrated in Figure 1.4.

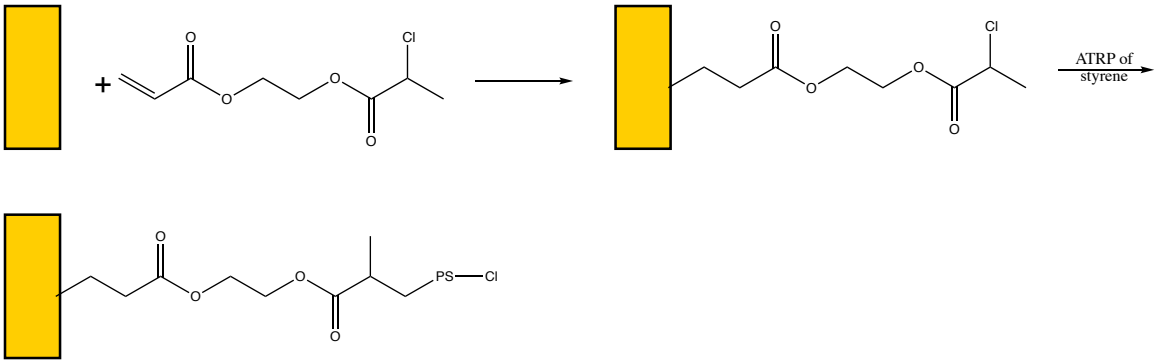

Figure 1.4 Functionalization of Terminal Ends[48]

1.3.2 UV Photografting

Early uses of ultraviolet light for surface modification involved the use of Norrish type I and II photoinitiators.[18] These photoinitiators had previously been used for polymerization reactions. The photoinitiator is excited by UV light. The excited photoinitiator then abstracts a hydrogen from a compound R-H to yield a radical ($R^{\cdot}$) that then goes on to react with the surface (Scheme 1.1). Frequently used photoinitiators include benzophenone, xanthone, benzoyl peroxide, and AIBN.[27]

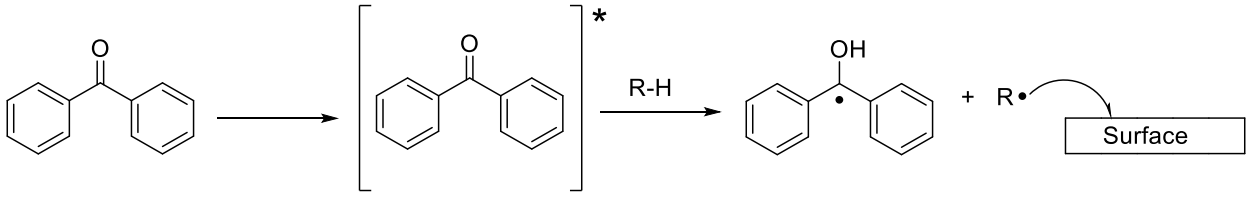

Scheme 1.1 Generation of Radicals using a Photoinitiatior for Surface Functionalization

More recently, metal catalysts have been used as a source of electrons for the derivatization of surfaces by radicals.[5] Photocatalysts (PC), such as $Ru(bpy)_3^{2+}$, are excited by the UV light. The excited catalyst (PC*) can then donate an electron to an organic compound with a leaving group (R-LG) to generate a radical ($R^{\cdot}$) and an anionic or neutral leaving group, see Scheme 1.2. That radical then goes on to interact with the surface.

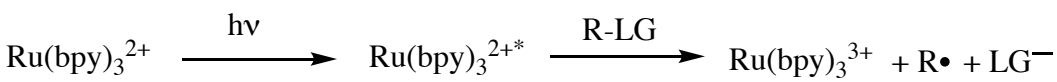

Scheme 1.2 Photocatalyst Initiated Radical Formation

1.4 Gold

Thin film growth has been studied on iron, gold, platinum, carbon, indium tin oxide, and silicon surfaces. Transition metals are commonly used in surface modification; particularly, gold

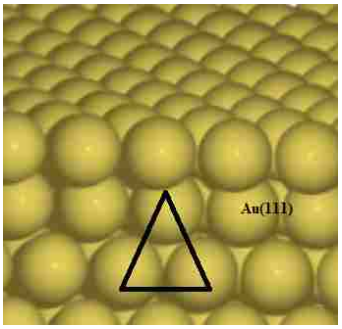

Figure 1.5 Face-centered Cubic Crystal (111) Index

has been shown to be an advantageous interface. The crystalline nature of gold means that the surface is well defined and has few defects. Figure 1.5 illustrates the (111) index of gold (one of three indices). The freshly prepared gold substrate has a face centered cubic crystal structure that arranges in a (111) index in which all of the atoms are surrounded in the plane. Au(111) is also the smoothest, most stable of the gold surfaces and has a higher substrate–molecule interaction. Most importantly, gold surfaces can be chemically modified and patterned easily and, unlike other metal surfaces, gold is relatively inert and not oxidized readily.

1.5 Surface Characterization Techniques

1.5.1 Grazing-angle Infrared Spectroscopy

Grazing-angle Infrared Reflection Absorption Spectroscopy (IRRAS) is a method in Fourier transform infrared (FTIR) spectroscopy. Grazing-angle FT-IRRAS allows a spectrum to be measured directly from a thin film on a surface. An IR fiber-optic cable is situated such that the incident radiation is at a grazing-angle to the reflective surface, usually with a fixed incidence angle of 80°.[30] Grazing-angle infrared spectroscopy is used to identify a variety of functional groups present on surfaces. It is generally applied to thin films on highly reflective surfaces such as gold and can determine if a surface is contaminated. A Fourier transform infrared spectrometer coupled with a grazing-angle attachment at a fixed angle of 80° is used for

characterization of surfaces. The infrared radiation is reflected from the surface of the sample, and the resultant spectrum reveals the functional groups present on the surface.

1.5.2 Contact Angle Goniometry

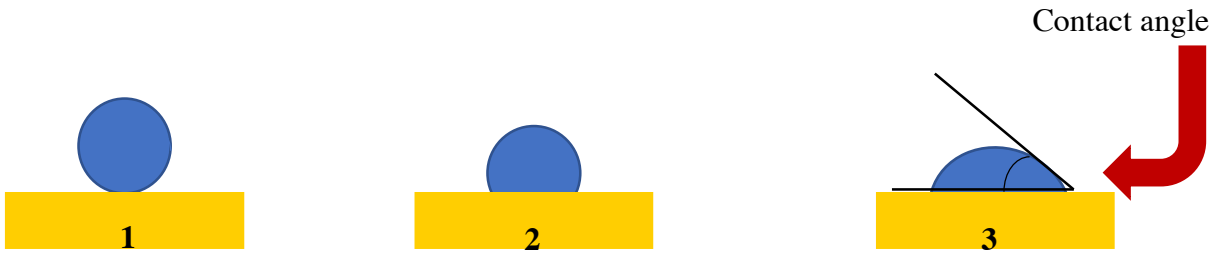

Figure 1.6 Surface Wettability

Water contact angles are used to measure surface wettability. The angle that is formed at the solid-liquid interface is defined as the contact angle. Complete wetting occurs when the contact angle is 0°. Figure 1.6 illustrates three examples of wettability. **1** is a non-wetting surface where the water droplet has a high contact angle. A wettable surface is shown in **2**, while a completely wet surface is shown in **3**. Freshly cleaned surfaces of bare substrates (such as gold) exhibit low water contact angles. Angles that are smaller than 90° are observed when the surface is considered hydrophilic.[33] Water contact angles greater than 90° indicate that the surface is hydrophobic. Surfaces with angles greater than 150° are considered superhydrophobic surfaces. Large angles are also observed for rough surfaces.

1.5.3 Atomic Force Microscopy

Atomic Force Microscopy (AFM) is a method of scanning probe microscopy used to measure properties of a surface. Measurable characteristics include height, friction, and topography. AFM was first developed in the mid 1980s.[34,35] The most common configuration for AFM imaging is illustrated in Figure 1.7. The AFM uses a cantilever with a tip to scan over

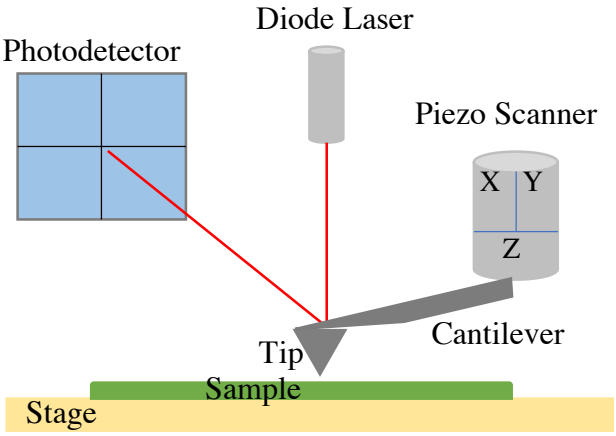

Figure 1.7 Basic Instrument Setup for Atomic Force

surfaces. The piezo scanner is used to maintain a constant force between the tip and the sample. The directional movements of the cantilever as a result of the tip coming into contact with the surface is recorded by the reflections of the diode laser source onto a photodetector. The resulting output from the photodiode is then translated into a depth analysis of the surface, known as a topographic image.

The AFM has multiple modes of operation. Contact mode and tapping mode are two of those methods. In contact mode the deflection of the cantilever is kept constant. This is used for traditional imaging. In tapping mode, the tip is oscillated at a variable frequency while the amplitude is kept constant. Tapping mode is used for nanoshaving and nanografting experiments. Imaging is usually achieved under low force conditions. Increased force is applied to a thin film in an effort to determine its stability relative to the force applied to the AFM tip. This increased force is used to remove any film that is not strongly bonded to the surface.

AFM can also manipulate the surface material by applying a high force onto the tip. The nanoshaving technique was first reported in 1994 for an n-alkanethiol self-assembled monolayer (SAM) on Au(111).[41] Nanoshaving was later done on an octadecyltriethoxysilane SAM on glass.[42] Since its inception, nanoshaving has been widely applied for nanoscale experiments[43-44] and for constructing nanoscale features.[45-46.] Nanoshaving is accomplished by sweeping the

cantilever across a small region with a higher mechanical force applied to the AFM tip. The sweeping action of the cantilever aims to remove or displace molecules of the thin film. By decreasing the force, nondestructive AFM imaging of the nanoshaved area is then possible. Nanoshaving can also be done in conjunction with other techniques such as particle lithography.

1.5.3.1 Particle Lithography

The patterning of surfaces allows organic thin films to address specific problems in nanoscience.[36,37] Particle lithography is a surface patterning method that enables spatial control over the deposition of the thin film. The deposition and annealing of a surface mask (*e.g.* silicon dioxide, latex, etc.) allows the deposition of thin film on areas not covered by the mask. These nano-patterning of the surface is achieved by covering the surface with mesospheres (latex, silicon dioxide, etc.). Figure 1.8 outlines the process of nanofabrication using a mesosphere mask. The masked surface **1** is then placed in the reaction solution **2**. After immersion, electrografting, or photografting the mask is removed to yield the coated surface **3**. The removal of the mask after deposition of the thin film leaves regions of bare substrate. These contact sites are called nanopores or nanoholes.

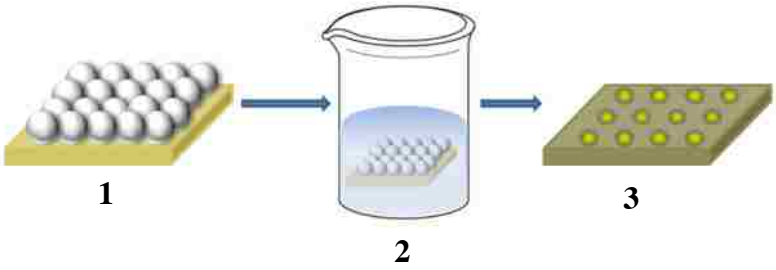

Figure 1.8 Particle Lithography using a Surface Mask

The coupling of AFM with particle lithography allows the depth of the thin film to be measured. After the coating of surface and removal of the mask, the surface can be scanned with

the AFM tip. The distance is measured between the site of bare substrate and the thin film. Thickness, topography, friction, and cursor profile information are obtained from this technique. Additionally, nanoholes are also potentially useful for data storage, information processing, and backfilling.[37]

1.5.4. X-ray Photoelectron Spectroscopy

X-ray photoelectron spectroscopy (XPS) is a technique widely used in surface science and surface analysis. XPS is accomplished by irradiating and exciting a sample surface with x-rays under ultra-high vacuum conditions.[50] An energy analyzer simultaneously measures the energy emitted by the photoelectrons. The resulting energy measurement provides information on the elemental composition, the chemical state, and the electronic state of elements present on or within the surface of a material.

1.6 Visible-Light Photoredox Catalysis with $Ru(bpy)_3^{2+}$

Kellogg,[38] Deronzier,[5] and Okada[49] pioneered the use of visible-light photoredox catalysis for the formation of small molecules in organic chemistry. The excited states of diamagnetic photocatalysts are often at once strong oxidizing and strong reducing agents. For example, the visible-light photocatalyst ruthenium (II) tris-2,2'-bipyridine $Ru(bpy)_3^{2+}$ is a work horse for visible-light photocatalysis. Figure 1.9 demonstrates the oxidative and reductive quenching cycles of tris(2,2'-bipyridine) ruthenium (II). Excitation of the ground state species $Ru(bpy)_3^{2+}$ (λ_{max}, MLCT=452m) with blue LEDs (λ_{max}=455nm) yields the active photocatalyst $Ru(bpy)_3^{2+*}$.

Upon absorption of a photon by a visible-light source, an electron from one of the metal t_{2g} orbitals is excited to a ligand π^* anti-bonding orbital. This transition is referred to as a metal

to ligand charge transfer (MLCT).[39] The excited photocatalyst $Ru(bpy)_3^{2+*}$ resulting from the MLCT is a better electron donor than its ground state species (Figure 1.10). $Ru(bpy)_3^{2+*}$ ($E_{1/2}^{III/II*}$= -0.81V vs SCE) can function as a reductant, reducing an electron acceptor (A) to the radical anion; the oxidized $Ru(bpy)_3^{3+}$ ($E_{1/2}^{III/II}$= +1.29V vs SCE) can later gain an electron from a donor and return to its ground state. Likewise, $Ru(bpy)_3^{2+*}$ ($E_{1/2}^{II*/I}$= +0.77V vs SCE) also serves as a stronger oxidant compared to the ground state catalyst. Similarly, $Ru(bpy)_3^{2+*}$ can be directly reduced by single electron transfer (SET) from a donor (D) to give a strong reductant $Ru(bpy)_3^{1+}$ ($E_{1/2}^{II*/I}$= +0.77V vs SCE). Upon loss of an electron $Ru(bpy)_3^{1+}$ ($E_{1/2}^{I/II}$= -1.33V vs

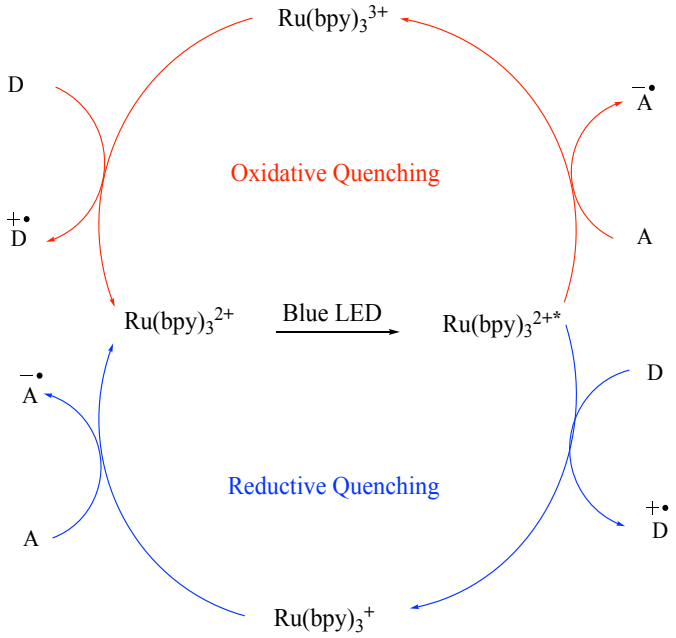

Figure 1.9 Reductive and Oxidative Quenching Cycle of $Ru(bpy)_3^{2+}$

SCE) returns to its ground state $Ru(bpy)_3^{2+}$.

Pinson and coworkers demonstrated that aryl diazonium salts could be reduced using $Ru(bpy)_3^{2+}$, and the resulting aryl radicals bind to gold surfaces forming layers with a thickness of less than 5nm that could not be removed with rinsing or ultrasonication.[5] The organic thin

films were characterized using water contact angle measurements, ellipsometry, Xx-ray photoelectron spectroscopy, and infrared reflectance-absorption spectroscopy.

1.7 References

1. Blodgett, K., *J. Am. Chem. Soc*. **1935**, *57*, 1007-1022.
2. Schoenfisch, M. H.; Pemberton, J. E., *J. Am. Chem. Soc*., **1998**, *120*, 4502-4513.
3. Combellas, C; Delamar, M.; Kanoufi, F; Pinson, J.; Podvorica, F., *Chem Mater*., **2005**, *17*, 3968-3975.
4. Bandyopadhyay, D.; Prashar, D.; Luk, Y. *Langmuir*, **2011**, *27*, 6124–6131.
5. Bouriga, M.; Chehimi, M. M.; Combellas, C.; Decorse, P.; Kanoufi, F.; Deronzier, A.; Pinson, J., *Chem. Mater.,* **2013**, *25*, 90-97.
6. (a) Jeon, L. J.; Nuzzo, R.G.; Xia, Mrksich, M.; Whitesides, G.M., *Langmuir*, **1995**, *11*, 3026. (b) Xia,Y.; Mrksich, M.; Kim, E., Whitesides, G. M., *J. Amer. Chem. Soc*., **1995**, *117*, 9576.
7. Krzywicki, J.W. *Metal Finishing*, **2006**, *104*, 28-37.
8. Wink, T.; van Zulien, S.J.; Bult, A.; van Bennekom, W.P., *Analyst*, **1997**, *122*, 43R-50R.
9. Chaki, N.K.; Vijayamohanan, K., *Biosensors and Bioelectronics*, **2002**, *12*, 1-12.
10. Sassolas, A.; Bouvier, B. D.; Blum, L. J., *Chem. Rev.,* **2008**, *108,* 109.
11. Arotiba, O.; Owino, J.; Songa, E.; Hendricks, N.; Waryo, T.; Jahed, N.; Baker, P.; Iwuoha, E., *Sensors*, **2008**, *8*, 6791.
12. (a) Bath, B. D.; Martin, H.B.; Wightman, R. M.; Anderson, M. R., *Langmuir*, **2001**, *17*,

7032. (b) Hermans, A.; Seipel, T.; Miller, C.E.; Wightman, R. M., *Langmuir*, **2006**, *22*, 1964.

13. Downard, A. J.; Roddick, A. D.; Bond, A. M., *Anal. Chim. Act.*, **1995**, *317*, 303–310.

14. Bourdillon, C.; Delamar, M.; Demaille, C.; Hitmi, R.; Moiroux, J.; Pinson, J., *J. Electroanal. Chem.*, **1992**, *336*, 113.

15. LeGoff, A.; Moggia, F.; Debou, N.; Jegou, P.; Artero, V.; Fontecave, M.; Jousselme, B.; Palacin, S.; *J. Electroanal. Chem.*, **2010**, *641*, 57.

16. McCreery, R. *Analytical Chemistry*, **2006**, *78*, 3491-3497.

17. Gates, B.D.; Xu, Q.; Stewart, M.; Ryan, D.; Wilson, C.G.; Whitesides, G.M., *Chem. Rev.*, **2005**, *105*, 1171-1196.

18. Belanger, D.; Pinson, J., *Chem. Soc. Rev.,* **2011**, *40*, 3995–4048.

19. Bigelow, W. C.; Pickett, D. L.; Zisman, W. A., *J. Colloid Sci.* **1946,** *1,* 513–538

20. Ulman, A., *Chem. Rev.*, **1996**, *96*, 1533-1554.

21. Nuzzo, R. G.; Allara, D. L., *J. Am. Chem. Soc.,* **1983**, *105*, 4481.

22. Troughton, E. B.; Bain, C. D.; Whitesides, G. M.; Allara, D. L.; Porter, M. D., *Langmuir*, **1988**, *4*, 365.

23. Sabatani, E.; Cohen-Boulakia, J.; Bruening, M.; Rubinstein, I., *Langmuir,* **1993**, *9*, 2974.

24. Ihs, A.; Uvdal, K.; Liedberg, B., *Langmuir*, **1993**, *9*, 733.

25. Edwards, T. R. G.; Cunnane, V. J.; Parsons, R.; Gani, D., *J. Chem. Soc., Chem. Commun.*, **1989**, 1041.

26. Li, T. T.-T.; Liu, H. Y.; Weaver, M. J., *J. Am. Chem. Soc.*, **1984**, *106*, 1233.

27. Deng, J.; Wang, L.; Liu, L.; Yang, W., *Progress in Polymer Science*, **2009**, *34*, 156–193.

28. Lussem, B.; Muller-Meskamp, L.; Karthauser, S.; Waser, R.; Homberger, M.; Simon, U.,

Langmuir, **2006**, *22*, 3021-3027.

29. Hasegawa, Y.; Avouris, P., *Science,* **1992**, *258*,1763-1765.

30. Hamilton, M. L.; Perston, B.B.; Harland, P.W.; Williamson, B.E; Thomson, M. A.; Melling, P. J., *Org. Process Res. Dev.*, **2005**, *9*, 337–343.

31. Ulman, A., *Characterization of Organic Thin Films*, Materials Characterization Series, Butterworth-Heinemann, Stoneham, **1995**.

32. Ferraro, J.R.; Basile, L.J., *Fourier Transform Infrared Spectroscopy – Applications to Chemical Systems*, 4, Academic Press, Inc., New York, **1985**

33. Yuan, Y., *Surface Science Techniques*, Springer Series in Surface Sciences, 51, Springer-Verlag, Berlin Heidelberg, **2013.**

34. Binnig, G.; Quate C.F.; Gerber, C., *Phys. Rev. Letters,* **1986**, *56*, 930.

35. Martin, Y.; Williams, C. C.; Wickramasinghe, H. K, *J. Appl. Phys.* **1987**, *61*, 4723.

36. Smith, R.K.; Lewis, P.A.; Weiss, P.S., *Progress in Surface Science*, **2004**, *75*, 1–68.

37. Gates, B.D.; Xu, Q.; Stewart, M.; Ryan, D.; Willson, C.G.; Whitesides, G.M., *Chemical Reviews*, **2005**, *105*, 1171-1196.

38. (a) Hedstrand, D. M.; Kruizinga, W. M.; Kellogg, R. M., *Tetrahedron Lett.*, **1978**, *19*, 1255. (b) van Bergen, T. J.; Hedstrand, D.M.; Kruizinga, W. H.; Kellogg, R. M., *J. Org. Chem.,* **1979**, *44*, 4953.

39. (a) McCusker, J. K., *Acc. Chem. Res.,* **2003**, *36*, 876. (b) Bock, C. R.; Connor, J. A.; Gutierrez, A. R.; Meyer, T. J.; Whitten, D. G.; Sullivan, B. P.; Nagle, J. K., *J. Am. Chem. Soc.* **1979**, *101*, 4815.

40. Amabilino, D.B., Surfaces for Supramolecular Systems, in *Supramolecular Chemistry at Surfaces*, **2015**, Royal Society of Chemistry 1-54.

41. Liu, G.-Y.; Salmeron, M. B., *Langmuir*, **1994**, *10*, 367- 370.

42. Xiao, X.-D.; Liu, G.-y.; Charych, D. H.; Salmeron, M., *Langmuir*, **1995**, *11*, 1600-1604.

43. Rosa, L. G.; Jiang, J.; Lima, O. V.; Xiao, J.; Utreras, E.; Dowben, P. A.; Tan, L., *Mater. Lett*. **2009**, *63*, 961-964.

44. Verberne-Sutton, S. D.; Quarels, R. D.; Zhai, X.; Garno, J. C.; Ragains, J. R., *J. Am. Chem. Soc*. **2014**, *136*, 14438-44.

45 Shao, J.; Josephs, E. A.; Lee, C.; Lopez, A.; Ye, T., *ACS Nano,* **2013**, *7*, 5421-5429.

46. Greene, M. E.; Kinser, C. R.; Kramer, D. E.; Pingree, L. S. C.; Hersam, M. C., *Microsc. Res. Techniq*., **2004**, *64*, 415-434.

47. Ihalainen, P.; Pettersson, F.; Pesonen, M.; Viitala, T.; Määttänen, A.; Österbacka, R.; Peltonen, J., *Nanotechnology*, **2014**, *25*, 94009.

48. Claes, M.; Voccia, S.; Detrembleur, C.; Jérôme, C.; Gilbert, B.; Leclère, Ph.; Geskin, V.M.; Gouttebaron,R.; Hecq, M; Lazzaroni, R.; Jérôme, R., *Macromolecules*, **2003**, *36*, 5926-5933.

49. Okada, K.; Okamoto, K.; Morita, N.; Okubo, K.; Oda, M., *J. Am. Chem. Soc*., **1991**, *113*, 9401. b) Okada, K.; Okamoto, K.; Oda, M., *J. Am. Chem. Soc*., **1988**, *110*, 8736. c) Okada, K.; Morita, N.; Okubo, K.; Oda, M., *Tetrahedron Lett*., **1992**, *33*, 7377.

50. Hollander, J.M.; Jolly, W. L., *Accounts of Chemical Research*, **1970**, *3*, 193-200.

CHAPTER 2: APPLICATION OF VISIBLE-LIGHT PHOTOCATALYSIS WITH PARTICLE LITHOGRAPHY TO GENERATE POLYNITROPHENYLENE NANOSTRUCTURES

2.1 Introduction to Diazonium Salts

Arenediazonium salts were first used in the production of dyes for textiles and photocopying.[1,2] Diazonium salts are unstable at high temperature and high pH due to their reactivity. The first electrochemical reduction of aryldiazonium salts was reported by Elofson.[3] He observed that the reduction of arenediazonium salts with mercury electrodes led to the formation of diphenyl mercury and phenylmercuric chloride. Electroreduction of diazonium salts saw further exploration in the synthesis of small molecules and even found uses in Heck reactions, Meerwin arylations, Sandmeyer-type reactions, in the preparation of thiophenols, and in additions to alkenes.[4] The electrografting of diazonium salts has been achieved on carbon, metals, semiconductors, oxides, and polymers.[1,4,5,6,7] The reduction of diazonium salts by electrodes occurs via a one electron reduction to the corresponding aryl radical with concomitant formation of nitrogen gas. At more negative potentials, the aryl radical is reduced to the aryl anion.[4] Electron withdrawing groups have been shown to increase the ease of arenediazonium reduction to the aryl radical (Scheme 2.1) while electron-donating substituents have been shown to stabilize the starting diazonium.[4]

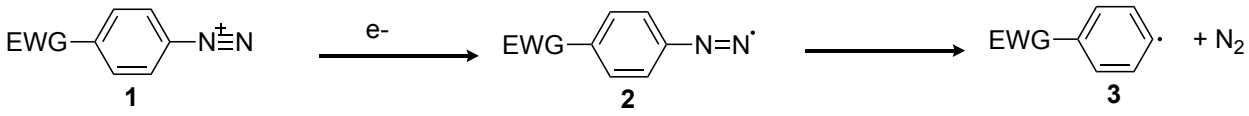

1 2 3

Scheme 2.1 Formation of Diazenyl Radical and Radical via One Electron Reduction

Photochemical reduction of arenediazonium salts have been shown to occur via radical decomposition[8] and light-induced homolytic cleavage[9] (Scheme 2.2, line 1). Radical-chain decomposition requires stoichiometric quantities of electron-donating compounds such as

dimethoxybenzene to form charge transfer complexes with the diazonium salt.[10,11] At low wavelengths (below 315nm), heterolytic cleavage occurs to give the aryl cation. The heterolytic pathway (Scheme 2.2, line 2) is a competing pathway with lower energy (λ<400nm) photodecomposition conditions.[4,9] Photografting of aryl radicals resulting from the reduction of

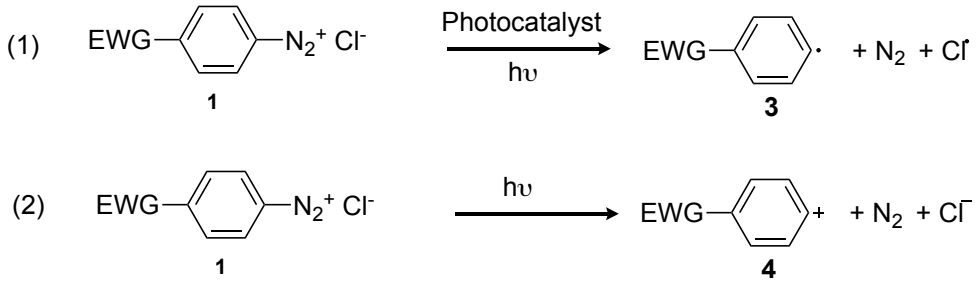

Scheme 2.2 Photochemical Cleavage of Diazonium Salts

arenediazonium salts via visible light photocatalysis has not been widely studied. Bouriga *et al*. demonstrated the use of $Ru(bpy)_3(PF_6)_2$ as a photocatalyst for the reduction of diazonium salts for the surface modification of both Au(111) and polyvinylchloride, a nonconductive polymer surface.[12] Similar approaches were demonstrated by Schroll *et al*.[13] and Busson *et al*.[14] The mild and user friendly conditions for visible light photocatalytic reduction of arenediazonium salts produce a carbon-centered aryl radical that grafts to both conducting and non-conducting surfaces.[1,4] The resulting aryl radicals (Scheme 2.2, line 1) bind to gold, polymers, and other surfaces forming layers with thicknesses of less than 10nm that could not be removed with rinsing or ultrasonication.[1,4,12-14] The organic thin films were characterized using water contact angle measurements, ellipsometry, XPS, and IRRAS. Spontaneous grafting led to a grafting rate of 5% compared to the method using $Ru(bpy)_3^{2+}$ as a photocatalyst.[12] Increasing the nucleophilicity of the solvent increased the amount of spontaneous grafting as was observed by Bouriga and coworkers. This evidence supported the earlier findings that solvents could induce dediazoniation by acting as electron donors.[12]

The covalently bound organic films produced with reduction of diazonium salts are more stable than self-assembled monolayers produced by chemisorption of *n*-alkanethiols.[12,15] As Chehimi[15] eloquently stated, "the advantage of aryl diazonium salts compared to other surface modifiers lies in their ease of preparation, rapid (electro)reduction, large choice of reactive functional groups, and strong aryl-surface covalent bonding." The ability to produce more stable films provides the benefits of long term storage and repeated use necessary for microelectronics,[12,16] electrochemical sensors,[17] biosensors,[12,16] medical devices,[12] and corrosion-resistant surfaces.[17] Furthermore, the patterning of surfaces coated with diazonium salts would be useful for biosensors if the photografting of the aryl radicals could be controlled. Nanolithography,[18-20] scanning electrochemical microscopy,[21] micro-contact printing,[22,23] silicon doping,[25] and particle lithography[24, 26, 27] techniques have all been applied in the patterning of organic thin films on surfaces by electrochemical reduction of diazonium salts. Therefore, we proposed that the preparation of periodic nanostructures can be accomplished efficiently with the combination of particle lithography and visible-light photoredox catalysis.[28]

We applied particle lithography (Chapter 1) using atomic force microscopy (AFM) analysis in an effort to determine the film thickness and topography of the surfaces produced from our photografting procedure. The nanoholes produced also provided the bare gold surface for further backfilling experiments that had not been previously done on electrochemically reduced surfaces of arenediazonium salts.

2.2 Results and Discussion

Four arenediazonium salt derivatives (**7a-7d)** were synthesized using tetrafluoroboric acid and sodium nitrite.[29] Aryldiazonium salts with weakly deactivating and electron-withdrawing

substituents were chosen as they were shown to increase the ease of reduction. The investigated arenediazonium salts can be seen in Scheme 2.3. Each aryldiazonium salt was grafted using visible light photocatalysis to determine the stability of the resulting film on an Au(111) surface.

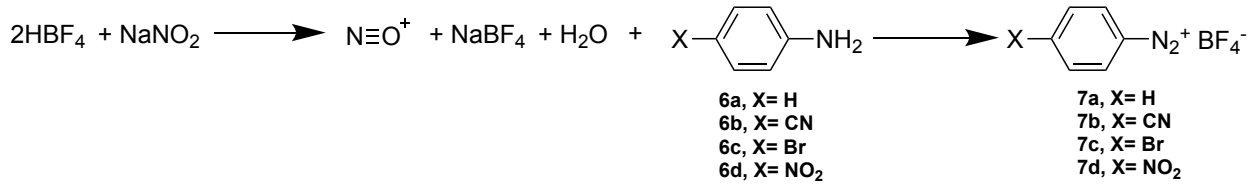

Scheme 2.3 Synthesis of Aryldiazonium Salts

Particle lithography with surface masks of silica mesospheres (d = 500 nm) was used to protect small regions of the Au(111) surface on a glass slide from photografting. This strategy for surface nanofabrication was adapted for ease of determination of surface modification, topography, layer thickness, and friction. Silicon dioxide masked gold surfaces (used for particle lithography) were initially immersed in solutions of 0.1M arenediazonium tetrafluoroborate **7** and 0.025M $Ru(bpy)_3(PF_6)_2$ in acetonitrile, stirred in a round-bottom flask, and irradiated for 30 minutes with blue LEDs.[12] The initial round bottom flask setup caused etching of the gold surface from the mica plate (see Procedures and Characterization) making it impossible to determine the areas of grafted organic thin film using AFM. After several alterations in setup (*i.e.* irradiation without stirring, irradiation in a petri dish, and continuous swirling) we determined that the solution needed to be continuously stirred in an effort to uniformly distribute the aryl radicals generated. An Erlenmeyer flask setup with stir bar and nitrogen inlet was determined to be the most effective photografting setup (see Appendix A).

Atomic force microscopy revealed that the visible-light photoredox catalyzed reduction of arenediazonium salts **7a** and **7b** did not contain any pattern on the surface and it is possible that films using these diazonium salts did not produce a film under our conditions. The lack of surface modification could be an indicator of one of the two phenomena: 1) the grafting of diazonium salts

7a and **7b** was not selective and thus grafting to the surface of the mesospheres as well as the gold surface occurred or 2) the organic films generated from the photografting of arenediazonium salts **7a** and **7b** was the result of physisorption and these films were removed during one of the various rinsing procedures.

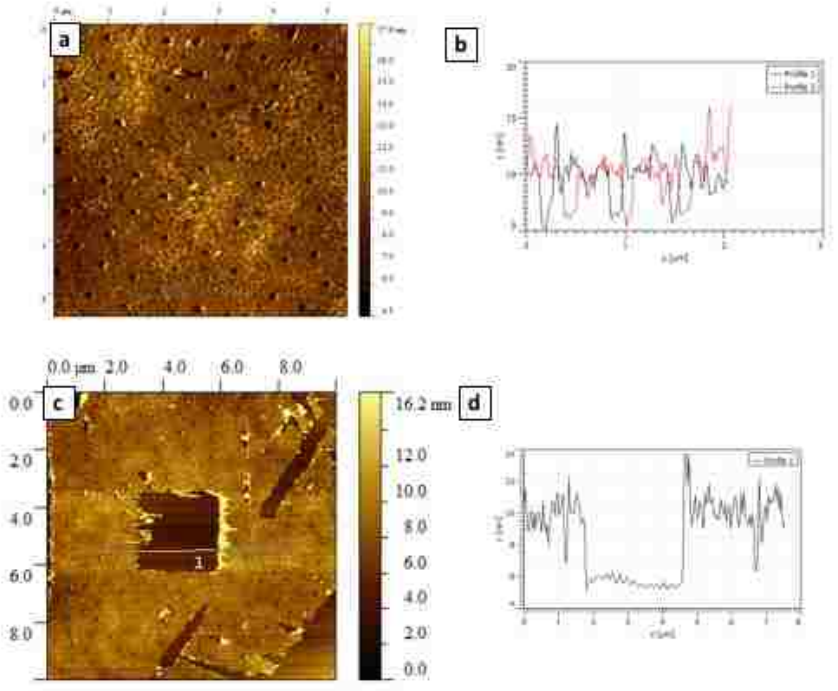

Figure 2.1 A photografted film of polybromophenylene formed on Au(111) generated with an initial concentration of 10^{-1}M **7c**, after 30 min irradiation. Nanopores were produced using immersion particle lithography. (a) Topography image (5 × 5 μm^2) acquired in air; (b) cursor profile for the lines in *a*;(c) the shaved area after additional force applied using AFM tip; (d) cursor profile for the line in *c* after nanoshaving.

However, nanografting of the Au(111) surfaces by the reduction of diazonium salts **7c** and **7d** was successfully demonstrated. The mask of mesospheres was removed by ultrasonication to generate nanopores in areas on the gold surface previously covered by mesospheres. The nanopores provide a baseline for thickness measurements of the organic thin films. AFM images obtained from the reduction of diazonium salt **7c** can be seen in Figure 2.1. The organic thin film exhibited the hexagonal packed arrangement expected after the removal of the silicon dioxide mesosphere mask. An average thickness of 10nm was observed. Such a thickness suggests the

formation of multilayers due to polymerization of the aryl radicals in situ. The increase of force applied to the AFM tip revealed that the organic thin film formed from the reduction of diazonium salt **7c** was removable with 10nN of force applied to the AFM tip.

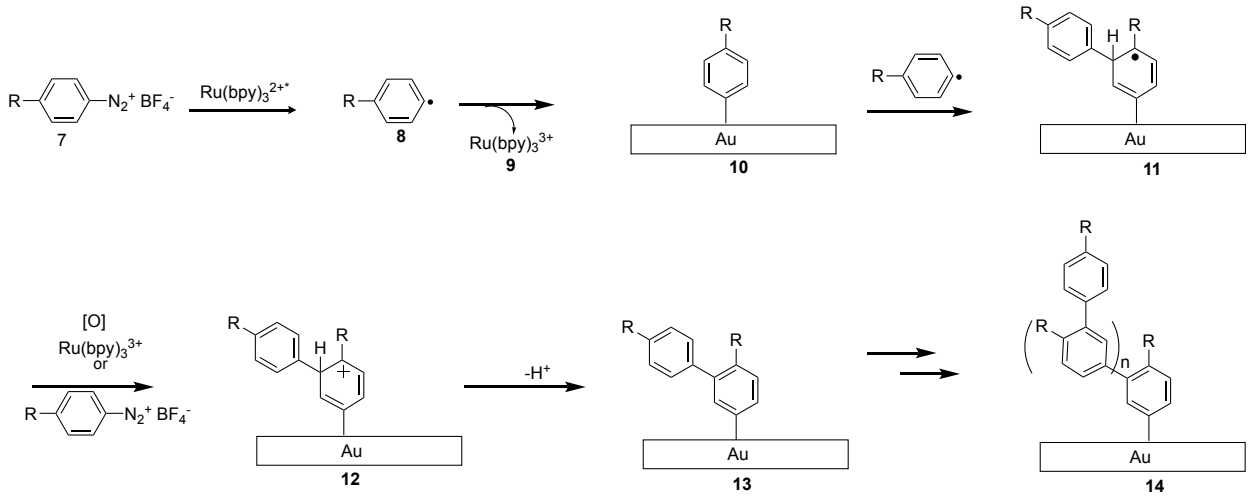

Scheme 2.4 Proposed Mechanism for the Photografting of Arenediazonium Salts

Gold surfaces masked with mesospheres were immersed in a solution of compound **7d** (*p*-nitrobenzenediazonium tetrafluoroborate (NBDT) and the photocatalyst $Ru(bpy)_3(PF_6)_2$ in acetonitrile and irradiated for varying time intervals to produce *p*-nitrophenyl radicals that bind to Au(111). Layer thicknesses revealed by AFM suggested the polymerization of *p*-nitrophenylradicals at the surface to form polynitrophenylene multilayers.[12] A proposed mechanism for the multilayer formation is outlined in Scheme 2.4. Upon irradiation, $Ru(bpy)_3^{2+}$ is excited to $Ru(bpy)_3^{2*}$. The excited photocatalyst donates an electron directly to aryldiazonium tetrafluoroborate **7**. The resulting aryl radical attaches to the gold surface (**10**). We propose that another aryl radical formed in situ attacks grafted *p*-nitrophenyl resulting in **11**. Oxidation of the intermediate **11** by $Ru(bpy)_3^{3+}$, the oxidized photocatalyst, or by another molecule of *p*-nitrobenzenediazonium tetrafluoroborate yields carbocation **12**. Concomitant removal of a proton regenerates aromaticity **13**. Successive attack of aryl radicals (**8**) results in the formation of

polyphenylene multilayers **14**.

Several irradiation times were investigated to determine the influence of time on multilayer thickness using this photografting procedure. A series of concentration and time dependence studies were conducted using diazonium salt **7d** to determine whether or not multilayer formation could be controlled. The resulting multilayer film formed from the photoreduction of 0.1M diazonium salt **7d** after 30 minutes of irradiation is presented in Figure 2. 2.The average depth of the organic thin film was measured at 89 ± 22 nm. Such organic thin film depths had not been previously reported using electrografting or photografting procedures with diazonium salts. A rough, irregular arrangement of surface structures surrounding nanopores was obtained from the topography measurement (Figure 2.2A). Reimaging of the organic thin film obtained from the 30-minute irradiation of diazonium salt **7d** after six months revealed that the surface was stable to oxidation and still resistant to applied AFM force.

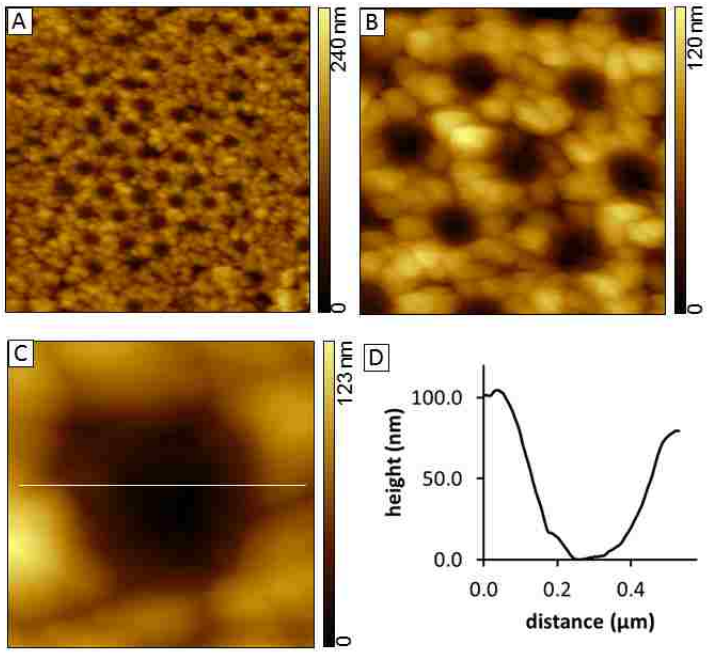

Figure 2.2 A photografted film of polynitrophenylene formed on Au(111) generated with an initial concentration of 10^{-1}M **7d** after 30 minutes of irradiation. Nanopores were produced using immersion particle lithography. (a) Topography image (5 × 5 μm^2) acquired in air; (b) zoom-in view (1.5 × 1.5 μm^2); (c) a single nanopore (500 × 500 nm^2); (d) cursor profile for the line in *c*.

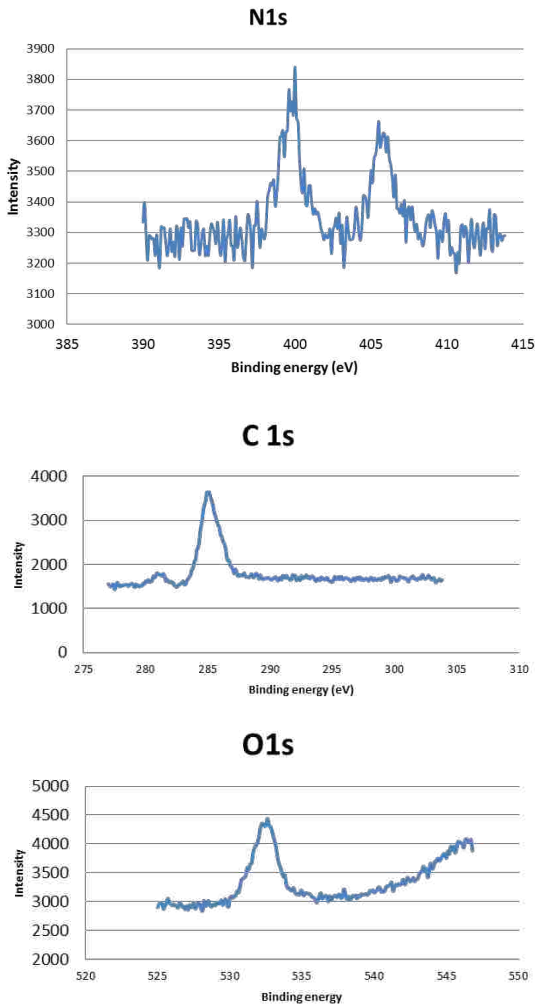

Figure 2.3 N1s, C1s, and O1s Photoelectron Spectra of the Deposited Polynitrophenylene Layers After Photografting.

The XPS data indicated that polynitrophenylene multilayers were present on the gold surface after irradiation with $Ru(bpy)_3^{2+}$ in acetonitrile. I observed nitrogen, oxygen, and carbon in the XPS spectra. I used the C1s spectra (285.1eV) to calibrate binding energies (Figure 2.3).[35] There were two major peaks observed in the N1s spectrum. The peaks were observed at 400eV and 405.9eV corresponding an azo-linkage (-N=N-) and a nitro-linkage ($-NO_2$). The O1s spectrum is broad with one major peak at 532.8eV. Water contact angle measurements yielded an average of 86° ± 2° indicating that the grafted surface is slightly hydrophilic. The XPS data and water

contact angle measurements were consistent with values previously published by Bouriga and coworkers.[12]

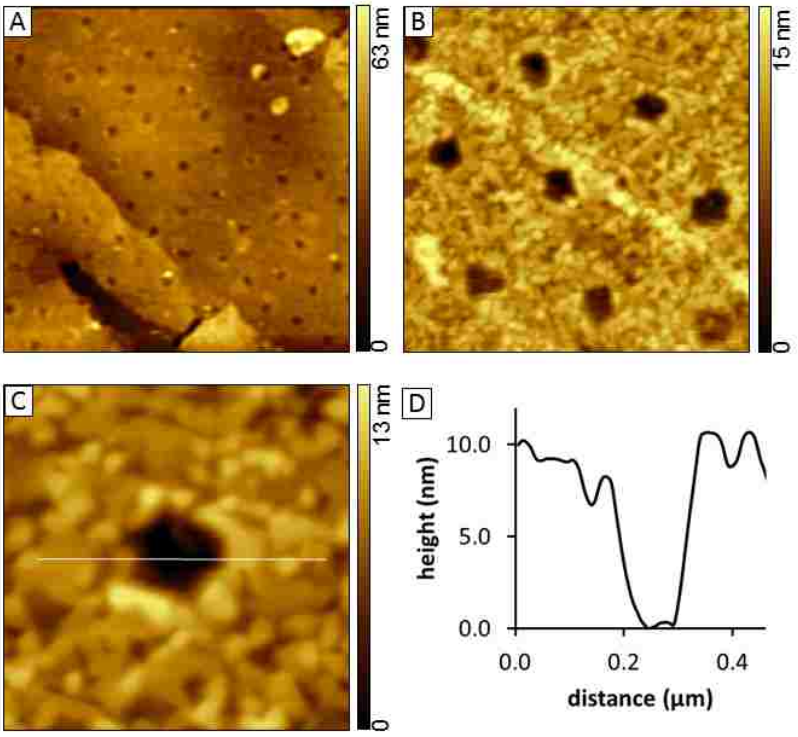

Figure 2.4 A photografted film of polynitrophenylene formed on Au(111) generated with an initial concentration of 10^{-1}M **7d** after 15 minutes of irradiation. Nanopores were produced using immersion particle lithography. (a) Topography image (5 × 5 μm^2) acquired in air; (b) zoom-in view (1.5 × 1.5 μm^2); (c) a single nanopore (500 × 500 nm^2); (d) cursor profile for the line in *c*.

After 15 minutes of irradiation at 0.1M NBDT **7d**, AFM images of the polynitrophenylene film revealed an organic thin film with one-seventh the thickness of the layer previously seen with the NBDT **7d** irradiated for 30 minutes. The film thickness was measured at approximately 13 ± 2 nm. The topography (Figure 2.4A) of the NBDT **7d** film after 15 minutes was much smoother than what had been previously observed. The hexagonally packed arrangement of the mesosphere masks left easily identifiable sites of bare gold. This can be seen in the dark 'holes' of Figure 2.4B.

After 5 minutes of irradiation of the 0.1M solution of NBDT **7d** (Figure 2.5), the dark regions are representative of the uncovered areas of the gold substrate and measure approximately

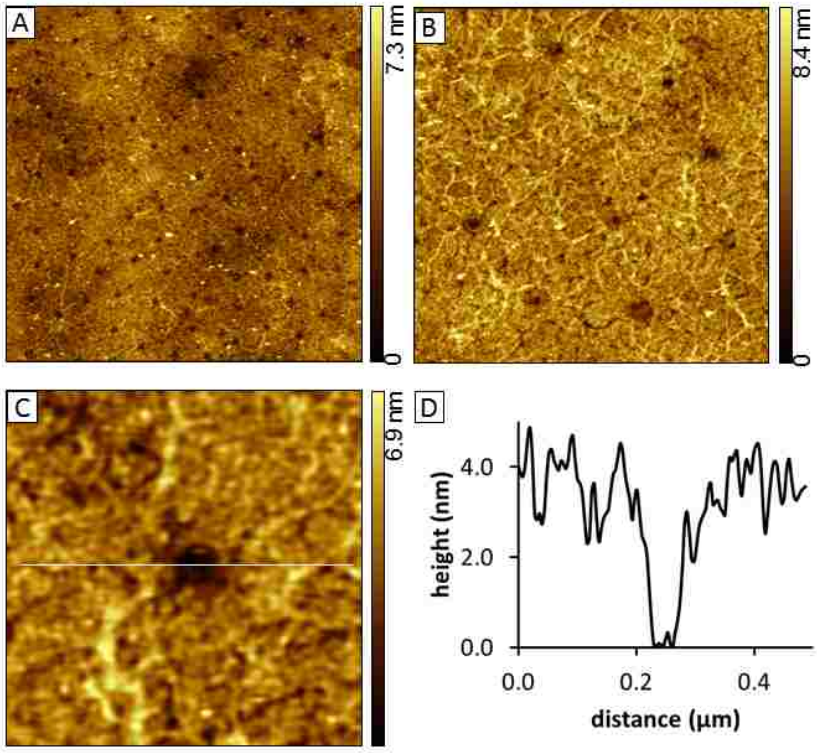

Figure 2.5 A photografted film of polynitrophenylene formed on Au(111) generated with an initial concentration of 10^{-1}M **7d** after 5 minutes of irradiation. Nanopores were produced using immersion particle lithography. (a) Topography image (5 × 5 μm^2) acquired in air; (b) zoom-in view (1.5 × 1.5 μm^2); (c) a single nanopore (500 × 500 nm^2); (d) cursor profile for the line in *c*.

18 % of the surface. The areas of the polynitrophenylene film are a slightly lighter shade of brown and fairly homogeneous in color. The continuity of color suggests a fairly uniform organic thin film composition throughout the sample. Although not as clearly visible as some of the other images, Figure 2.5B demonstrates the hexagonally packed arrangement of the mesospheres resulting from the irradiation of NBDT after 5 minutes. The cursor profile of a single nanopore is shown in Figure 2.5D reveals an average thickness of the 3.5 ± 0.9 nm for the photografted film. Though irradiation time was shown to effectively control grafting efficiency, monolayer formation was not achieved.

A decrease in concentration was explored in an effort to obtain monolayer thickness. The concentration was decreased to 10^{-3}M and 10^{-5}M (100 and 10,000-fold dilutions respectively). The

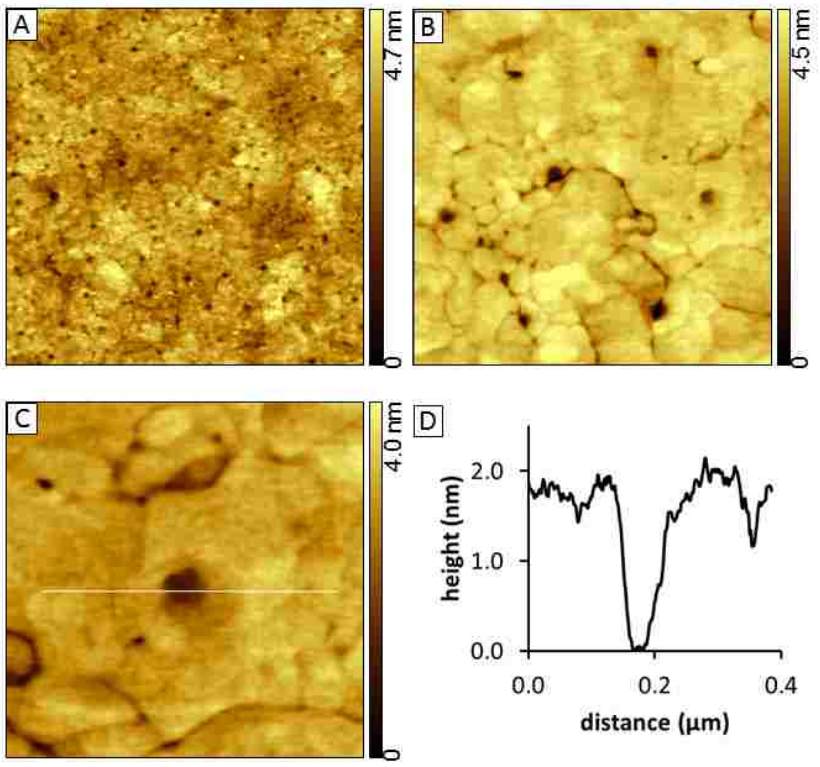

Figure 2.6 A photografted film of polynitrophenylene formed on Au(111) generated with an initial concentration of 1 mM **7d**, after 30 min irradiation. Nanopores were produced using immersion particle lithography. (a) Topography image (5 × 5 μm^2) acquired in air; (b) zoom-in view (1.5 × 1.5 μm^2); (c) a single nanopore (500 × 500 nm^2); (d) cursor profile for the line in *c*.

10,000-fold decrease in concentration did not produce any detectable organic film by AFM. After thirty minutes of irradiation at a 1mM (100-fold dilution) concentration of NBDT **7d**, a densely-packed film of polynitrophenylene was observed. The periodic arrangement of nanopores was detected via AFM in contact mode. Characteristic terraces, scars and domains of the underlying Au(111) substrate were evident within Figure 2.6A, the topography image.

Interestingly, the films do not exhibit molecular vacancy islands that are characteristic of Au surface reconstruction typically observed with *n*-alkanethiol monolayers.[32] Figure 2.6B shows a hexagonal packed arrangement of nanopores. Figure 2.6C shows a magnified view of an individual nanopore. The depth of the nanopore in Figure 2.6C is shown in the cursor profile in Figure 2.6D. The images in Figure 2.6 are representative of multiple areas of the sample. The

average depth measured was 2.6 ± 0.2 nm for the polynitrophenylene film prepared after 30 minutes of irradiation at 1mM.

The exposed surfaces sites of the substrate located within the nanopores were backfilled with a ω-functionalized *n*-alkanethiol which contains a carboxylic acid headgroup. Mercaptoundecanoic acid (MUA) was chosen because of its ability to be further functionalized. MUA in ethanol (0.6 mM) was added to the sample shown in Figure 2.5 (0.1 M NBDT, 5 min. irradiation). A close-up view of the sample is presented in Figure 2.7a. The shapes and arrangement of 16 nanopores within the film of polynitrophenylene were observed. After 24 hours of immersion in MUA, multilayers of this thiol were observed in the former exposed areas of the sample (Figure 2.7c).

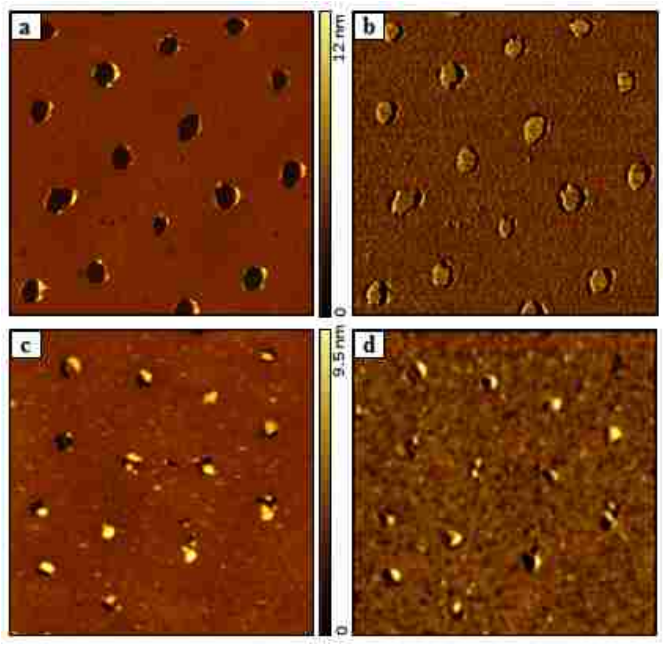

Figure 2.7 After backfilling with an *n*-alkanethiol, nanostructures formed within exposed sites of the nanopores. (a) Topography image of nanopores within a matrix film of polynitrophenylene (2 × 2 μm^2); (b) simultaneously acquired lateral force image. (c) After backfilling with MUA (topography, 2 × 2 μm^2); (d) corresponding lateral force image.

The use of increased force was applied to the surface of the backfilled sample for a side-by-side comparison of the stability of the diazonium-derived film versus thiol-bound MUA (Figure

2.7). We anticipated that the thiol molecules could be displaced from the surface using a process known as nanoshaving.[33] A single nanostructure of MUA is shown in Figure 2.8a. Before backfilling with MUA, the depth of the nanopore measured 3.0 ± 0.2 nm. Under low force, images can be acquired without disturbing the shapes of the nanostructures. Figure 2.8b is a single nanopore that has been immersed in MUA solution for 24 hours. In consideration of the thiol nanostructure measuring 8.7 nm, such a thickness corresponds to a multilayer of MUA formed by interactions between acid headgroups.[34] The area containing the nanostructure and the surrounding organic thin film was nanoshaved at higher force (swept 20x) to shave away the surface film. The 10nN of force was sufficient to remove thiol molecules, however, the photografted film of polynitrophenylene persisted (Figure 2.8c). No evidence of exchange or adsorption of MUA with the organic thin film was visible throughout the course of the backfilling or nanoshaving investigations.

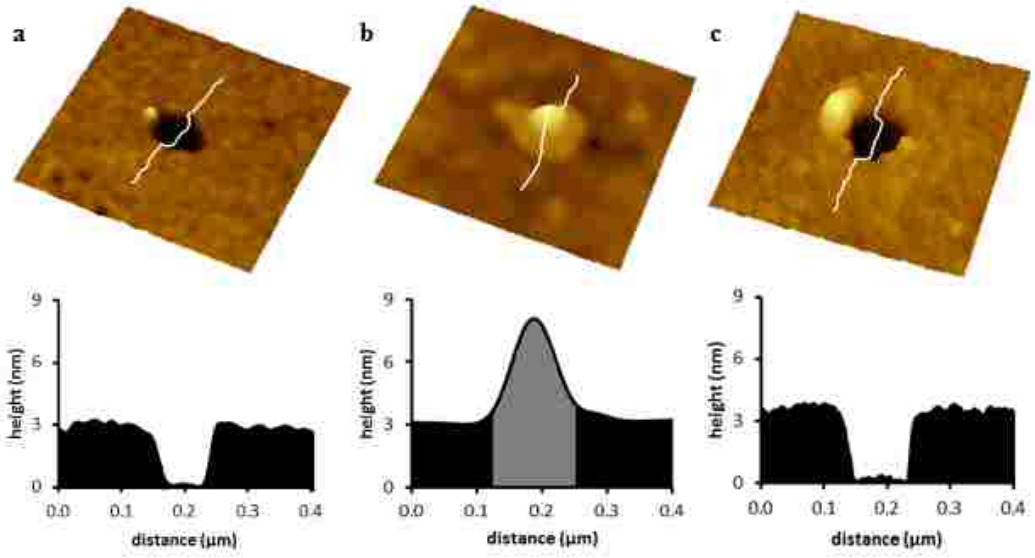

Figure 2.8. Steps for backfilling and shaving the nanopores filled with MUA. Topography images (500 × 500 nm^2) of (a) a single nanopore within the polynitrophenylene matrix film; (b) nanostructure of MUA formed within a nanopore; (c) the same area of the MUA nanostructure.

2.3 Conclusion

Overall, a highly efficient method for grafting polyphenylene moieties onto Au(111) surfaces was developed using visible light photoredox catalysis. The pore depth of the polyphenylene coating was controlled by both the duration of irradiation and the initial concentration of the diazonium salt. Further attempts at manipulating the organic thin were illuminating. We demonstrated that the nanopores on the photografted substrate could be backfilled with mercaptoundecanoic acid. Additionally, the alkanethiol layer could be selectively removed without harming the organic film generated from the polymerization of *p*-nitrophenyl radicals. As previously mentioned, AFM imaging of the "30 minute 10^{-1}M sample" after six months revealed that the organic film was robust and stable to oxidation.

2.4 Experimental and Tabulated Data

2.4.1 Experimental Section

Materials and Reagents. Sodium nitrite (99.8% ACS certified) was obtained from Fisher Scientific. $Ru(bpy)_3(PF_6)_2$ (97%), 4-nitroaniline (99%), tetrafluoroboric acid (48% aqueous), anhydrous diethyl ether (99.0% ACS reagent grade), acetone (99.5% ACS reagent grade), and mercaptoundecanoic acid (95%) were purchased from Sigma-Aldrich and used without further purification. ^{1}H NMR and ^{13}C NMR spectroscopy were performed on a Bruker AV-400 spectrometer. Unless otherwise noted, all materials were purchased from Sigma-Aldrich and used without further purification. Glassware was flamed dried under vacuum and backfilled with dry nitrogen prior to use. Deuterated solvents were obtained from Cambridge Isotope Labs. Solvents were purified according to the method published by Pangborn et al.[31] The irradiation source for

photografting reactions was two 4 W sapphire blue LED flex strips from Creative Lighting Solutions, Cleveland Ohio.

Preparation of gold surfaces with a mesosphere mask. Template-stripped, ultraflat gold substrates were prepared by a previously reported procedure.[36] Gold films were prepared on mica(0001) by evaporative deposition. Glass discs were glued to freshly-prepared gold films using an epoxy (EPO-TEK, Billerica, MA). Pieces of ultraflat gold/glass were stripped from mica to expose a clean, atomically-flat Au (111) surface. Size-sorted silica mesospheres with an average diameter of 500 nm (Thermo Scientific) were cleaned by centrifugation and suspension in water (three cleaning cycles). A 40 μL drop of the silica mesosphere suspension was placed onto the template-stripped gold substrates, dried in air for 2 h, and then oven dried at 150°C for at least 14 h. The final heating step was used to temporarily anneal the silica spheres to the substrate to prevent displacement during chemistry steps of immersion in solutions. After completing the steps of chemical reactions, removal of the surface mask was accomplished by sonication in clean solvents.

Photografting Procedure. Acetonitrile (MeCN) from a solvent purification system[31] was dried over 3 Å molecular sieves for 24 h. A solution of 4-nitrobenzenediazonium tetrafluoroborate (NBDT, 47.4 mg, 0.2 mmol) and $Ru(bpy)_3(PF_6)_2$ (2.97 mg, 0.005 mmol) in 2 mL of anhydrous MeCN was wrapped in foil, stirred, and deoxygenated three times using the freeze-pump-thaw protocol. A lower concentration (10^{-3} M) of NBDT was prepared via dilution. A 20 uL aliquot of the 10^{-1} M solution of 4-nitrobenzenediazonium tetrafluoroborate was transferred to a separate round bottom flask wrapped in foil. Anhydrous MeCN (1.98 mL) was then added to achieve the desired concentration (10^{-3} M). This solution was also deoxygenated three times using the freeze-pump-thaw protocol. A stir bar and the masked gold substrates were placed in a 125 mL Erlenmeyer flask so that the stir bar did not touch the sample. The Erlenmeyer flask was sealed

with a rubber septum and sparged with nitrogen for 30 min. The deoxygenated solution of 4-nitrobenzenediazonium tetrafluoroborate and $Ru(bpy)_3(PF_6)_2$ in anhydrous MeCN was added to the 125 mL Erlenmeyer flask containing the masked gold sample and stir bar. The suspension was magnetically stirred and irradiated. After irradiation for the desired period of time, the solution was decanted. The masked gold sample was washed twice with 2 mL of deionized water and twice with 2 mL of ethanol to remove material that was not strongly attached to the gold surface. The samples were sonicated in ethanol for 1 min to remove the mesospheres and any remaining non-covalently bound residues.

Backfilling the nanopores with mercaptoundecanoic acid (MUA). A solution of MUA in ethanol was prepared by dissolving 0.0014 g of MUA in 10 mL ethanol and stirred until completely dissolved (0.6 mM). The solution was injected into a liquid cell (Sonimoto Laboratories, West Bloomfield, MI) that supports imaging samples in a liquid environment. Fresh aliquots (1 mL) of the MUA solution were replenished each hour to replace liquid lost by evaporation.

Atomic Force Microscopy (AFM). The samples were imaged using a model 5500 or model 5420 atomic force microscope with Pico View v.1.12 software (Agilent Technologies, Chandler, AZ). Non-conductive imaging probes from Bruker (MSCT, 0.01 – 0.6 N/m) were used to acquire contact-mode images. Images were processed and analyzed using Gwyddion (v. 2.22), an open-access processing software designed for AFM images, supported by the Czech Metrology Institute.

2.4.2 Procedures and Characterization

Representative procedure of the preparation of diazonium tetrafluoroborate:

The aryl diazonium tetrafluoroborate was prepared according to a method similar to that of Vogel using an aniline derivative .[49] Tetrafluoroboric acid (HBF_4) (3.6 mL, 27 mmol) was added to a round-bottom flask containing 5 mL of deionized water. A solution of the aniline derivative (10

mmol) was added in three portions to the round-bottom flask and stirred. The resulting olive-green solution was cooled to 0°C in an ice-water bath. A solution of sodium nitrite (0.69 g, 10 mmol) in deionized water (2 mL) was prepared and then added dropwise to the aqueous solution of 4-nitroaniline and HBF_4 over a period of 30 min under N_2 at 0°C. As the resulting cloudy green mixture became difficult to stir, the stirring rate was increased. The round-bottom flask was wrapped in foil and the mixture was stirred for an additional 1 h at 0°C. The resulting mixture was filtered and washed with 2 mL of cold deionized water. The resulting solid was added to a 250 mL Erlenmeyer flask and dissolved in 30 mL of acetone. The remaining precipitate was removed by filtration and washed with 2 mL of acetone. 20 mL of anhydrous diethyl ether was added at once to the resulting filtrate. The precipitated diazonium salt was filtered using a Büchner funnel, washed with 10 mL of anhydrous diethyl ether, and dried under high vacuum for 1 h. Due to its low stability at room temperature, the diazonium salt was used immediately or stored at –2°C prior to use.

Synthesis of 7a:

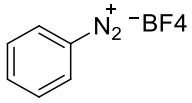

Tetrafluoroboric acid (HBF_4) (3.6mL, 27mmol) was added to a round-bottom flask containing 5mL of deionized water. Aniline (0.91mL, 10mmol) was added in three portions to the round-bottom flask and stirred. The resulting olive-green solution was cooled to 0°C in an ice-water bath. A solution of sodium nitrite (0.69g, 10mmol) and deionized water (2mL) was prepared and then added dropwise to the aqueous solution of 4-nitroaniline and HBF_4 over a period of 30 minutes under N_2 at 0 °C. As the resulting cloudy green mixture became difficult to stir, the stirring rate was increased. The round-bottom flask was wrapped in foil and the mixture was allowed to stir for

an additional hour at 0°C. The resulting mixture was filtered and washed with 2mL of cold deionized water. The resulting solid was added to a 250mL Erlenmeyer flask and dissolved in 30 mL of acetone. The remaining precipitate was removed by filtration and washed with 2mL of acetone. 20mL of anhydrous diethyl ether was added at once to the resulting filtrate. The precipitated diazonium salt was filtered using a Büchner funnel, washed with 10mL of anhydrous diethyl ether, and dried under high vacuum for 1hr. Due to its low stability at room temperature; the diazonium salt was used immediately or stored at −2°C prior to use.0.8341g (44%) $C_6H_5N_2BF_4$ (192.05g/mol) was isolated. ^{1}H NMR (250MHz, CD_3CN): δ 8.48(d, 2H, J=Hz), 8.24(t, 1H, J=4.83Hz), 7.91(t, 2H, J=4.83Hz)

Synthesis of 7b:

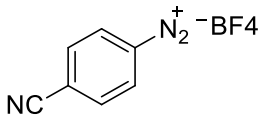

Prepared using the same method as the synthesis of **1** from 1.182g of 4-aminobenzonitrile. 0.8875g (41%) $C_7H_4N_3BF_4$ (217.04g/mol) was isolated. ^{1}H NMR (250MHz, CD_3CN): δ 8.59(d, 2H, J=5.68Hz), 8.24(d, 2H, J=3.28Hz)

Synthesis of 7c:

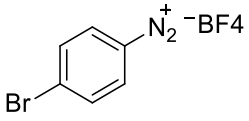

Prepared using the same method as the synthesis of **1** from 1.7202g of 4-bromoaniline. g (%) $C_6H_4N_2BrBF_4$ (269.96g/mol) was isolated. ^{1}H NMR (250MHz, CD_3CN): δ 8.35(d, 2H, J=8.60Hz), 8.13(d, 2H, J=8.70Hz)

Synthesis of 7d:

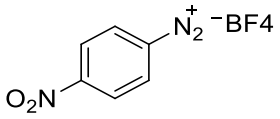

Prepared using the same method as the synthesis of **1** from 1.3812g of 4-nitroaniline. 1.2344g (52.1%) $C_6H_4N_3O_2BF_4$ (237.03g/mol) was isolated. ^{1}H NMR (400MHz, CD_3CN): δ 8.74 (d, 2H, J=9.32Hz), 8.63 (d, 2H, J=9.32Hz); ^{13}C NMR (100MHz, CD_3CN): ● 155.3, 135.5, 126.7, 121.6.

2.5 References

1. Belanger, D.; Pinson, J., *Chem. Soc. Rev.*, **2011**, *40*, 3995-4048.
2. Zollinger, H., *Diazo Chemistry*, Wiley, New York, 2004.
3. Elofson, R.M., *Can. J. Chem.,* **1958**, *36*, 1207.
4. Galli, C., *Chem. Rev.,* **1988**, *88*, 765.
5. M. Delamar, M.; Hitmi, R.; Pinson, J.; Saveant, J.- M., *J. Am. Chem. Soc.,* **1992**, *114*, 5883.
6. Allongue, P.; Delamar, M.; Desbat, B.; Fagebaume, O.; Hitmi, R.; Pinson, J. Saveant, J.-M., *J. Am. Chem. Soc.*, **1997**, *119*, 201.
7. Barriere, F.; Downard, A.J., *J. Solid State Electrochem.*, **2008**, *12*, 1231.
8. Fomin, G.V.; Mordvintsev, P.I.; Mkhitarov, R.A.; Gordina, T. A**.,** *Zh. Fiz. Khim.,* **1980**, *54*, 240-242.
9. Ando, W. *The Chemistry* of *Diazonium and Diazo Groups;* Patai, *S.,* Ed.; Wiley: New York, **1978;** Part 1, Chapter 9, 341.

10. Busson, M.; Berisha, A.; Combellas, C.; Kanoufi, F.; Pinson, J., *Chem. Commun.*, **2011**, *47*, 12631.

11. Kosynkin, D., Bockman, T.M., and Kochi, J.K. *J. Am. Chem. Soc.*, **1997**, *119*, 4846.

12. Bouriga, M.; Chehimi, M. M.; Combellas, C.; Decorse, P.; Kanoufi, F.; Deronzier, A.; Pinson, J., *Chem. Mater.,* **2013**, *25*, 90-97.

13. Schroll, P.; Fehl, C.; Dankesreiter, S.; König, B. *Org. Biomol. Chem.,* **2013**, *11*, 6510-6514.

14. Busson, M.; Berisha, A.; Combellas, C.; Kanoufi, F.; Pinson, J., *Chem. Commun.*, **2011**, *47*, 12631-23633.

15. Chehimi, M. M.; Hallais, Matrab, G. T.; Pinson, J.; Podvorica, F.I., *J. Phys. Chem. C,* **2008**, *112*, 18559.

16. Ramin, L.;Jabbarzadeh, A., *Langmuir*, **2011**, *27*,16, 9748–9759.

17. Schoenfisch, M. H.; Pemberton, J. E., *J. Am. Chem. Soc.*, **1998**, *120*, 18, 4502-4513.

18. Ghorbal, A.; Grisotto, F.; Laude, M.; Chadier, J.; Palacin, S., *Journal of Colloid and Interface Science,* **2008**, *328*, 308-313.

19. Brooksby, P. A.; Downard, A. J., *Langmuir,* **2005**, *21*, 1672-1675.

20. Anariba, F.; DuVall, S. H.; McCreery, R. L., *Analytical Chemistry,* **2003**, *75*, 3837-3844.

21. Azevedo, J. l.; Fillaud, L.; Bourdillon, C. l.; Noël, J.-M.; Kanoufi, F. d.; Jousselme, B.; Derycke, V.; Campidelli, S. P.; Cornut, R., *J. Am. Chem. Soc.,* **2014**, *136*, 4833-4836.

22. Garrett, D. J.; Lehr, J.; Miskelly, G. M.; Downard, A. J., *J. Am. Chem. Soc.,* **2007**, *129*, 15456-15457.

23. Lehr, J.; Garrett, D. J.; Paulik, M. G.; Flavel, B. S.; Brooksby, P. A.; Williamson, B. E.; Downard, A. J., *Anal. Chem.,* **2010**, *82*, 7027-7034.

24. Liu, G.; Bocking, T.; Gooding, J. J., *J. Electroanal. Chem,.* **2007**, *600*, 335-344.

25. Charlier, J.; Palacin, S.; Leroy, J.; Del Frari, D.; Zagonel, L.; Barrett, N.; Renault, O.; Bailly, A.; Mariolle, D., *J. Mater. Chem,* **2008**, *18*, 3136-3142.

26. Corgier, B. P.; Belanger, D., *Langmuir,* **2010**, *26*, 5991-5997.

27. Santos, L.; Ghilane, J.; Lacroix, J.-C. *Electrochem. Comm.* 2012, *18*, 20-23.

28. Saner, C. K.; Lusker, K. L.; LeJeune, Z. M.; Serem, W. K.; Garno, J. C. *Beilstein Journal of Nanotechnology,* **2012**, *3*, 114-122.

29. Vogel, A.I., P*ractical Organic Chemistry*, 5th ed., John Wiley and Sons, Inc., New York, 1989.

30. Necăs, D.; Klapetek, P. *Central Eur. J. Phys.*, **2012**, *10*, 181–188.

31. Pangborn, A. B.; Giardello, M. A.; Grubbs, R. H.; Rosen, R. K.; Timmers, F. J., *Organometallics*, **1996**, *15*, 1518.

32. Poirier, G. E., *Langmuir,* **1997**, *13*, 2019-2026.

33. Liu, G. Y.; Xu, S.; Qian, Y. L., *Acc. Chem. Res.* **2000**, *33*, 457-466.

34. Kelley, A. T.; Ngunjiri, J. N.; Serem, W. K.; Lawrence, S. O.; Yu, J. J.; Crowe, W. E.; Garno, J. C. *Langmuir,* **2010**, *26*, 3040-3049.

35. NIST X-ray Spectroscopy Database, Version 4.1; National Institute of Standards and Technology: Gaithersburg, MD, **2012**.

36. Wagner, P.; Zaugg, F.; Kernen, P.; Hegner, M.; Semenza, G., *J. Vac. Sci. Technol. B,* **1996**, *14*, 1466–1471.

CHAPTER 3: APPLICATION OF VISIBLE-LIGHT PHOTOCATALYSIS FOR THE FORMATION OF ALKYL-RADICAL DERIVED THIN FILMS

3.1 Introduction to Alkyl Radical Grafting

Electrografting is a well-known technique for the formation of radical-derived thin films.[1] Methods for the electro- and photografting of aryl radicals have been widely explored using a variety of small molecules including diaryliodonium [1,2] salts and arenediazonium salts.[1,4] In contrast, methods for the production of alkyl radicals for grafting have not been as widely developed. This slow development is due in part to several limitations of the alkyl radical precursors. Alkyl halides, Grignard reagents, and carboxylic acids have all been studied as alkyl radical precursors. Over-reduction to the carbanion (alkyl halides), over-oxidation to carbocation (carboxylic acids), and low functional group tolerance (Grignard reagents) are the most common issues to plague the use of alkyl radicals for thin film growth.

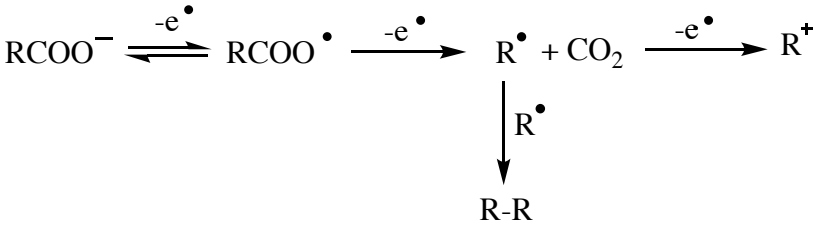

Scheme 3.1 Kolbe Electrolysis Reaction Mechanism

High potentials are required for anodic oxidation of carboxylate anions to carboxyl radicals. [5,7,8] The rapid loss of CO_2 generates alkyl radicals that can attach to the surface of a substrate. The formation of the alkyl radical is fast; however, the radical is easily oxidized relative to the starting carboxylate, thus resulting in the formation of carbocations. The mechanism of this reaction is similar to that of the Kolbe electrolysis reaction (Scheme 3.1). Carboxylate oxidation has been demonstrated using both 2-arylacetates and alkanoates.[1, 8]

Grignard reagents undergo anodic oxidation to generate grafting radicals on silicon surfaces.[11-15] Grignard reagents have also been thermally activated to generate lower quality thin films. Though quite useful, Grignard reagents require oxygen-free conditions and are sensitive to adventitious moisture.

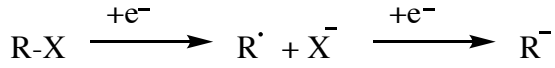

Scheme 3.2 Reduction of Alkyl Halides

Andrieux and coworkers studied the electoreduction of various alkyl halides using cyclic voltammetry. Tertiary iodides were reduced by single electron transfer resulting in the cleavage of the carbon-iodine bond.[5,6] Andrieux and coworkers observed a second wave corresponding to the reduction of the tertiary radical to the carbanion. *Sec*-butyl and *n*-butyl iodides were also studied; however, reduction potentials for the formation of the alkyl radical and the alkyl anion were very similar, owing to the ease of over-reduction (radicals to carbanions). Alkyl bromides also exhibited similar reduction potentials for the halide itself and the radical.[6] Additionally, photografting of alkyl halides on silicon, carbon, and metal[1,31,32] surfaces have been explored and the resulting films characterized. Unfortunately, these methods are plagued by over-reduction, functional group intolerance, and uncontrolled spontaneous attachment.[1, 31,32]

3.2 Phthalimide Esters

N-(acyloxy)phthalimides (or phthalimide esters) are a precursor to alkyl radicals and are synthesized in one step from the corresponding carboxylic acid.[24] The phthalimide ester is inert to many reaction conditions.[29] Single electron reduction of *N*-(acyloxy)phthalimides was first demonstrated by Okada and coworkers.[16-20] Okada[16-20] and Overman[21-22] have demonstrated (Scheme 3.3) that visible-light irradiation of the photocatalyst $Ru(bpy)_3^{2+}$ results in the formation of an excited state $Ru(bpy)_3^{2+*}$ that can accept an electron from benzyl nicotinamide (BNAH) to

generate $Ru(bpy)_3^{1+}$, a strong reducing agent. Single-electron transfer from $Ru(bpy)_3^{1+}$ to phthalimide esters turns over the photocatalyst and results in the formation of carbon dioxide, a phthalimide anion, and an alkyl radical. The alkyl radicals resulting from the reduction of the phthalimide esters can undergo reduction, [16-20] halogenation, [16-20] selenation, [16-20] and conjugate addition to electron-poor alkenes.[21]

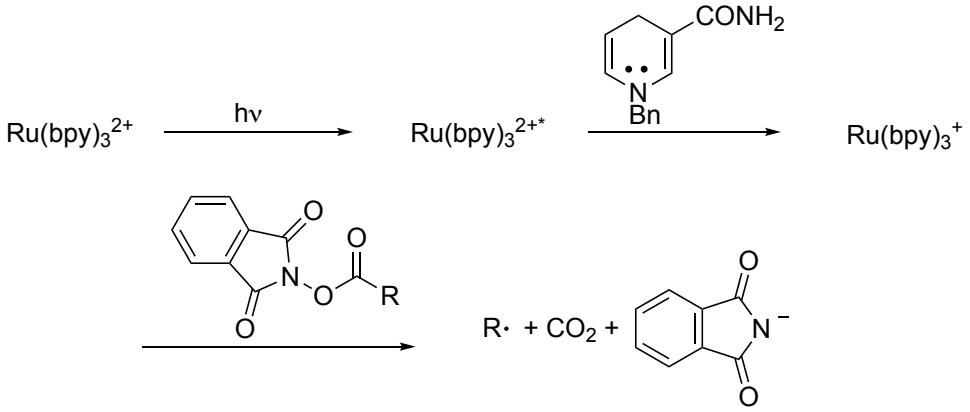

Scheme 3.3 Phthalimide Ester Reduction to Alkyl Radical

We proposed that the alkyl radicasl generated from the reduction of phthalimide esters would graft to Au surfaces for the formation of alkyl-radical-derived thin films. This method would address the issues of over-reduction and functional group tolerance seen with other alkyl radical precursors. Alkyl radicals are expected to attach swiftly to the surface substrate. The use of *N*-(acyloxy)phthalimides for the surface modification of Au(111) has not been previously investigated. We anticipated that the stability of the as-formed Au-C bond would also provide increased stability to oxidation, thermal decomposition, applied force, chemical rinsing, and long term storage when compared to alkane thiol SAM counterparts.

We believed that the combination of photocatalytic grafting of phthalimide-ester-derived alkyl radicals with particle lithography (Chapter 1 Scheme 1.6) would be beneficial to the study of alkyl-radical-derived thin films. We proposed that the patterning of the Au surface with a silicon dioxide (d=500nm) mesosphere mask and photografting of the masked gold surface followed by

removal of the mask would reveal an alkyl radical-derived thin film with nanopores of bare gold. It is imperative that I reiterate that these sites are important for the measurement of film thickness and determination of the stability of the thin film.

3.3 Synthesis of Phthalimide esters

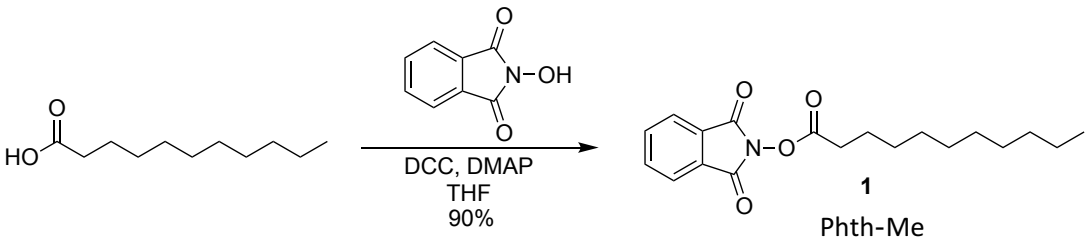

Scheme 3.4 Synthesis of Undecanoic Phthalimide Ester

As previously mentioned, all of the phthalimide esters were synthesized from carboxylic acids as seen in Scheme 3.4.[24] Commerically available undecanoic acid was used to synthesize phthalimide ester **1** (Phth-Me). Substrate **1** was synthesized as a proof of concept to ensure that the alkyl radical produced by the photocatalytic reduction would graft to the Au(111) surface. Additional phthalimide esters were synthesized fin hopes of further functionalization of their terminal groups.

Phthalimide esters **3** and **4** were prepared from commercially available 11-aminoundecanoic acid. Boc protection of the amine gave compound **2**.[23] Carboxylic acid **2** was then converted to the phthalimide ester **3** (Phth-NHBoc), Boc-protected terminal amine.[24] Deprotection of **3** with trifluoroacetic acid gave phthalimide ester **4** with a free terminal amine.[25] The transformations can be seen in Scheme 3.5. Phthalimide esters **3**, **4**, **11**, and **12** were synthesized with the goal of peptide and protein functionalization of the end groups.

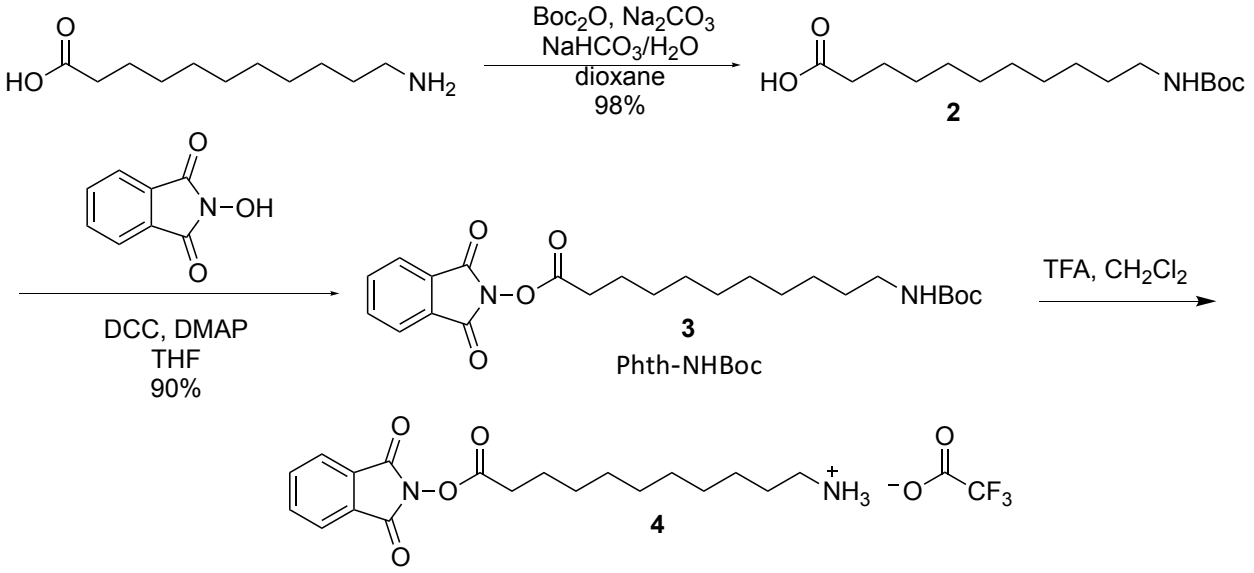

Scheme 3.5 Synthesis of Phthalimide Esters with Amine Terminus

Phthalimide esters **7** and **8** were prepared from methyl 10-hydroxydecanoate. Protection of the free alcohol of methyl 10-hydroxy decanoate with methoxyethyoxymethyl chloride (MEM-Cl) gave intermediate **5**.[26] Hydrolysis of the methyl ester **5** yielded carboxylic acid **6**.[27] Compound **6** was then converted to the MEM ether phthalimide ester **7**(Phth-OMEM). Phthalimide ester **7** was then deprotected to yield phthalimide ester **8** (Phth-OH), a terminal alcohol.[28] Jones oxidation of phthalimide ester **8** was expected to yield a phthalimide ester with a terminal carboxylic acid; however, with the release of the phthalimide ester ion in situ and possible deprotonation of the

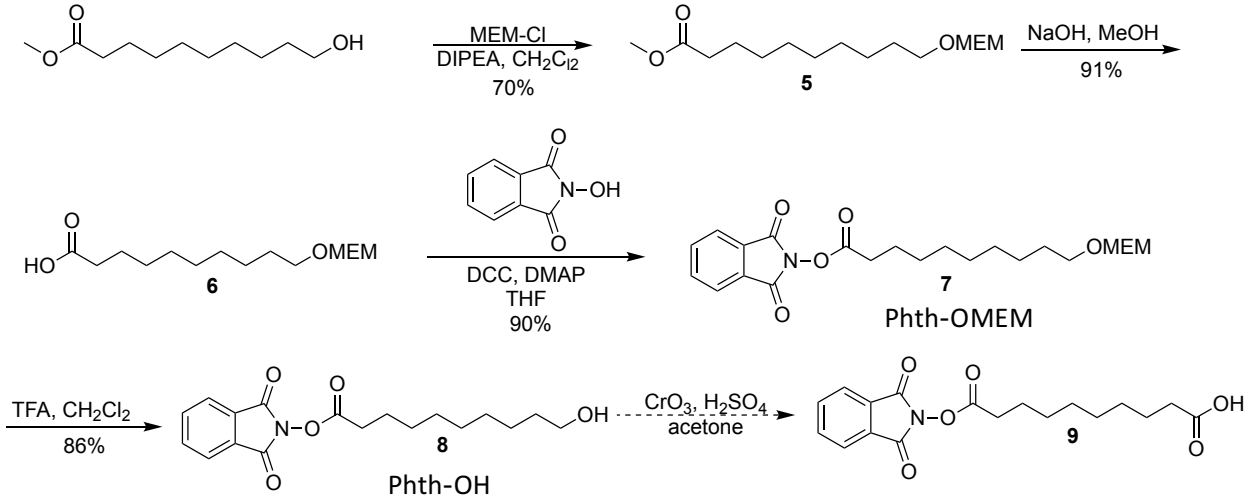

Scheme 3.6 Synthesis of Alcohol Terminated Phthalimide Ester

terminal carboxylic acid. Such a reactive species would likely produce undesirable byproducts, potentially increasing the difficulty upon characterization of the resulting thin film.

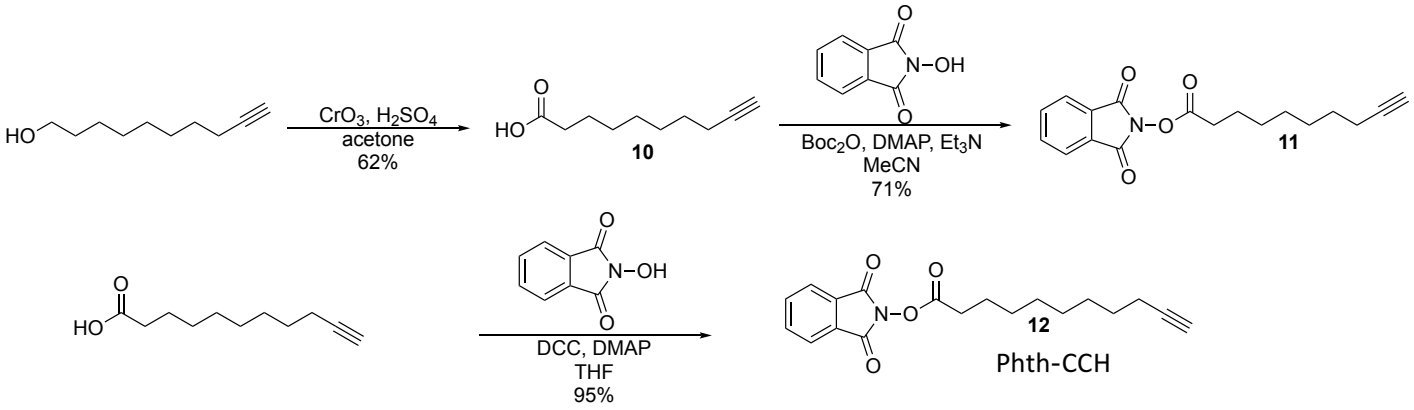

Scheme 3.7 Synthesis of Phthalimide esters with Terminal Alkyne

Phthalimide ester **11** was synthesized from 9-decyn-1-ol according to Scheme 3.7 with the hope of further tethering the chain using click chemistry. Oxidation of the primary alcohol to the carboxylic acid gave intermediate **10**.[30] Carboxylic acid **10** was then converted to phthalimide ester **11** bearing terminal alkyne, as outlined in Scheme 4.[24] Initially, phthalimide ester **11** was expected to graft efficiently and be a viable intermediate for click chemistry. After additional reading, we realized that terminal alkynes can graft directly to Au (111) surfaces. Thus, protection of the alkyne seemed necessary.[33] Synthesis of a phthalimide ester with a protected alkyne terminus was investigated, but after several failed attempts (removal of protecting group during Jones oxidation and competing reactions while attempting to protect the alkyne at the carboxylic acid stage) was discontinued. Commercially available 10-undecynoic acid could also be converted to phthalimide ester **12** (Phth-CCH).

3.4 Results and Discussion

For the purposes of this research "Au-FG" (e.g. Au-Me, Au-OH, Au-NHBoc, Au-CCH, and Au-OMEM) will be used to describe the thin films with various terminal functional groups

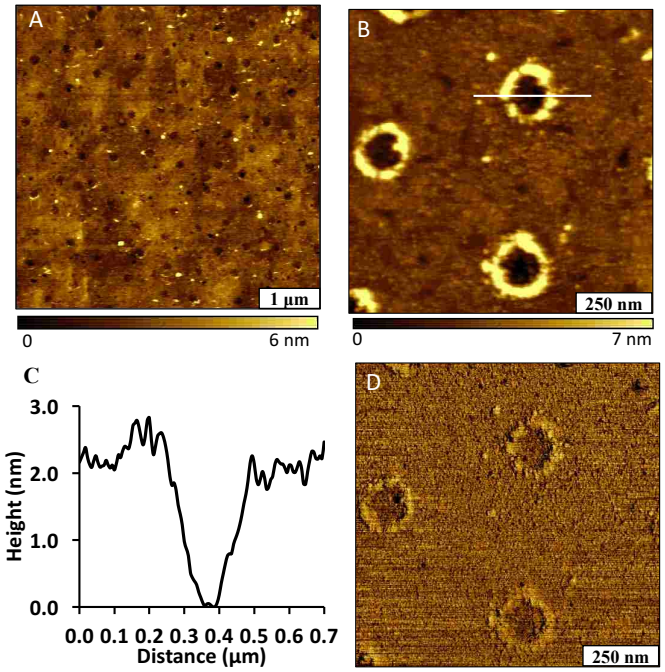

Figure 3.1 A photografted film of Au-Me generated after 30 min irradiation of a solution of 10^{-1}M Phth-Me **1**. Nanopores were produced using immersion particle lithography. (a) Topography image (1 × 1 µm^2) acquired in air; (b) zoom-in view area (250 × 250 nm^2); (c) cursor profile for the line in B; (d) phase image of B (250 × 250 nm^2).

onto Au surfaces. Au(111) surfaces were masked with mesospheres, immersed in a heterogeneous mixture of phthalimide ester, benzyl nicotinamide (BNAH), and $Ru(bpy)_3Cl_2$ in acetonitrile (this mixture became homogeneous upon irradiation), and irradiated for 30 minutes. After the irradiation, the mask was removed from the organic thin film coated substrate by rinsing with ethanol and water followed by ultrasonication. The resulting thin films (*i.e.* Figure 3.1) on Au were subjected to AFM analysis. Additional methods were used to characterize the resulting films. Commercially available glass-backed slides of polycrystalline Au were irradiated in the presence of phthalimide ester, benzyl nicotinamide and $Ru(bpy)_3Cl_2$ for a duration of 3 h. The resulting thin films were subjected to contact angle goniometry and IRRAS analysis (Chapter 1).

AFM characterization of the photoreduction of phthalimide ester **1** revealed patterning on the Au(111) surface with the Phth-Me **1** after 30 minutes of irradiation at 0.1M. The hexagonal packed arrangement of the silicon dioxide mask can be readily identified in Figure 3.1A. The dark

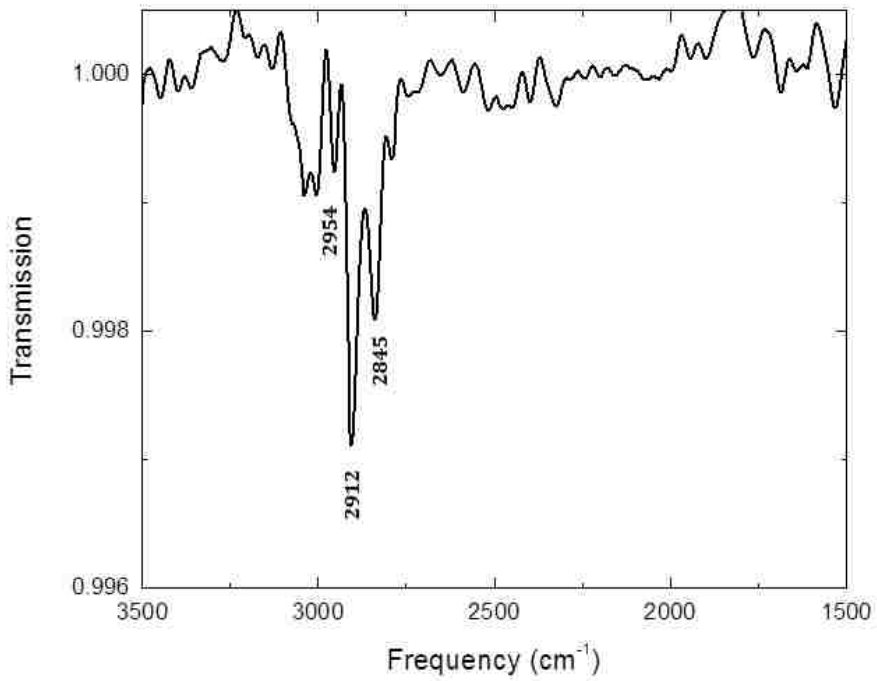

Figure 3.2 Grazing angle IRRAS Spectrum for Au-Me

brown holes seen are the sites of bare gold after the removal of the SiO_2 mesosphere mask. The surface coverage is fairly uniform as shown in Figure 3.1A. Figure 3.1B is a zoom-in view of three nanopores. The edges of the nanoholes are rounded and distinct. A close-up view of a single nanopore in Figure 3.1B is shown in the cursor profile in Figure 3.1C. The average thickness of the photografted Au-Me thin film is approximately 2 nm. Grazing-angle infrared reflectance-absorption spectroscopy (IRRAS) for the Au-Me film (Figure 3.2) displayed charaacteristic C-H stretching frequencies. The stretches at 2954, 2912, and 2845 cm^{-1} correspond to the $-CH_3$ asymmetric, the $-CH_2$ antisymmetric, and the $-CH_2$ symmetric stretches.[35] An IR spectrum of Phth-Me can be found in Appendix B for reference. Notably absent are the phthalimide ester carbonyl stretches at 1742, 1788, and 1815 cm^{-1}. The lack of these characteristic peaks suggests a clean conversion of precursor to alkyl radicals without adsorption of unreacted Phth-Me **1** to the surface. However, medium alkene (=C-H) stretches corresponding to cis and trans alkenes were observed

at 3001 and 3021c cm^{-1}. This suggests alkene formation possibly due to radical-radical disproportionation may be taking place within the alkyl chains.

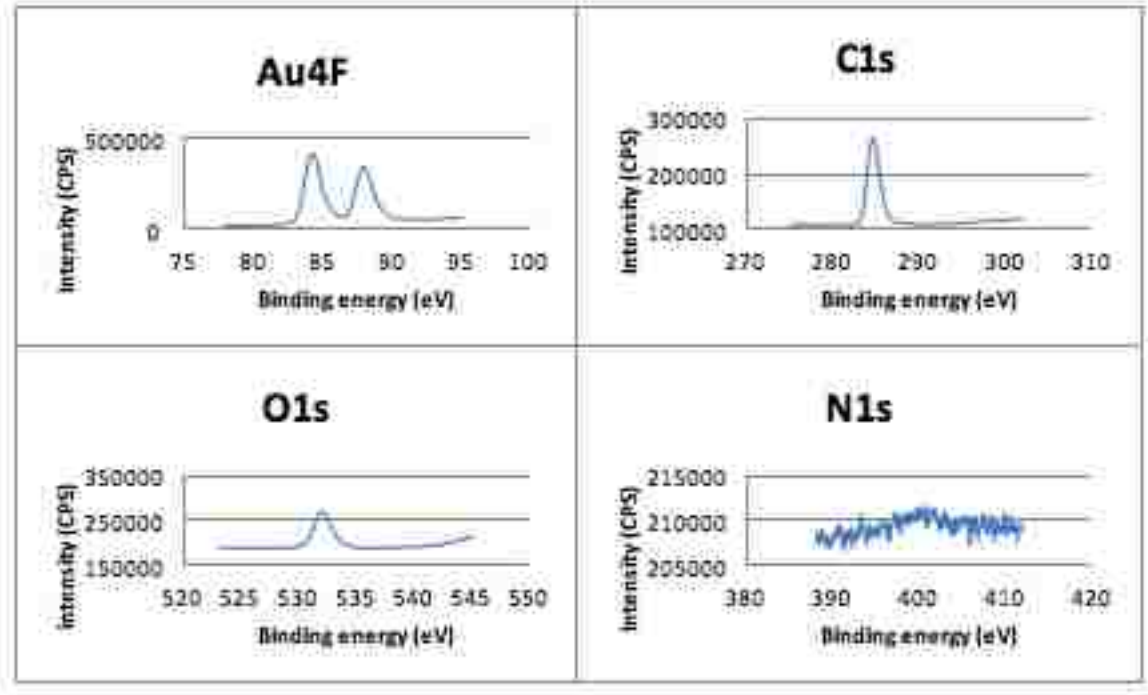

Figure 3.3 Au4f, C1s, O1s, and N1s Photoelectron Spectra of Au-Me Organic Thin Film

The XPS data indicates that the decyl-chains are attached to the gold surface of the Au-Me organic thin film (Figure 3.3). Au, C, O, and N were present on the XPS spectra. The $Au4f_{7/2}$ and $Au4f_{5/2}$ were observed at 84.0eV and 87.7eV, respectively, and were used to calibrate the binding energies of the other elements.[43] The presence of the Au photoelectron peaks is consistent with the low thin film thickness observed by AFM. The C1s spectrum of the Au-Me film revealed a peak at 284.3eV that could be assigned to methylene carbons ($-CH_2-$) present within the decyl-chains.[43,44] A binding energy of 531.9eV was observed for the O1s spectrum of the Au-Me thin film, this peak can be assigned to carbonyl containing compounds (-C=O).[43,44] The O1s spectra suggests the presence of carboxylate group or the incorporation of phthalimide within the Au-Me thin film; however, carbonyl structures indicative of phthalimide were not observed on IR.

Although the signal-to-noise was poor, the N1s spectrum suggests that presence of nitrogen containing compound attached to Ru. This indicated that some adventitious $Ru(bpy)_3^{2+}$ photocatalyst maybe be trapped within the Au-Me film.[43,45]

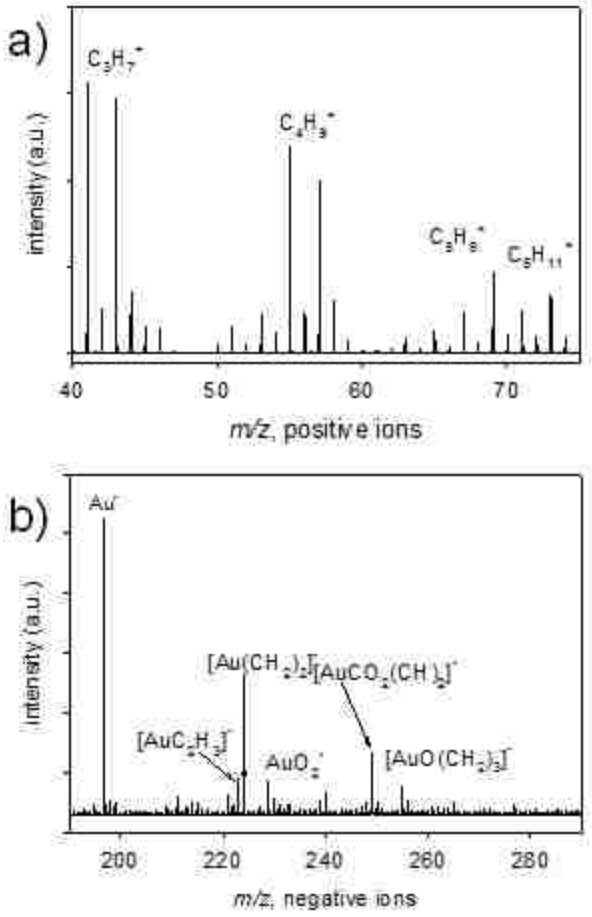

Figure 3.4 TOF SIMs Spectra Obtained for Au-Me Thin Film a) positive ion mass spectrum and b) negative ion mass spectrum.

The positive ion mass spectrum of the Au-Me film (Figure 3.4a) supports my assertion that the decyl-chains (*i.e.* $C_3H_7^+$, $C_4H_9^+$, $C_5H_{11}^+$) have been photografted onto the gold surface. Negative ion mass spectra of the Au-Me film indicate the formation of both Au-C and Au-O bonds (Figure 3.4b). Ions of the form $[Au(CH_2)_2]^-$ and $[Au(C_2H_3)]^-$ support our hypothesis that the reduction of Phth-Me **1** with $Ru(bpy)_3^{2+}$ and BNAH in the presence of an Au (111) substrate would form Au-C

bonds. Additionally, Au-O bonds were also observed in the form of $[AuO_2]^-$, $[Au\ CO_2(CH_2)]^-$, and $[AuO(C_2H_3)]^-$. These ions are indicative of Au-carboxylates.[45] Water contact angle measurement of 91° ± 4° was observed for the Au-Me thin film, demonstrating that the thin film was hydrophobic. The water contact angle obtained for the Au-Me film is smaller than that observed with decanethiol SAMs (109° ± 2°).[47] This suggests that the water droplet of the Au-Me film interact with the methylene-rich chains as opposed to interacting with the terminal methyl groups, as is customary with alkane thiol SAMs. It can also be inferred that the Au-Me film is disordered compared to the decanethiol SAM.

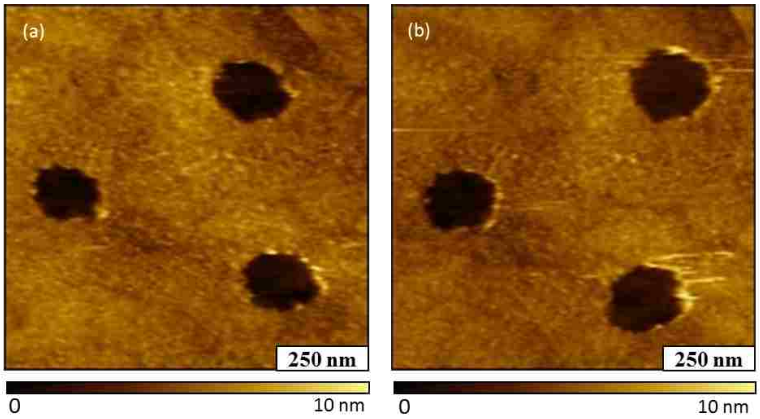

Figure 3.5 Attempted nanoshaving of photografted Au-Me film. (a) Topography image of nanopores within the film; (b) topography image acquired after nanoshaving; the film was not displaced.

The robustness of the Au-Me film was tested with increased force of the AFM tip. Three nanopores were investigated for this experiment. Figure 3.5a is the reference image of the three nanoholes before nanoshaving. The force of the AFM tip was increased to 10nN and applied to the region shown in Figure 3.5a. After 10 sweeps of the tip over the mentioned regions, the image in Figure 3.5b was acquired. There is no noteable displacement of Au-Me film. The nanopores maintained their orginial shape. Scratches of the Au-Me film were observed on areas near the nanopore. The inability of the AFM tip to remove the Au-Me film with increased force (10nN)

suggests the thin film is robust compared to thiol counterparts which are easily removed at these high forces.[36]

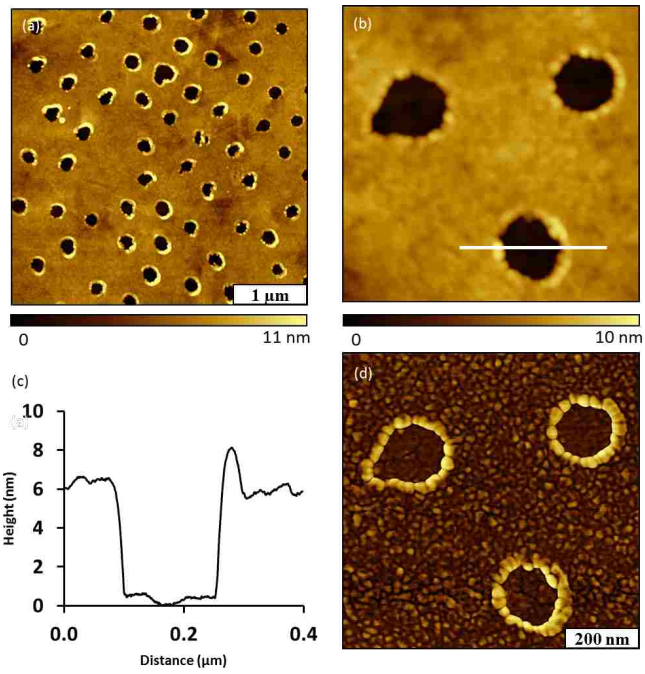

Figure 3.6 A photografted thin film of Au-NHBoc generated after 30 min irradiation of a solution of 10^{-1}M Phth-NHBoc **3**. Nanopores were produced using immersion particle lithography. (a) Topography of nanopores; (b) zoom-in topography view of nanopores; (c) cursor profile for the line in *b*; (d) corresponding phase image of *b*.

The organic thin film formed from the irradiation of Phth-NHBoc **3** (concentration = 0.1M) in the presence of $Ru(bpy)_3Cl_2$ and BNAH in MeCN with a masked Au(111) surface was examined next. After 30 minutes of irradiation, the mesosphere mask was removed with an ethanol and water wash followed by ultrasonication. Removal of the SiO_2 template yielded the thin film seen in Figure 3.6. Although there is clear evidence of the mesosphere mask, there are distinct defects in several areas. The hexagonal-packed arrangement is still more easily distinguishable in some regions. Figure 3.6B is a magnified view of three nanopores. The film is relatively smooth as evidenced by the cursor profile in Figure 3.6C. The initial thickness of the Au-NHBoc film was measured at approximately 6nm. The Au-NHBoc thin film provides a terminal end that, after

deprotection, can be further conjugated to amino acids, peptides, or other molecules of biological relevance. The IR spectrum of Au-NHBoc (Figure 3.7) displays characteristic C-H stretching, similar to what was previously observed with Au-Me. Frequencies at 2953, 2917, and 2847 cm^{-1} were easily identifiable as $-CH_3$ asymmetric, $-CH_2$ antisymmetric, and $-CH_2$ symmetric stretching, respectively. A characteristic carbamate carbonyl stretch was observed at 1696cm^{-1}. There is an unidentified carbonyl stretch observed at 1749cm^{-1}. This stretch does not directly correlate to the presence of unreacted Phth-NHBoc **3**, however, we posit that it could be phthalimide produced *in situ* trapped within the Au-NHBoc film. Additional unidentified stretches were seen under 1650cm^{-1}. An average water contact angle measurement of 93° ± 3° was observed, indicating that the Au-NHBoc film is hydrophobic. These results also suggest that the film is disordered compare to alkylthiol SAMs with a similar structure.[47]

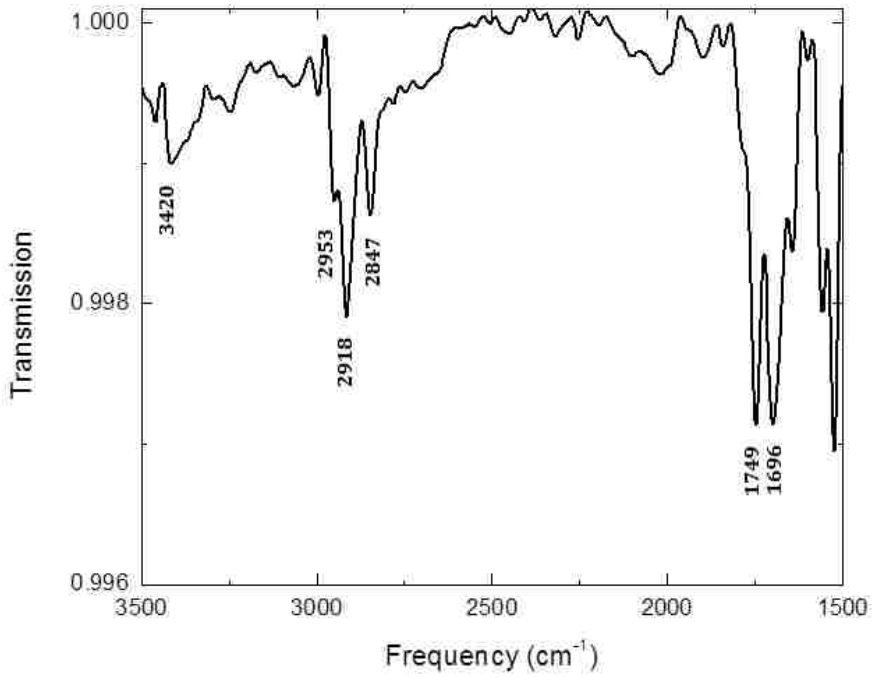

3.7 Grazing angle IRRAS Spectrum for Au-NHBoc

The robustness of the Au-NHBoc film was investigated after long term storage. The Au-NHBoc organic thin film was imaged using AFM (Figure 3.8) six months after it was prepared by

irradiation of the photocatalyst in the presence of Phth-NHBoc **3**. The hexagonal packed arrangement of the nanopores was still visible. However, the thickness of the Au-NHBoc film had drastically decreased from the orginial thickness of about 6nm to 2.5nm. Although layer decomposition was observed, the remaining film attached was highly robust.

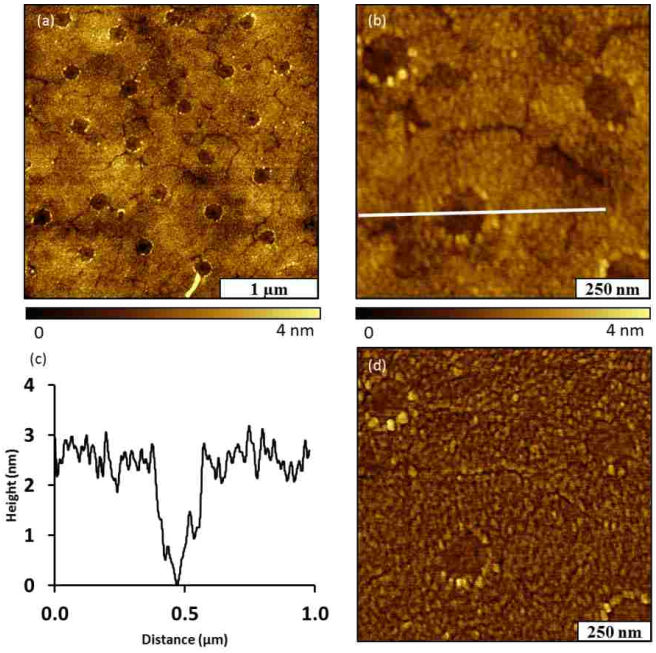

Figure 3.8 The photografted Au-NHBoc film after storage in ambient conditions for six months. (a) Topography image; (b) zoom-in view of nanopores; (c) cursor profile for the line in *b*; (d) corresponding phase image of *b*.

Imaging of the Au-OMEM organic thin film revealed patterning on the Au(111) surface with the Phth-OMEM **7** after 30 minutes of irradiation at 0.1M. The hexagonal packed arrangement of the silicon dioxide mask can be readily identified in Figure 3.9A. Triangular facets characteristic of the gold surface can be readily identified in the topographic image. The triangular features are a result of the orientation of Au(111) on the mica plate suggesting that the film was not very thick.[36] This was confirmed with thickness determination using cursor profiles. The dark brown nanohole in Figure 3.9B is a site of bare gold after the removal of the SiO_2 mask. The cursor profile of the single nanopore in Figure 3.9B if featured in Figure 3.9C. The surface is not as

uniform as seen with other photografted organic thin films. The average thickness of the organic thin is less than 1nm. Figure 3.9D is the phase image corresponding to the topography image in Figure 3.9B.

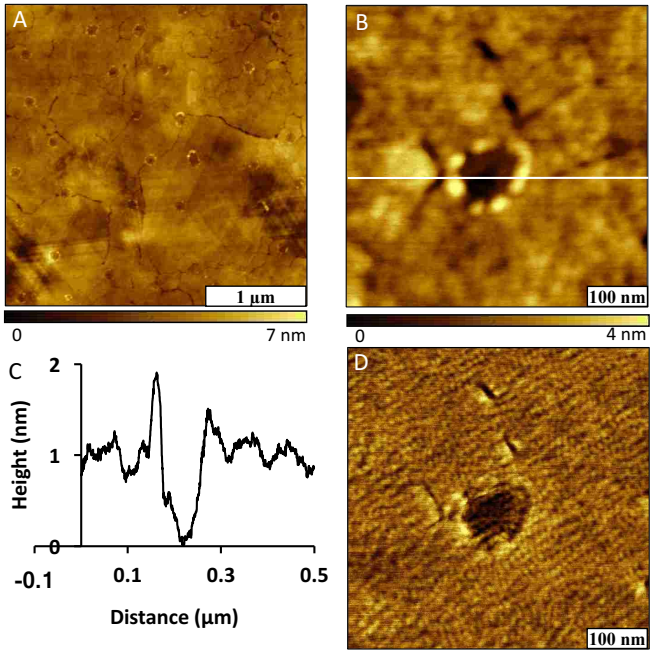

Figure 3.9 A photografted thin film of Au-OMEM generated after 30 min irradiation of 10^{-1}M Phth-OMEM **7**. Nanopores were produced using immersion particle lithography. (a) Topography of nanopores; (b) zoom-in topography view of nanopores; (c) cursor profile for the line in *b*; (d) corresponding phase image of *b*.

Characterization of the Au-OH organic thin film using AFM revealed patterning on the Au(111) surface with the Phth-OH **8** after 30 minutes of irradiation at 0.1M. Figure 3.10A illustrates the efficient hexagonal packing of the silicon dioxide mask. The surface of the photografted organic thin films appears uniform. Characteristic features of the gold surface could not be readily identified as previously seen with organic thin films with smaller thicknesses. A high-resolution image of a single nanopore can been seen in Figure 3.10B. Figure 3.10C features the cursor profile of the single nanopore in Figure 3.10B. The phase image corresponding to the single nanopore is shown in Figure 3.10D. The average thickness of the organic thin is approximately 6nm indicating multilayer formation.

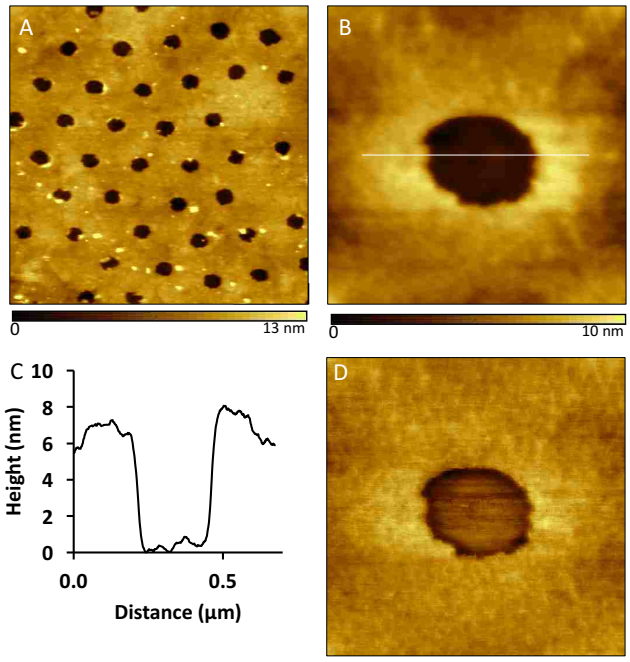

Figure 3.10 A photografted thin film of Au-OH generated after 30 min irradiation of 10^{-1}M Phth-OH **8**. Nanopores were produced using immersion particle lithography. (a) Topography of nanopores; (b) zoom-in topography view of nanopores; (c) cursor profile for the line in *b*; (d) corresponding phase image of *b*.

The Au-CCH organic thin film was characterized using AFM. Topographic images conformed patterning of the Au (111) surface with the Phth-CCH **12** after 30 minutes of irradiation at 0.1M. The hexagonal packing of the silicon dioxide mask is shown in Figure 3.11A. There are noticeable defects in the packing indicating that the packing and annealing of the mesospheres was not as efficient as seen with previous samples. However, the surface of the photografted Au-CCH film is fairly uniform. A high-resolution image of one nanopore is shown in Figure 3.11B. The cursor profile (Figure 3.11C) of the nanopore shows that the thin film around the pore has a thickness of about 6nm, supporting evidence for multilayer formation. Figure 3.11D is the phase image corresponding to the nanopore shown in Figure 3.11B. Characterization of the Au-CCH film with IRRAS did not reveal any alkyne stretches. This suggests that radicals were potentially adding onto alkynes present within the film.

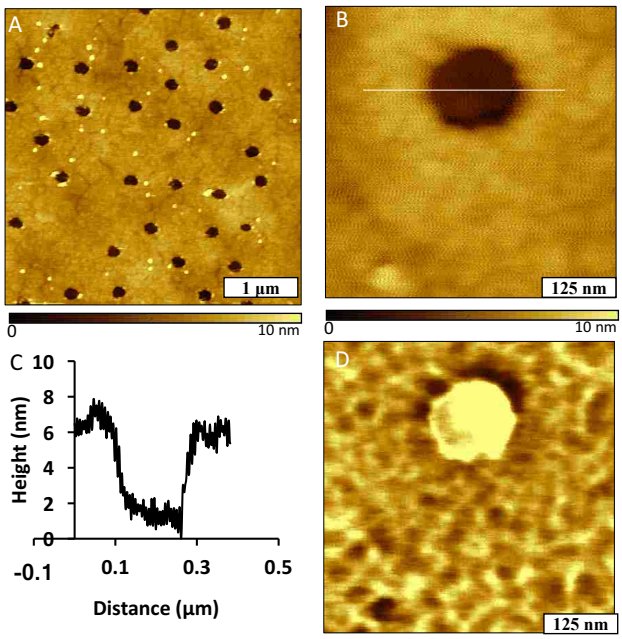

Figure 3.11 A photografted thin film of Au-CCH generated after 30 min irradiation of 10^{-1} M Phth-CCH **12**. Nanopores were produced using immersion particle lithography. (a) Topography of nanopores; (b) zoom-in topography view of nanopores; (c) cursor profile for the line in *b*; (d) corresponding phase image of *b*.

As previously expressed, we assert that these films are disordered and also have a thickness similar to or greater than the length of corresponding alkyl radicals in the all-anti conformation. This suggests that multilayers are formed in all cases (Au-Me, Au-NHBoc, Au-OMEM, Au-OH, and Au-CCH). A mechanism for such multilayer formation has been previously suggested,[48] and we elaborate on this with detailed mechanistic proposals (Schemes 3.8 - 3.10). The formation of Au-carboxylate bonds is less understood and requires further investigation. Schemes 3.8 - 3.10 should be treated as hypotheses of the possible radical reactions within the thin film. These proposals do not outline the exact mode of attachment of alkyl to Au or the frequency of gauche defects.

The initial attachment of a photochemically-generated alkyl radical (see Scheme 3.3) such as the decyl radical (from Phth-Me **1**) to an Au (111) surface will result in a disordered monolayer

represented by **13** and **14** (Scheme 3.8). Then, a decyl radical will abstract hydrogen **15**, likely from one of the secondary carbons of an already-grafted decyl chain to generate the surface-bound radical seen in **16**. Finally, the combination of the radical in **17** with another decyl radical will result in the formation of the branched hydrocarbon chain in **18**. The resulting branched alkyl chains could then undergo subsequent hydrogen abstractions and combinations of surface-bound radicals with decyl radicals from solution as a means for the formation of multilayers.

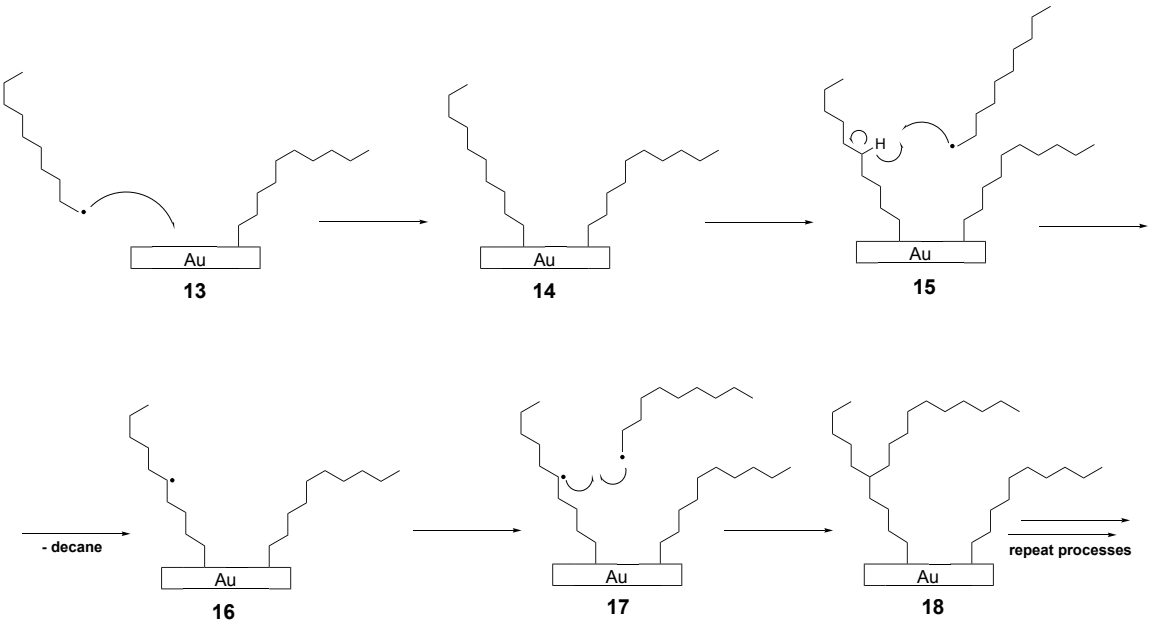

Scheme 3.8 Mechanistic Hypothesis for the Branching of Decyl-chains

Similarly, a decyl radical could abstract hydrogen from an already-grafted decyl chain to generate the radical seen in **16**. Another surface-bound decyl radical could then abstract a hydrogen from another decyl chain attached to the surface resulting in **19** (Scheme 3.9). Finally, the combination of the two secondary radicals in **19** would yield the cross-linked film **20**. The resulting alkyl chains could then undergo subsequent hydrogen abstractions and radical-radical combination as a means for the formation of cross-linked multilayers.

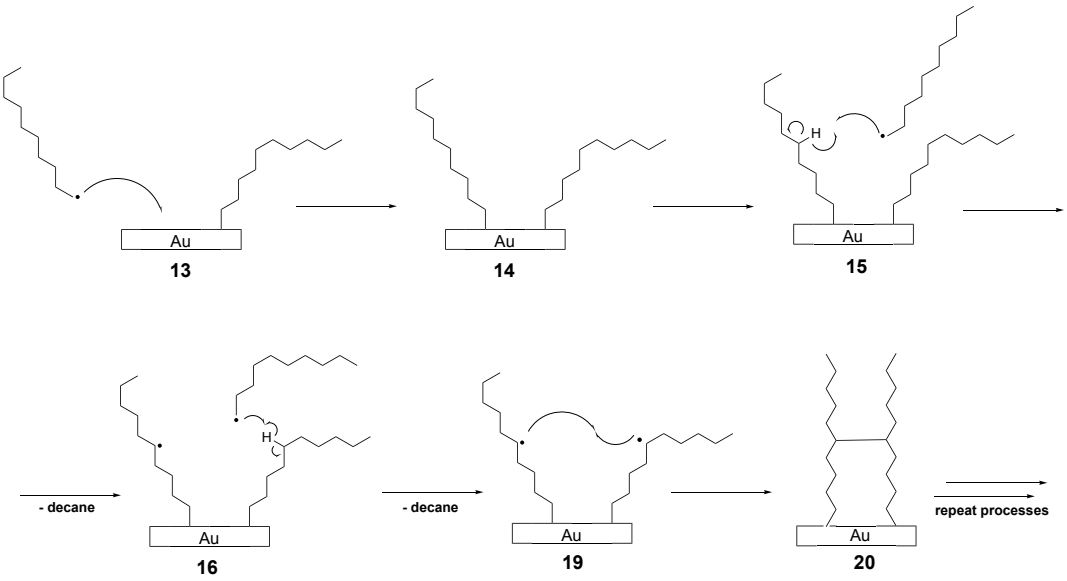

Scheme 3.9 Mechanistic Hypothesis for the Cross-linking of Decyl-chains

Alternatively, Scheme 3.10 illustrates a possible mechanism for the formation of alkenes. A decyl radical could abstract hydrogen from an already-grafted decyl chain to generate the radical seen in **16**. Another surface-bound decyl radical could then abstract a hydrogen from an adjacent carbon on the same decyl chain attached to the surface. Concomitant combination of the two secondary radicals results in the formation of alkene **21**. The resulting substituted alkyl chains

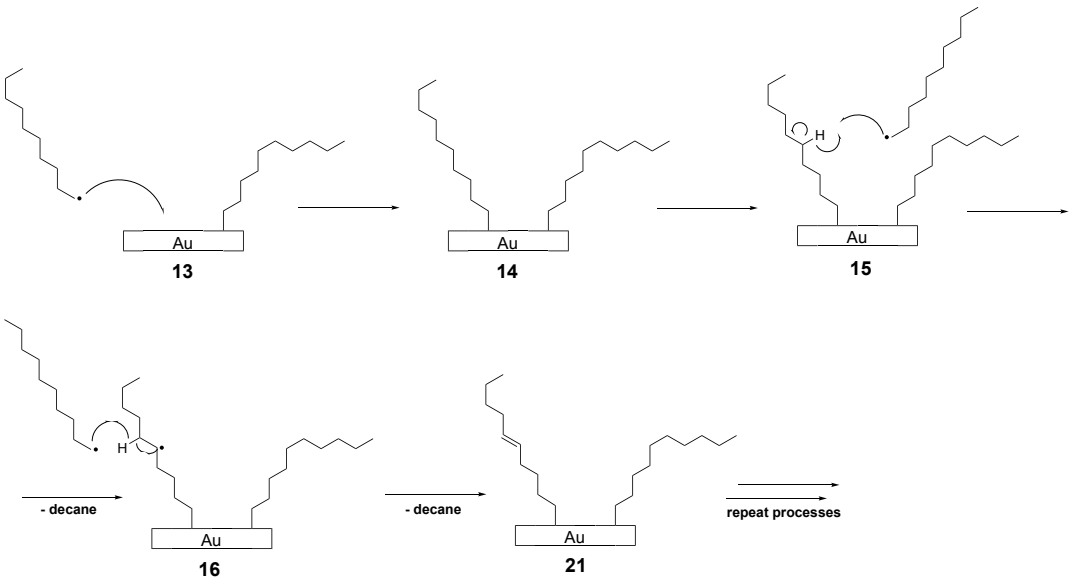

Scheme 3.10 Mechanistic Hypothesis for the Formation of Alkenes

could then undergo subsequent hydrogen abstractions and radical-radical combination as a means for the formation of substituted multilayers. Additionally, we acknowledge that a combination of these three processes is possible within the thin film generated by our proposed method of surface modification for the generation of alkyl radical-derived thin film.

3.5 Conclusion

In the work described herein, visible-light-photocatalytic reduction of phthalimide-ester-derived alkyl radicals was combined with particle lithography to generate alkyl thin films from the covalent attachment of alkyl radicals to Au(111). The use of visible-light photocatalysis for the reduction of phthalmide esters in the presence of $Ru(bpy)^{2+}$and BNAH was shown to be amenable to several functional groups (alkyl chains, carbamates, alcohols, and alkynes). The resulting nanostructured thin films were derived from Phth-CH_3, Phth-NHBoc, Phth-OMEM, Phth-OH, and Phth-CCH. Strong attachment of the alkyl films to Au substrate is likely to be dependent on Au-C and Au-O_2C bonds in addition to substitution, radical-radical recombination, and cross-linking between alkyl chains. The resulting alkyl thin films also proved to be disordered; this finding was supported by contact angle goniometry, IRRAS, and TOF SIMS. The generation of multilayers is likely a consequence of Au-attached alkyl groups that undergo a series of radical processes after initial attachment to the Au surface.

The film thicknesses were measured using AFM cursor profiles of the nanopores. A nanoshaving experiment using 10 nN of force showed that the Au-CH_3 organic thin film could not be easily removed with force. Although some degradation was observed after six months with the Au-NHBoc film, the remaining layers were still robust when reimaged using AFM. However, the Au-OH, Au-CCH, and Au-OMEM layers were not as robust as attempts at reimaging did not reveal patterned surfaces after three months.

3.6 Experimental and Tabulated Data

3.6.1 General Methods

Materials and Reagents. 11-aminoundecanoic acid (97%), *N*-hydroxyphthalimide (97%), *N, N'*-dicyclohexylcarbodiimide (99%), 4-(dimethylamino)pyridine (99%, Reagent Plus), di-*tert*-butyldicarbonate (99%, Reagent Plus), 4Å molecular sieves, ethanol (99.5%), 2-methoxyethoxymethyl chloride (technical grade), methyl 10-hydroxydecanoate (90%, technical grade) and $Ru(bpy)_3Cl_2$ (99.95%) were purchased from Sigma-Aldrich and used without further purification. Undecanoic acid (98%), 9-decyn-1-ol (94%), and 10-undecynoic acid (98%), and 1-benzyl-1,4-dihydronicotinamide (BNAH, 95%) were purchased from TCI and used without further purification. ^{1}H and ^{13}C NMR spectroscopy was performed on a Bruker AV-400 spectrometer. Glassware was flame-dried under vacuum and backfilled with dry nitrogen prior to use. Acetonitrile for grafting procedures was purified according to the method published by Pangborn *et al.*[37] Deuterated solvents were purchased from Cambridge Isotope Labs. The irradiation source for photografting reactions was two 4W sapphire blue LED flex strips from Creative Lighting Solutions (Cleveland, OH, USA) wrapped around a crystallizing dish.

Preparation of Gold Surfaces with a Mesosphere Mask. Template-stripped gold substrates were prepared by a previously reported procedure. Glass discs were glued to freshly prepared gold films using an epoxy (EPO-TEK, Billerica, MA).[46] The glass discs were stripped from mica to expose a clean, atomically flat Au(111) surface. Size-sorted silica mesospheres with an average diameter of 500 nm (Thermo Scientific) were cleaned by centrifugation and suspension in water (three cleaning cycles). A 10 μL drop of the silica mesosphere suspension was placed on to the template-stripped gold substrates, dried in air for 2 h, and then oven-dried for at least 96 h. The final heating step was used to temporarily anneal the silica spheres to the substrate to prevent

displacement during immersion in solutions. After completion of the photografting procedures, removal of the surface mask was accomplished by sonication in ethanol.

Photografting Procedure for Preparation of Samples for AFM Analysis. Acetonitrile (MeCN) from a solvent purification system was dried over 4 Å molecular sieves for at least 24 h. Phthalimide ester (0.2 mmol), BNAH (0.2 mmol), and $Ru(bpy)_3Cl_2$ (0.0056 mmol) were added to a 50 mL Erlenmeyer flask charged with a stir bar. The Au(111) substrate with mesospheres (*vide supra*) was then added. The flask was then sealed with a rubber septum and a dry N_2 line was introduced. MeCN (2 mL) was added and the reaction mixture was stirred until only the $Ru(bpy)_3Cl_2$ remained undissolved ($Ru(bpy)_3Cl_2$ remained undissolved until irradiation). Stirring was performed carefully so as to avoid contact between the Au(111) substrate and the stirbar. The reaction mixture was then irradiated with blue LEDs for 30 minutes (see SI for photo). Upon completion of irradiation, the reaction mixture was decanted. The Au(111) substrate was washed twice with 2 mL deionized water and twice with 2 mL 99.5% ethanol. The substrate was then ultrasonicated for 2 minutes in 99.5% ethanol followed by ultrasonication for 2 minutes in deionized water before imaging. These samples were also analyzed with XPS and TOF SIMS.

Photografting Procedure for Preparation of Samples for PM-IRRAS and Contact Angle Goniometry. Polycrystalline 100 nm Au-film-coated glass slides obtained from Platypus Technologies (catalog number Au.1000.SL1) were cut into sections of approximately 1x1 inch and cleaned using UV/ozone for 24 hours. To a 125 mL Erlenmeyer flask charged with a stirbar was added phthalimide ester (0.4 mmol), BNAH (0.4 mmol), and $Ru(bpy)_3Cl_2$ (0.0056 mmol). The freshly-cleaned Au film-coated glass was then added. The flask was then sealed with a rubber septum and a dry N_2 line was introduced. MeCN (4 mL) was added and the reaction mixture was stirred until only the $Ru(bpy)_3Cl_2$ remained undissolved (*vide supra*). Stirring was performed

carefully so as to avoid contact between the Au substrate and the stirbar. The reaction mixture was then irradiated with blue LEDs for 3 hours (see SI for photo). After irradiation, the reaction mixture was decanted. The Au substrate was washed with 10 mL deionized water and 10 mL of 99.5% ethanol before analysis.

Atomic Force Microscopy (AFM). Model 5500 and 5420 scanning probe microscopes (Keysight Technologies, Santa Rosa, CA) were used to characterize samples. Images were collected with Pico View v 1.12 software. Tips with an average spring constant of 40 N/m (Budget Sensors, Innovative Solutions Bulgaria Ltd.) were used to acquire topography and corresponding phase images with tapping mode. Nanoshaving experiments were conducted using a liquid cell containing ethanolic solution. Contact mode in liquid was used for nanoshaving using tips with an average spring constant of 0.6 N/m (Bruker Instruments, Camarillo, CA, USA). Digital images were processed with Gwyddion (v 2.30) software.

Polarization Modulation Infrared Reflectance Absorbance Spectroscopy (PM-IRRAS). PM-IRRAS spectra were recorded using a Bruker Tensor 27 instrument equipped with a liquid N_2-cooled MCT probe and an 80 Spec polarization modulation attachment from Pike Technologies. For each sample, 2056 scans were accumulated with a spectral resolution of 4 cm^{-1}. Before recording each spectrum, a freshly-cleaned, Au-film-coated glass slide (*vide supra*) was recorded as background.

Contact Angle Goniometry (Water Contact Angles). Water contact angles were measured with a VCA Optima instrument (AST Products, Inc.). Two μL of deionized water were deposited on the top of each sample in the horizontal position. At least six measurements were calculated for each sample using VCA Optima software.

X-Ray Photoelectron Spectroscopy (XPS). Photoelectron spectra were obtained using a PHI 5000 VersaProbe Scanning ESCA Microprobe (Physical Electronics, Chanhassen, MN) and a Perkin Elmer 5000 ESCA system each equipped with a monochromatic Al Kα X-ray source (E_p = 1486.7 eV). Typically, the pressures of the chambers were <7 x 10^{-10} mbar during analysis. The XPS spectra were measured with a pass energy of 23.5 eV and energy step 0.125 eV, and collected at 45 ^{o} to the normal of the sample surface. The binding energies (E_B) were calibrated using the Au $4f_{7/2}$ photoelectron peak (E_B = 84.00 eV).

Time-of-Flight Secondary Ion Mass Spectrometry (TOF SIMS). Time-of-flight secondary ion mass spectra were measured using an ION TOF IV spectrometer (ION TOF Inc., Chestnut Hill, NY) equipped with a Bi liquid metal ion gun. Briefly, the spectrometer consists of three vacuum chambers each separated by a gate valve. Samples are introduced via a loadlock. The preparation and analysis chambers are maintained at ≤7 x 10^{-9} mbar. The primary Bi^+ ions had a kinetic energy of 25 keV, were contained within a ~100 nm diameter probe beam, and were rastered over a (100 × 100) μm^2 area. All spectra were obtained in the static regime using a total ion dose of less than 10^{10} ions cm^{-2}. The secondary ions were extracted into a time-of-flight mass spectrometer using a potential of 2kV and reaccelerated to a kinetic energy of 10 keV before arriving at the detector. At least three areas were examined for each

3.6.2 Procedures and Characterization

Synthesis of undecanoic phthalimide ester:

1

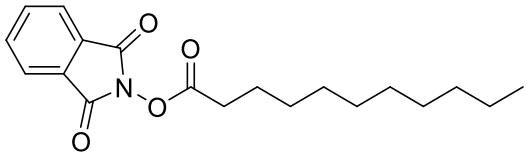

This compound was prepared according to a reported procedure with another carboxylic acid .[21] To a 25°C solution of undecanoic acid (2.00g, 10.7mmol) in THF (40mL) was added *N*-hydroxyphthalimide (2.98g, 18.3 mmol), 4-dimethylaminopyridine (0.0656g, 0.537 mmol), and *N,N'*-dicyclohexylcarbodiimide (3.32 g, 16.1mmol) in succession. After the addition of *N,N'*-dicyclohexylcarbodiimide, the reaction vessel was sealed and a nitrogen line was added. The reaction was magnetically stirred at 25°C and monitored by TLC until completion. Upon completion, the reaction was filtered using a Buchner funnel. The filter cake was washed with 30mL CH_2Cl_2. The filtrate was concentrated in vacuo. Column chromatography using 10% ethyl acetate/hexane afforded 2.54g (71%) of a white solid. ^{1}H NMR (400MHz, $CDCl_3$): δ 7.88 (dd, 2H, *J*=3.0Hz), 7.78 (dd, 2H, *J*=2.4Hz), 2.66 (t, 2H, *J*=7.5), 1.78 (m, 2H, *J*=7.4Hz), 1.44 (m, 2H, *J*=5.1Hz), 1.27 (m, 12H), 0.87 (t, 3H, *J*=6.7Hz); ^{13}C NMR (100MHz, $CDCl_3$): δ 169.9, 162.2, 134.9, 129.2, 124.2, 32.1, 31.2, 29.7, 29.6, 29.5, 29.3, 29.0, 24.9, 22.9, 14.3; HRMS m/z calculated for $C_{19}H_{25}NO_4Na$ $(M+Na)^+$ 354.1676, found 354.1686.

Synthesis of 9-decynoic acid:

10

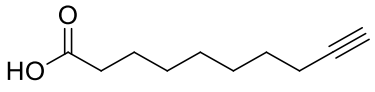

A solution of 9-decyn-1-ol (0.89mL, 5.0mmol) in 15mL of acetone was cooled to 0°C in an ice-water bath under nitrogen. Jones reagent (2.7mL, 2.7M) was added dropwise over the course of 20 minutes at 0°C. The reaction was allowed to stir at 0°C for an additional 2 hours. Upon completion, the stir bar was removed and the reaction mixture was concentrated in vacuo. The reaction mixture was extracted with 2 x 25mL of THF. The organic layer was washed with brine,

dried over Na_2SO_4, filtered, and concentrated in vacuo. Column chromatography resulted in the isolation of 0.5235g (62%) of a colorless oil. ^{1}H NMR (400MHz, $CDCl_3$): δ 12.00 (s, 1H), 2.35 (t, 2H, *J*=7.16Hz), 2.17 (m, 2H),1.95 (s, 1H) 1.62 (t, 2H, *J*=6.2Hz), 1.50 (m, 2H, *J*=6.8Hz), 1.40 (m, 2H), 1.38 (m, 4H). Spectral data match literature. [40]

Synthesis of 11-tertbutylcarbamate undecanoic acid:

2

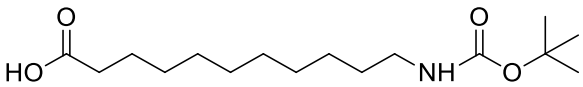

This compound was prepared according to a procedure similar to that reported in Reference 41. To a suspension of 11-aminoundecanoic acid (1.00 g, 5.0 mmol) in a solution (10.6 mL) of $NaHCO_3$ at half saturation was added sodium carbonate (0.530 g, 5.0 mmol). The resulting suspension was cooled to 0^{o}C in an ice-water bath. A solution of di-*tert*-butyldicarbonate (1.31g, 6.0 mmol) in 1,4-dioxane (4.2 mL) was prepared and added to the suspension all at once. The reaction mixture was allowed to warm to room temperature and stirred overnight. Upon completion, the stir bar was removed and the reaction mixture was concentrated in vacuo to remove 1,4-dioxane before being washed with Et_2O (2x25mL) to remove excess di-*tert*-butyldicarbonate. The aqueous layer was treated with cold 1M HCl dropwise until pH =2. Saturated NaCl (20mL) was added to the aqueous layer which was then extracted with 6 x15mL of EtOAC. The combined organic layers were dried over $MgSO_4$, filtered, and concentrated. Column chromatography using 30% ethyl acetate/hexane resulted in the isolation of 1.47g (98%) of a white solid. The ^{1}H NMR of this compound was consistent with a previous report.[3] ^{1}H NMR (400MHz, $CDCl_3$): δ 4.52 (bs,

1H), 3.10 (m, 2H), 2.34 (t, 2H, *J*=7.4 Hz), 1.62 (m, 2H), 1.52 (s, 2H), 1.44 (s, 9H), 1.27 (s, 12H). Spectral data matched literature. [42]

Synthesis of of *N-tert*-butoxycarbonylamino undecanoic phthalimide ester:

3

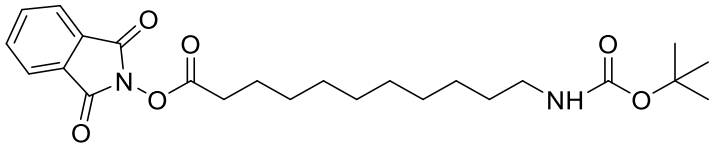

This compound was prepared according to the method used for the synthesis of undecanoic acid phthalimide (Phth-Me) ester starting instead with *N-tert*-butoxycarbonyl-11-aminoundecanoic acid (0.682 g, 2.26mmol). Column chromatography (20% EtOAc/Hexanes) resulted in the isolation of 0.911 g (90%) of a white solid. ^{1}H NMR (500 MHz, $CDCl_3$): δ 7.88 (dd, *J* = 5.4, 3.1 Hz, 1H), 7.79 (dd, *J* = 5.5, 3.1 Hz, 1H), 4.50 (s, 1H), 3.11 (m, 2H), 2.66 (t, 2H, *J*=7.5Hz), 1.78 (p, *J* = 7.5 Hz, 1H), 1.56 (m, 2H), 1.44 (m, 12H), 1.29 (s, 9H); ^{13}C NMR (125 MHz, $CDCl_3$): δ 169.9, 162.2, 134.9, 129.2, 124.2,79.2, 40.9, 31.2 30.3, 29.6, 29.5 29.4, 29.3, 29.0, 28.9, 28.7, 27.0, 24.9; HRMS m/z calculated for $C_{24}H_{34}O_6N_2Na$ $(M+Na)^+$ 469.2309, found 469.2318.

Synthesis of methyl 10-((2-methoxyethoxy)methoxy)decanoate:

5

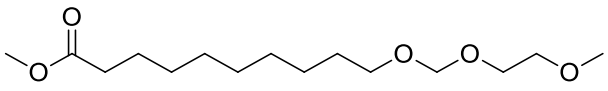

To a stirred solution of methyl 10-hydroxydecanoate (2.00mL, 9.89mmol) in CH_2Cl_2 (2mL) was added diispropylethylamine (2.60mL, 14.8mmol) was added and allowed to stir. 2-methoxyethoxymethyl chloride (1.70mL, 14.8mmol) was added to the reaction mixture. After 30

minutes, the reaction was no longer able to stir due to precipitation. An additional 4mL of CH_2Cl_2 was added to the reaction which was allowed to stir overnight. The reaction was quenched with 15mL of aqueous $NaHCO_3$ and extracted with CH_2Cl_2 (3x 20mL). The combined organic layers were washed with 20mL H_2O, 20mL brine, dried over $MgSO_4$, filtered, and concentrated in vacuo. Column chromatography resulted in the isolation of 2.00g (70%) of a yellow oil. ^{1}H NMR (500MHz, $CDCl_3$): δ 4.70 (s, 2H), 3.68 (d, 2H, *J*=4.4Hz), 3.66 (s, 3H), 3.56-3.51 (m, 4H), 3.39 (s, 3H), 2.30 (t, 2H, *J*=7.5Hz), 1.62-1.53 (m, 4H),1.28 (m,10H); ^{13}C NMR (125MHz, $CDCl_3$): δ 174.5, 95.7, 72.0, 68.1, 66.9, 59.2, 51.6, 34.3, 29.9, 29.6, 29.4, 29.3, 26.4, 25.1; HRMS m/z calculated for $C_{15}H_{30}O_5Na$ $(M+Na)^+$ 313.1985, found 313.1980.

Synthesis of 10-((2-methoxyethoxy)methoxy)decanoic acid:

6

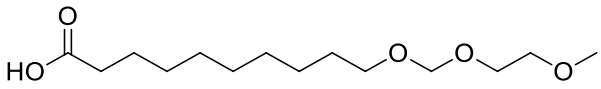

A solution of methyl 10-((2-methoxyethoxy)methoxy)decanoate (2.00g, 6.89mmol) in 3mL MeOH was cooled to 0ºC in an ice-water bath. An aqueous solution of 2N NaOH (20mL) was added and the reaction was allowed to stir for an additional 10 minutes at 0ºC before being removed from the ice-bath. The resulting mixture was stirred for 4h at room temperature until complete via TLC analysis. The reaction mixture was poured into 10mL of 2N HCl that had been previously cooled to 0ºC. Column chromatography resulted in the isolation of 1.73g (91%). ^{1}H NMR (500MHz, $CDCl_3$): δ 4.72 (s, 2H), 3.70 (dd, 2H, *J*=4.4Hz), 3.58 (dd, 2H, *J*=3.0Hz), 3.54(t, 2H, *J*=6.7Hz), 3.40 (s, 3H), 2.34 (t, 2H, *J*=7.5Hz), 1.63 (m, 2H, *J*=7.1Hz), 1.58 (m, 2H, *J*=7.6Hz),1.30

(m, 10H); ^{13}C NMR (125MHz, $CDCl_3$): δ 179.8, 95.6, 72.0, 68.1, 66.8, 59.2, 53.6, 34.2, 29.8, 29.5, 29.3, 29.2, 26.3, 24.8; HRMS m/z calculated for $C_{14}H_{29}O_5$ $(M+H)^+$ 277.201, found 277.2002.

Synthesis of 10-((2-methoxyethoxy)methoxy)decanoic phthalimide ester:

7

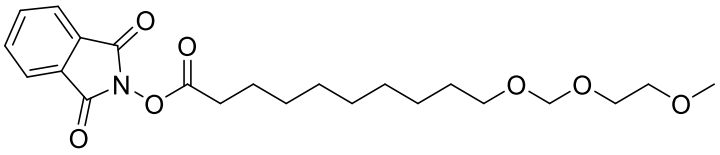

Prepared according to the method used in the synthesis of undecanoic phthalimide ester starting from 10-((2-methoxyethoxy)methoxy)decanoic acid (1.5078g, 5.46mmol).[21] Column chromatography resulted in the isolation of 2.07g (90%). ^{1}H NMR (500MHz, $CDCl_3$): δ 7.89 (dd, 2H, *J*=1.8Hz), 7.79 (dd, 2H, *J*=1.1Hz), 4.71 (s, 2H), 3.69 (t, 2H, *J*=3.6Hz), 3.56 (m, 4H), 3.40 (s, 3H), 2.66 (t, 2H, *J*=7.4Hz) 1.78 (m, 2H, *J*=7.5Hz), 1.59 (m, 2H, *J*=6.6Hz)), 1.44 (m, 2H), 1.33 (m, 8H); ^{13}C NMR (125MHz, $CDCl_3$): δ 169.8, 162.2, 134.9, 129.2, 124.2, 95.7, 72.1, 68.2, 66.9, 59.2, 31.2, 29.9,29.54, 29.51, 29.3, 29.0, 26.4, 24.9; HRMS m/z calculated for $C_{22}H_{31}NO_7Na$ $(M+Na)^+$ 444.1993, found 444.2003.

Synthesis of 10-hydroxydecanoic phthalimide ester:

8

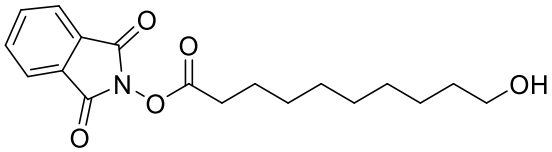

A 1:1 solution of trifluoroacetic acid (3.90mL, 50.8mmol) in CH_2Cl_2 (3.90mL) was added to 10-((2-methoxyethoxy)methoxy)decanoic phthalimide ester (1.07g, 2.54mmol) and allowed to stir

until completion. The reaction mixture was poured into a saturated solution of $NaHCO_3$ (20mL) at room temperature and extracted with Et_2O (3 x 20mL). The organic layer was washed with H_2O (20mL), brine (20mL), dried over Na_2SO_4, filtered, and concentrated in vacuo. Column chromatography resulted in the isolation of 0.7305g (86%). ^{1}H NMR (400MHz, $CDCl_3$): δ 7.89 (dd, 2H, *J*=3.1Hz), 7.79 (dd, 2H, *J*=3.0Hz), 4.35 (t, 2H, *J*=6.7Hz), 2.74 (m, 1H) 2.66 (t, 2H, *J*=7.4Hz) 1.77 (m, 4H), 1.35-1.47 (m, 10H); ^{13}C NMR (125MHz, CD_3CN): δ 169.8, 162.2, 135.0, 129.2, 124.2, 68.5, 31.2, 29.3, 29.2, 29.1, 28.9, 28.3, 25.7, 24.8; HRMS m/z calculated for $C_{18}H_{24}NO_5$ $(M+H)^+$ 334.1649, found 334.1660.

Synthesis of 9-decynoic phthalimide ester:

11

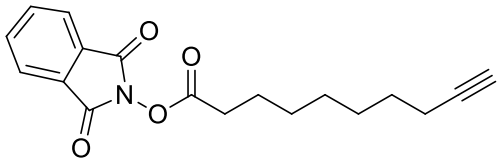

Prepared according to the method used in the synthesis of undecanoic phthalimide ester from 9-decynoic acid (0.2230g, 1.32mmol).[21] Column chromatography resulted in the isolation of 0.2940g (71%) of a white solid. ^{1}H NMR (500MHz, $CDCl_3$): δ 7.88 (dd, 2H, J=2.00Hz), 7.79 (dd, 2H), 2.67 (t, 2H, J=7.24Hz), 2.19 (t, 2H), 1.93 (s, 1H), 1.80 (p, 2H, J=7.00Hz), 1.54 (p, 2H, J=7.12Hz), 1.45 (m, 4H), 1.37 (m, 2H); ^{13}C NMR (125MHz, $CDCl_3$): δ 169.8, 162.2, 134.9, 129.2, 124.2, 84.8, 68.4, 32.1, 28.9, 28.8, 28.6, 28.5, 24.8, 18.6; HRMS m/z calculated for $C_{18}H_{20}NO_4$ $(M+H)^+$ 314.1387, found 314.1395.

Synthesis of 10-undecynoic phthalimide ester:

12

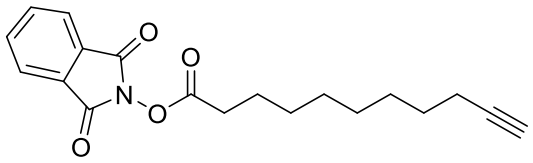

Prepared according to the method used in the synthesis of undecanoic phthalimide ester starting from commercially available 10-undecynoic acid (0.9313g, 5.11mmol).[21] Column chromatography resulted in the isolation of 1.591g (95%) of a white solid. ^{1}H NMR (500MHz, $CDCl_3$): δ 7.88 (dd, 2H, *J*=2.4Hz), 7.79 (dd, 2H, *J*=2.4Hz), 2.67 (t, 2H, *J*=7.5Hz), 2.19 (dt, 2H), 1.93 (s, 1H), 1.79 (m, 2H, *J*=7.6Hz), 1.54 (m, 2H, *J*=7.8Hz), 1.45 (m, 4H), 1.34 (m, 4H); ^{13}C NMR (125MHz, $CDCl_3$): δ 169.8, 162.2, 134.9, 129.2, 124.2, 84.9, 68.3, 31.2, 29.1, 29.0, 28.9, 28.8, 28.6, 24.8, 18.6; HRMS m/z calculated for $C_{19}H_{22}NO_4$ $(M+H)^+$ 328.1543, found 328.1539.

3.7 References

1. Belanger, D.; Pinson, J., *Chem. Soc. Rev.*, **2011**, *40*, 3995-4048.
2. Vase, K., *Novel Approaches for Electrochemically assisted Covalent Modification of Carbon Surfaces*, PhD Thesis, University of Aarhus, DK, **2007**.
3. Kosynkin, D.; Bockman, T. M.; Kochi, J. K., *J. Am. Chem.* Soc., **1997**, *119*, 4846.
4. Bouriga, M.; Chehimi, M. M.; Combellas, C.; Decorse, P.; Kanoufi, F.; Deronzier, A.; Pinson, J. *Chem. Mater.,* **2013**, *25*, 90-97.
5. Andrieux, C. P.; Gonzalez, F., Saveant, J.-M.; *J. Am. Chem. Soc.,* **1997**, *119*, 4292.
6. Andrieux, C. P.; Gallardo, I., Saveant, J.-M.; Su, K.-B., *J. Am.Chem. Soc.,* **1986,** *108,* 2628.

7. Brooksby, P. A.; Downard, A. J.; Yu, S. S. C., *Langmuir,* **2005**, *21*, 11304.

8. Wayner, D. D. M.; McPhee, D. J; Griller, D., *J. Am. Chem Soc*., **1988**, *110*, 132.

9. Kolbe, H.; Liebigs, J., *Ann. Chem*., **1849**, *69*, 257.

10. A. Wurtz, *Ann., Chim. Phys*., **1855**, *44*, 291.

11. Gros-Jean, M.; Herino, R.; Chazalviel, J.-N and Ozanam, F.; *Mater. Sci. Eng., B*, **2000**, *69*, 77.

12. Fidelis, A.; Ozanamand, F.; Chazalviel, J.-N*., Surf. Sci*., **2000**, *444*, L7.

13. Fellah, S.; Teyssot, A.; Ozanam, F; Chazalviel, J.-N.; Vigneron, J.; Etcheberry, A., *Langmuir*, **2002**, *18*, 5851.

14. Fellah, S.; Teyssot, A.; Chazalviel, J.-N.; Vigneron, J.; Etcheberry, A.; Stchakovsky, M., *J. Phys. Chem. B*, **2006,** *110*, 1665.

15. Fellah, S.; Amiar, A.; Ozanam, F.; Chazalviel, J.-N.; Vigneron, J.; Etcheberry, A.; Stchakovsky, M., *J. Phys. Chem. B*, **2007**, *111*, 1310.

16. Okada, K.; Okamoto, K.; Oda, M., *J. Am. Chem. Soc*., **1988**, *110*, 8736–8738.

17. Okada, K.; Okamoto, K.; Oda, M., *J. Chem. Soc., Chem. Commun.,* **1989**, 1636–1637.

18. Okada, K.; Okamoto, K.; Morita, N.; Okubo, K.; Oda, M., *J. Am. Chem. Soc*., **1991**, *113*, 9401– 9402.

19. Okada, K.; Okubo, K.; Morita, N.; Oda, M., *Tetrahedron Lett.,* **1992**, *33*, 7377–7380.

20. Okada, K.; Okubo, K.; Morita, N.; Oda, M., *Chem. Lett*., **1993**, *22*, 2021–2024.

21. Schnermann, M. J.; Overman, L. E., *Angew. Chem., Int. Ed.,* **2012**, *51*, 9576–9580.

22. Pratsch, G.; Lackner, G. L.; Overman, L. E., *J. Org. Chem.*, **2015**, *80*, 6025–6036.

23. Li, P.; Evans, C. D.; Wu, Y.; Cao, B.; Hamel, E.; Joullie, M. M., *J. Am. Chem. Soc.*, **2008**, *130*, 2351–2364.

24. Basel, Y.; Hassner, A., *Tetrahedron Lett.,* **2002**, *43*, 2529-2533.

25. Shendage, D.M.; Froehlich, R.; Haufe, G., *Org. Lett.*, **2004**, *6*, 3675.

26. Corey, E.J.; Gras, J.-L.; Ulrich, P., *Tetrahedron Lett.*, **1976**, *17*, 809.

27. Ohba, Y.; Takatsuji, M.; Nakahara, K.; Fujioka, H.; Kita, Y., *Chem. Eur. J.*, **2009**, *15*, 3526-353.

28. Quindon, Y.; Morton, H.E.; Yoakim, C., *Tetrahedron Lett.*, **1983**, *24*, 3969.

29. Prier, C. K.; Rankic, D. A.; MacMillan, D. W. C**.,** *Chem. Rev.*, **2013**, *113*, 5322–5363.

30. Harding, K. E.; May, L. M.; Dick, K. F., *J. Org. Chem.*, **1975**, *40*, 1664-1665.

31. Smentkowski, V. S.; Yates Jr., J. T., *Science,* **1996**, *271*, 193.

32. Yang, L.; Lua, Y.-Y.; Lee, M. V.; Lindford, M. R., *Acc. Chem. Res.*, **2005**, *38*, 933.

33. Love, J.C.; Estroff, L.A.; Kriebel, J.K.; Nuzzo, R.G.; Whitesides, G.M., *Chem. Rev.,* **2005**, *105*, 1103-1169.

34. Laibinis, P.E.; Whitesides, G.M.; Allara, D.L.; Tao, Y.-T.; Parikh, A.N.; Nuzzo, R.G., *J. Am. Chem. Soc.,* **1991**, *113*, 7152-7167.

35. Ozaki, Y.; Morita, S.; Hirano, Y., *Advanced Chemistry of Monolayers at Interfaces*, Imae, T., Ed. Elsevier, Ltd.: Amsterdam, **2007**, 309-359.

36. Verberne-Sutton, S. D.; Quarels, R. D.; Zhai, X.; Garno, J. C.; Ragains, J. R., *J. Am. Chem. Soc.,* **2014**, *136*, 14438-44.

37. Pangborn, A. B.; Giardello, M. A.; Grubbs, R. H.; Rosen, R. K.; Timmers, F. J., *Organometallics,* **1996**, *15*, 1518−1520.

38. Wagner, P.; Zaugg, F.; Kernen, P.; Hegner, M.; Semenza, G., *J. Vac. Sci. Technol. B,* **1996**, *14*, 1466−1471.

39. Nečas, D.; Klapetek, P., *Cen. Euro. J. Phys.,* **2011**, *10*, 181-188.

40. Theeramunkong, S.; Galli, U.; Grolla, A. A; Caldarelli, A.; Travelli, C.; Massarotti, A.; Troiani, M. P.; Alisi, M. A.; Orsomando, G.; Genazzani, A. A.; Tron, G. C., *Med. Chem. Comm.,* **2015**, *6*, 1891-1897.

41. Shendage, D.M.; Fröhlich, R.; Haufe, G., *Org. Lett.*, **2004**, *6*, 3675-3678.

42. Amara, N.; Mashiach, R.; Amar, D.; Krief, P.; Spieser, S.A.H.; Bottomley, M.J.; Aharoni, A.; Meijler, M.M. *J. Am. Chem. Soc.* **2009**, *131*, 10610–10619.

43. NIST X-ray Spectroscopy Database, Version 4.1; National Institute of Standards and Technology: Gaithersburg, MD, **2012**.

44. Hooper, A.; Fisher, G.L.; Konstadinidis, K.; Jung, D.; Nguyen, H.; Opila, R.; Collins, R.W.; Winograd, N.; Allara, D.L., *J. Am. Chem. Soc.* **1999**, *121*, 8052-8064.

45. Khan, M.M.T.; Srivastava, S., *Polyhedron*, **1988**, *7*, 1063.

46. Wagner, P.; Zaugg, F.; Kernen, P.; Hegner, M.; Semenza, G., *J. Vac. Sci. Technol. B* **1996**, *14*, 1466–1471.

47. Mendoza, S.M.; Arfaoui, I.; Zanarini, S.; Paolucci, F.; Rudolf, P., *Langmuir* **2007**, *23*, 582-588.

48. Chehimi, M.M.; Hallais, G.; Matrab, T.; Pinson, J.; Podvorica, F.I., *J. Phys. Chem. C* **2008**, *112*, 18559-18565.

CHAPTER 4: CARBOHYDRATE CHEMISTRY

4.1 Introduction to Oligosaccharides

The promise of sugar chemistry lies in its applications in physical organic chemistry, synthetic organic chemistry, biochemistry, and in the biological and medicinal sciences. Traditional methods for the synthesis of carbohydrates are taxing. Techniques to improve the stereoselectivity and efficiency of synthetic transformations using carbohydrates still need to be explored in order to mimic the complexity seen in nature. Oligosaccharide synthesis is especially important to the field of glycobiology, because of the importance of oligosaccharides as molecular recognition elements in biological processes (*e.g.* cell-cell recognition, cellular adhesion, and cellular transport).[1] Glycobiology is the study of the structure, function, and biological activity of carbohydrates.[1] The biological roles of glycoproteins, glycolipids, and proteoglycans is a growing area of interest.[2] Oligosaccharides have also found uses in the synthesis of vaccines and cancer research.[4,5] *O*-glycosidic compounds are the most abundant carbohydrates found in nature; however, the development of simple, efficient, and stereoselective methods for the synthesis of glycosidic linkages is a major challenge in carbohydrate and organic chemistry.

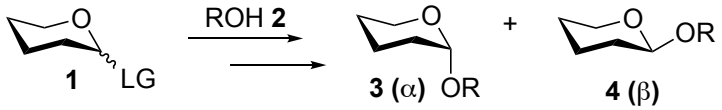

Scheme 4.1 Glycosidic Bond Formation

Glycosidic bonds, such as **3** and **4**, are formed when a nucleophile displaces a leaving group attached to the anomeric carbon (the carbon containing the leaving group) of a carbohydrate donor **1** (see Scheme 4.1). The glycosyl donor **1** is the electrophile that 'donates' the anomeric carbon, while the glycosyl acceptor is the nucleophile that attacks the anomeric carbon. If the nucleophile is a hydroxyl acceptor **2** (ROH) the process is termed *O*-glycosylation. The first glycoside syntheses were reported by Michael and Fischer.[6] Advances by Koenig and Knorr led to the

development of a large number of glycosylation methods.[7,8,9] Though glycosylation reactions play an important role in carbohydrate chemistry, the development of a widely applicable glycosylation method is still a significant synthetic challenge.

4.2 Mechanism of Glycosylation

The most common glycosylation is the formation of a single glycosidic bond between two monosaccharides. At least one of the monosaccharides must donate its anomeric carbon to form the new acetal linkage (such as **3** and **4** in Scheme 4.1). A new bond formed between an anomeric carbon (donor) and a hydroxyl group of a non-anomeric carbon (acceptor) generates a reducing disaccharide and can act as a reducing agent due to hemiacetal formation. While a glycosidic bond (an *O*-linkage) formed between two anomeric carbons generates a non-reducing disaccharide.[2] The configuration of the newly formed acetal bond can be *alpha* **3** or *beta* **4**. The mechanism of the glycosylation gives us important information about the reaction. Monosaccharides and oligosaccharides linked to non-carbohydrate containing molecules occurs frequently in nature. The non-carbohydrate containing moiety is called an aglycon, while the carbohydrate is referred to as the glycone.[2]

Issues with stereochemical control of the glycosidic bond occur as a result of the difficulties associated with obtaining S_N2 (Scheme 4.2) attack of an *O*-nucleophile at the anomeric carbon. Scheme 4.2 illustrates the two major pathways for formation of new glycosidic bonds. In the S_N2 pathway, the aglycon **X** on donor **5** is activated by a promotor **P+** to generate intermediate **6**. The activated aglycon **6** is then displaced via backside attack by a glycosyl acceptor (ROH). Removal of a proton by base yields a disaccharide with inversion of stereochemistry **7α**. Similarly, in the S_N1-type reaction pathway the aglycon **X** on donor **5a** is activated by a promoter **P+** to yield intermediate **6a**. The ring oxygen readily participates in the nucleophilic displacement of the

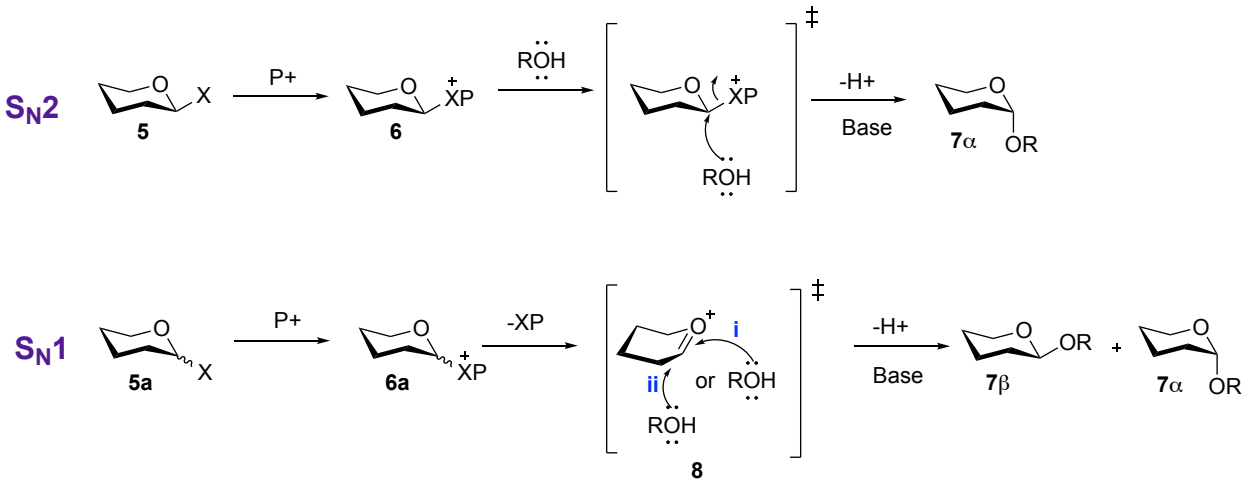

Scheme 4.2 Major Glycosylation Reaction Pathways

activated aglycon +**XP** to give oxocarbenium cation **8**. The oxocarbenium cation **8** can then be attacked from either face resulting in a mixture of anomers **7α** and **7β**. This phenomenon renders stereochemistry difficult to control, as the S_N1-type pathway generates the 1,2 trans-glycosidic linkage (**7β**) and the 1,2-cis-glycoside bond (**7α**).

4.2.1 Protecting Groups

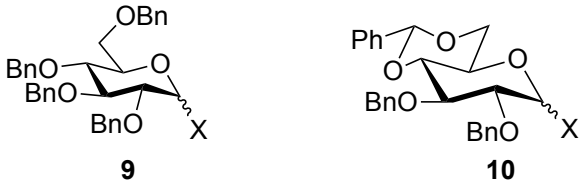

Scheme 4.3 Protecting Groups in Glycosylation Reactions

There are many phenomena that influence the selectivity of *O*-glycosylations. The use of protecting groups is one method employed by carbohydrate chemists. Protecting groups and strategies for protection are essential in carbohydrate chemistry. There are two basic types of protecting groups (Scheme 4.3) to consider, temporary protecting groups **10** and permanent protecting groups **9**. Permanent protecting groups **9** remain on the sugar until the end of the synthesis, while the temporary protecting groups **10** are liberated during synthetic modifications.

Removal of temporary protecting groups precedes glycosylation, *e.g.* release of a hydroxyl acceptor (ROH). Protecting groups are also used to control regioselectivity, increase reactivity, and influence stereochemistry. For example, it is well established that acylated donors are less reactive than benzylated donors.[10] This phenomenon will be discussed in more detail in section 4.4.

4.2.2 Anomeric Effect

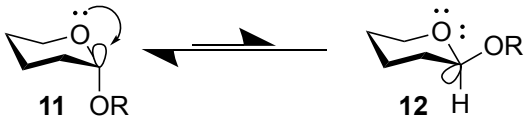

Scheme 4.4 Anomeric Effect

The anomeric effect (Scheme 4.4) or the Edward-Lemieux effect is the tendency of substituents adjacent to a heteroatom (oxygen, nitrogen, or sulfur) within a cyclohexane ring to be in an axial position **11** rather than the equatorial position **12**.[15] The axial anomer is stabilized by the ability of a lone pair from the heteroatom to donate directly into the antibonding orbital of the adjacent bond.[15] The hyperconjugation **11** between the lone pair on the ring oxygen in the ring and the sigma* orbital of the C-OR bond provide increased stability to the molecule due to electron delocalization. Substituents in the axial position **11** also confer a reduced molecular dipole moment for the system.[15] When the substituent is in the axial position, the dipoles associated with the C-OR and C-O_{ring} bonds oppose each other. Thus, substituents in the equatorial position **12** are not as stable.

4.2.3 Neighboring Group Participation and Directing Groups

The stereochemical outcome of *O*-glycosylation can also be affected by neighboring group participation. 1,2-*Trans*-glycosides can be diastereoselectively synthesized using neighboring group participation. This is most commonly achieved using *O*-acetyl, *O*-benzoyl, or *O*-pivaloyl

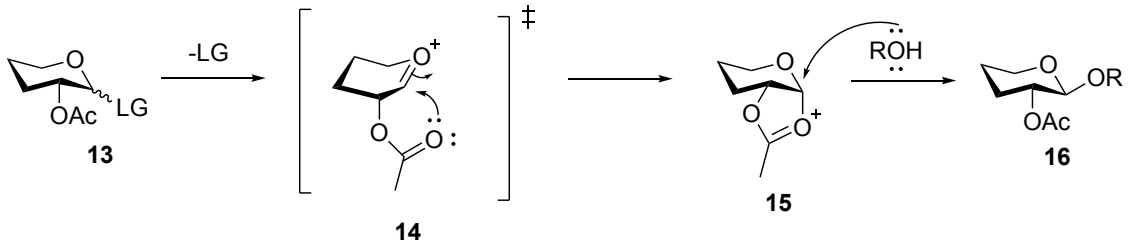

Scheme 4.5 Neighboring Group Participation

substituents at the C_2 position.[2] Such a substitution is an example of the use of protecting groups to direct the stereochemical outcome of *O*-glycosylation. Similar to the S_N1 mechanism, the oxocarbenium cation **14** is formed; however, the intermediate can be readily attacked by a lone pair of electrons from the ester carbonyl. This dioxolenium cation **15** is a critical intermediate in the formation of many 1,2-*trans*-glycosides.[2] This can be seen in Scheme 4.5. The efficient blocking of the bottom face directs nucleophilic attack to the top of the anomeric carbon by S_N2-like attack. The predominant product is the *beta* glycoside **16** (*trans*).

Additionally, neighboring group participation and directing group methods have been developed for the formation of 1,2-*cis*-glycosides (*alpha* selectivity). Auxiliaries can be used to control the effectively block the top face of the sugar either by neighboring group participation or by the use of a bdirecting group. Boons and Demchenko have been able to exploit the use of auxiliaries for diastereoselective control of glycosylation (see Scheme 4.6).[3,13,14]

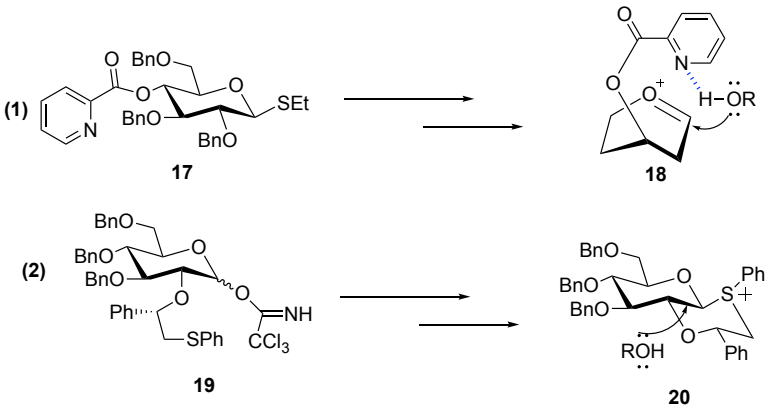

Scheme 4.6 Chiral Auxiliaries

Boons and coworkers used the preference of sulfur **19** at the anomeric carbon to attack in the beta position, effectively leaving the alpha position primed for nucleophilic attack **20**. [13] Similarly, Demchenko and coworkers have used picoloyl ethers and picolinyl esters **17** to hydrogen bond to the proton on the acceptor **18**, thus, directing the formation of the new glycoside bond.[3,14] The use of auxiliaries that can later be removed showcase the importance of protecting groups in oligosaccharide synthesis.

4.2.4 Solvent Effects

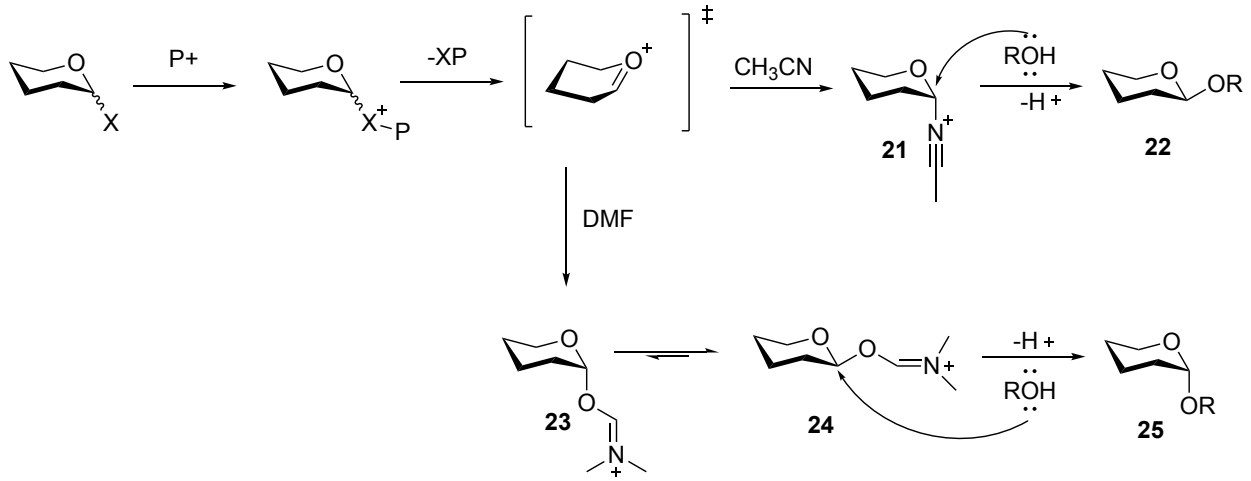

Scheme 4.7 The Influence of Solvents on *O*-Glycosylations

Solvents can play many roles in glycosylation reactions. The effect of solvents on glycosylations have been widely studied. In general, nonpolar solvents like dichloromethane, toluene, and dichloroethane are used for glycosylation as they do not participate in the glycosylation. Solvent participation has also been used to achieve stereoselective glycoside formation. Ethereal solvents like diethyl ether,[16] tetrahydrofuran,[16] and dioxane[17] drive the formation of α-glycosides via attack on the oxocarbenium cation. *N*,*N*-dimethylformamide (DMF) has also proven to be a useful solvent and cosolvent in the preparation of α-glycosidic linkages (Scheme 4.7).[18,19] DMF has a stereodirecting effect. Kinetic attack of DMF on the oxocarbenium

ion gives the alpha *O*-imidate **23**, however, equilibration gives the more stable beta *O*-imidate **24** resulting in *alpha* selectivity **25** by backside displacement. The use of acetonitrile [20,21] as a solvent has been shown to form β-glycosides **22** linkages selectively. The 1,2-*cis* nitrilium **21** species is kinetically favored. Displacement by ROH, a hydroxyl acceptor, results in 1,2-*trans* selectivity.

4.3 Glycosyl Acceptor

The reactivity of the glycosyl acceptor can play a large role in the stereochemical outcome of the newly formed glycoside bond. In general, the more reactive the hydroxyl acceptor, the lower the selectivity of the reaction. Primary alcohols are more reactive than secondary alcohol

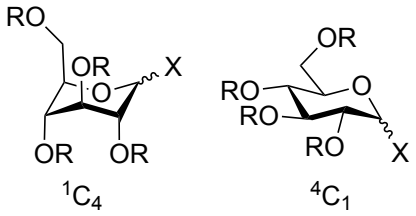

Scheme 4.8 Chair Confirmations

acceptors. Hydroxyl acceptors in the equatorial position are more reactive than acceptors in the axial position. Thus, it is important to consider the effect protecting groups exhibit on the conformation of the ring between $^4C_1$ and $^1C_4$ (Figure 4.8), as protecting groups alter the spatial orientation of the hydroxyl acceptor. As previously mentioned, protecting groups can change the conformation of the sugar. Acetates, benzoates, pivaloates, and other acyl-protecting groups lower the nucleophilicity of neighboring hydroxyl groups due to electron withdrawal.[22] This has been shown to improve the glycosylation stereoselectivity.[23]

4.4 Glycosyl Donor

Similar to glycosyl acceptors, protecting groups can also determine the reactivity of glycosyl donors. Participation of an acyl protecting group at the C_2 position has been used for the stereoselective formation of 1,2-*trans*-glycosides. Likewise, the use of auxiliaries at the C_2 or the

C_4 position have been shown to give 1,2-*cis*-glycosides.[3,13,14] Fraser-Reid and coworkers demonstrated that the benzylidiene protection of the C_4 and C_6 hydroxyl groups can improve the selectivity of the newly formed glycosidic bond. The cyclic nature of the 4,6-benzylidene protecting group reduces the flexibility of the sugar and causes torsional deactivation of the glycosyl donor.[42]

The aglycon also plays an important role in determining the stereoselectivity of the glycoside bond. The reactivity of the glycosyl donor can be tuned by the type of activation required for the aglycon.[25] The potential development of glycosyl donors that require mild methods for activation of the aglycon and that contain an aglycon that is stable toward common carbohydrate protecting group manipulations is still an area of interest. Herein, I will discuss several common classes of glycosyl donors.

4.4.1 Glycosyl Halides

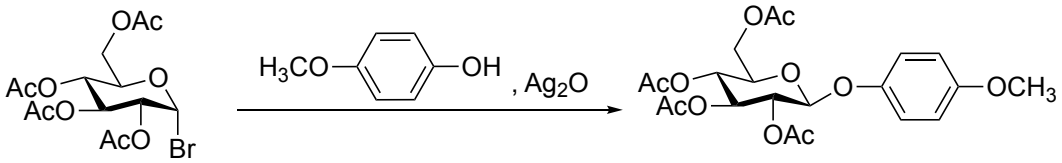

26 **27**

Scheme 4.9 Koenigs-Knorr Glycosyl Halide Example

Glycosyl bromides and chlorides were the first type of glycosyl donor used for the complex synthesis of oligosaccharides. α-Glycosyl halides are more stable than β-glycosyl halides due to the anomeric effect. The stability of the glycosyl halide is influenced by the sugar protecting groups. Benzyl ether protecting groups destabilize glycosyl halides and increase their reactivity, while acetate protecting groups decrease their reactivity. Glycosyl halides can not be easily purified and can not be stored for long periods of time. Glycosylations using glycosyl chlorides and bromides were originally promoted by heavy metal (particularly halophilic mercury and silver)

activation for glycosylation reactions (Scheme 4.9).[7] Since their initial use, milder means of glycosyl halide activation have since been developed. The use of Lewis acids, Bronsted acids, and iodine for activation resulted in an increase in the use of glycosyl chlorides and bromides in glycosylation reactions.[26-30] However, the stability of glycosyl halides was drastically improved with the development of glycosyl fluoride donors.[31] These compounds have a long shelf-life and can be easily purified.[2,31] The C_1-F bond is significantly more stable than the C_1-Br or C_1-Cl bond, but required specialized conditions for activation.[2,31] Glycosyl halides have also been used as precursor compounds for the preparation of *n*-pentenyl glycoside and thioglycoside donors.[10,11]

4.4.2 *n*-Pentenyl Glycosides

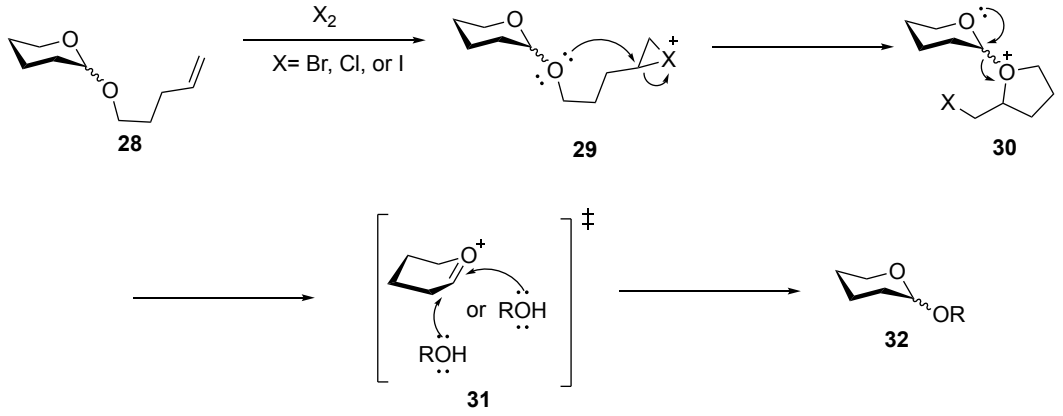

Scheme 4.10 Activation of *n*-Pentenyl Glycosyl Donors

n-Pentenyl glycosides **28** (Scheme 4.10) were first introduced by Fraser-Reid and coworkers in 1988. This class of compounds exhibits excellent stability compared to glycosyl halides and is stable to most protecting group manipulations of the sugar backbone. However, these compounds require harsh conditions for activation. *n*-Pentenyl glycosyl donors **28** are activated by halonium formation.[7] The halonium ion **29** is then attacked by the exo-anomeric oxygen to give a cyclized intermediate **30**. Dissociation of the aglycon results in formation of the oxocarbenium ion **31**, followed by attack of the hydroxyl acceptor and base removal of a proton

results in disaccharide **32**. It is important to note that the acylated *n*-pentenyl glycoside donors react more slowly than the benzylated counterparts.[7]

4.4.3 Trichloroacetimidates

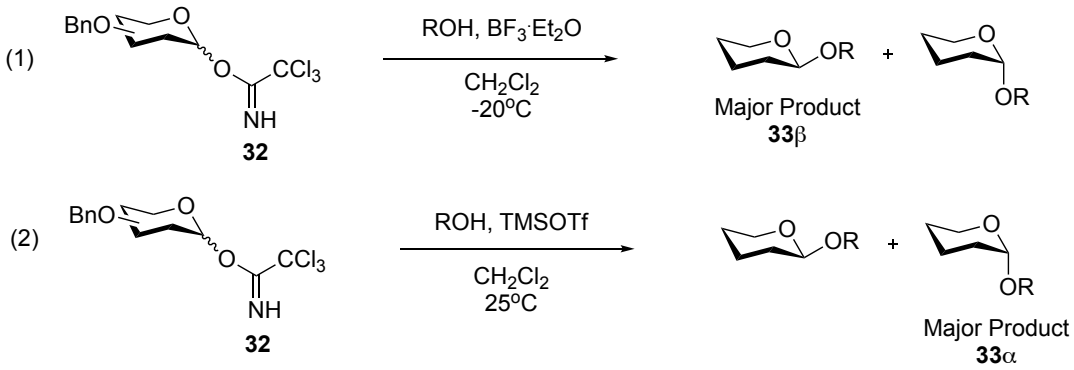

Scheme 4.11 Reactivity of Glycosyl Tricholoracetimidates

Since their development in 1980 by Schmidt and coworkers, glycosyl trichloroacetimidates have been widely used as glycosyl donors in the synthesis of oligosaccharides.[34-36] This class of donors is activated with Bronsted or Lewis acids (Scheme 4.11), but is relatively stable under basic conditions. The selection of an activator is essential to the stereochemical outcome of the glycosylation using TCAI donors. For example, the use of $BF_3{\cdot}Et_2O$ (equation 1) favors the formation of 1,2-*trans*-glycosides while the use of TMSOTf (equation 2) preferentially yields 1,2-*cis*-glycosides.[34-36] Trichloroacetimidates are highly reactive glycosyl donors but require immediate use upon synthesis and readily decompose in solution. An inverse procedure was developed to combat the decomposition: the glycosyl trichloroacetimidate is added to a mixture of the glycosyl acceptor and the acid catalyst.

4.4.4 Thioglycosides

Thioglycoside donors can be readily prepared by thiol attack on the anomeric carbon of 1,2-*trans*-acetates, glycosyl halides, or trichloroacetimidates.[2] Thioglycosides are remarkably stable to common carbohydrate manipulations of the sugar backbone and have long shelf-lives.

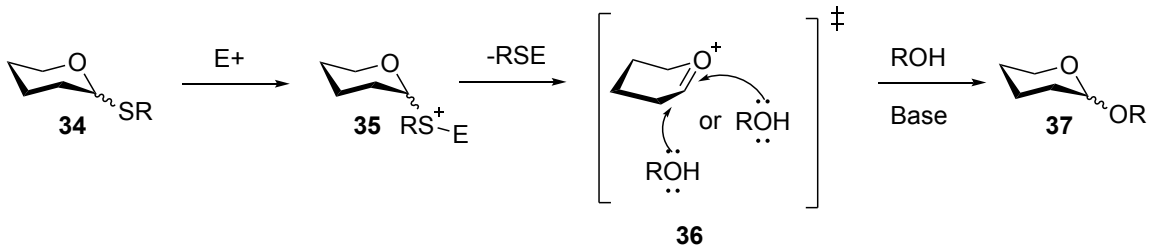

Scheme 4.12 Methods of Thioglycoside Donor Activation

These compounds are also inert to some traditional *O*-glycosylation methods, allowing their use as glycosyl acceptors in the one-pot multistep synthesis of oligosaccharides. Early methods of electrophilic activation of thioglycosides required the use of heavy metals such as mercury or lead (Scheme 4.12).[37,38] More recently, other electrophilic reagents have been employed for the direct activation of the sulfur atom, but they are still limited in their method of activation. The use of halogenating agents[41], methylating agents[39], and thiophiles[41] have been developed for the activation of thioglycoside donors. Although milder in nature than the use of heavy metals, these methods of activation often cause side reactions that decrease the yield and selectivity of O-glycosylation reactions.

4.5 References

1. Sznaidman, M., *Bioorganic Chemistry*: *Carbohydrates*, Oxford University Press, New York, **1999**, 1-56.
2. Levy, D.E.; Fügedi, P., *The Organic Chemistry of Sugars*. CRC Press, Boca Raton, **2005**.
3. Nigudkar, S.S.; Demchenko, A.V., *Chem Sci*., **2015**, *6*, 2687–2704.
4. Robbins, J. B.; Lee, C. J.; Rastogi, S. C.; Schiffman, G.; Henrichsen, J., *Infect. Immun*., *1979*, 26, 1116–1122.
5. (a) Ragupathi, G.; Koide, F.; Livingston, P. O.; Cho, Y. S.; Endo, A.; Wan, Q.; Spassova, M. K.; Keding, S. J.; Allen, J.; Ouerfelli, O.; Wilson, R. M.; Danishefsky, S. J., *J. Am.*

Chem. Soc., **2006**, *128*, 2715–2725. (b) Yin, Z.; Huang, X., *J. Carbohydr. Chem.,* **2012**, *31*, 143–186.

6. Mydock, L. K.; Demchenko, A. V., *Org. Biomol. Chem.*, **2010**, *8*, 497–510.

7. Koenigs, W.; Knorr, *E. Chem. Bericte*. **1901**, *34*, 957-981.

8. Igarashi, K. Adv.*Carbohydr. Chem. Biochem.*, **1997**, *34*, 243-283.

9. (a) Zemelen, G.; Gerecs, *A. Chem.Bericte*. **1930**, *62B*, 2720-2729. (b)Helferich, B.; Zirner, J., *Chem. Bericte.*, **1962**, *95*, 2604-2611.

10. Mootoo, D.R.; Konradsson, P.; Fraser-Reid, B.; *J. Am. Chem. Soc.*, **1988**, *110*, 55883-85584.

11. Fraser-Reid, B.; Radatus, B., *J. Chem. Soc. D*, **1970**, 779-780.

12. Zhong, W.; Boons, G.-J., *Handbook of Chemical Glycosylation*. Demchenko, A.V., editor. Wiley-VCH, Weinheim; Germany, **2008**, 261–303.

13. Boltje, T.J.; Kim, J.-H.; Park, J.; Boons, G.-J., *Nature Chemistry,* **2010**, *2*, 552–557.

14. Yasomanee, J.P.; Demchenko, A.V., *J. Am. Chem. Soc.* **2012**, *134*, 20097–20102.

15. IUPAC, *Compendium of Chemical Terminology*, 2nd ed. (the "Gold Book") **1997**. Online corrected version: **1996** "Anomeric Effect.

16. Wulff, G. and Rohle, G., *Angew. Chem., Int. Ed. Engl.,* **1974**,*13*, 157–170.

17. Demchenko, A. V., Stauch, T., Boons, G.-J. *Synlett,* **1997**, *7*, 818–820.

18. Liu, C.-Y.I.; Mulani, S.; Mong, K.-K.T., *Adv. Synth. Catal.* **2012**, *354*, 3299–3310.

19. Kaeothip, S.; Yasomanee, J.P.; Demchenko, A.V., *J. Org. Chem.* **2012**, *77*, 291–299.

20. Eby, R. and Schuerch, C. *Carbohydr. Res.* **1974**, *34*, 79–90.

21. Chao, C.S.; Lin, C.Y.; Mulani S.; Hung W.C.; Mong K.K., *Chem.-Eur. J.*, **2011**, *17*, 12193–12202.

22. **(a)** Sinay P., *Pure Appl. Chem.*, **1978**, *50*, 1437–1452. **(b)** Paulsen H., *Angew. Chem., Int. Ed. Engl.,* **1982**, *21*,155–173.

23. Kaeothip, S.; Akins, S..J.; Demchenko, A.V., *Carbohydr. Res.*, **2010**, *345*, 2146–2150.

24. Benzylidiene (a) Crich, D.; Cai, W., *J. Org. Chem.,* **1999**, *64*, 4926–4930. (b) Crich, D.; Chandrasekera, N.S., *Angew. Chem., Int. Ed.,* **2004**, *43,* 5386–5389. (c) Huang, M.; Garrett, G.E.; Birlirakis, N.; Bohe, L., Pratt, D.A., Crich, D., *Nat. Chem.*, **2012**, *4*, 663–667.

25. Tuning: Moitessier, N.; Chapleur, T., Tetrahedron Lett., **2003**, *44*, 1731-1735.

26. Milder (Lewis acid) conditions: Ogawa, T. and Matsui, M., *Carbonhyr. Res.*, **1976**, *51*, C13-C18.

27. Lubineau, A. and Malleron, A., *Tetrahedron Lett.*, **1985**, *26*, 1713-1716.

28. Lubineau, A.; Le Gallic, J.; Malleron, A., *Tetrahedron Lett.*, **1987**, *28*, 5041-5044.

29. Iodine: Kartha, K.P.R.; Aloui, M., Field, R.A., *Tetrahedron Lett.*, **1996**, *37*, 8807-8810.

30. TfOH: Mukaiyama, T.; Jona, H.; Takeuchi, K., *Chem. Lett.*, **2000**, *29*, 696-697.

31. Fluorides: Toshima, K., *Carbohydr. Res.*, **2000**, *327*, 15-26.

32. Marra, A.; Esnault, J.; Veyrieres, A.; Sinay, P., *J. Am. Chem. Soc.*, **1992**, *114*, 6354–6360.

33. Boons, G. J.; Isles, S., *Tetrahedron Lett.* **1994**, *35*, 3593-3596.

34. Schmidt, R. R., *Angew. Chem. Int. Ed.*, **1986**, *25*, 212-235.

35. Zhu, X. M.; Schmidt, R. R., *Angew. Chem. Int. Ed.* **2009**, *48*, 1900-1934.

36. Schmidt, R. R.; Castro-Palomino, J. C.; Retz, O. *Pure Appl. Chem.* **1999**, *71*, 729-744.

37. Mercury: Ferrier, R.J.; Hay, R.W.; Vethaviayasar, N.A.; *Carbohydr. Res.,* **1973**, *27*, 55-61.

38. Lead: Takeda, K.; Tsuboyama, K.; Torii, K.; Furuhata, K.; Sato, N.; Ogura, H., *Carbohydr. Res.*, **1990**, *203*, 57-63.

39. Methylating agents: Lonn, H., *J Carbohydr. Chem.,* **1987**, *6*, 301-306.

40. Halogenation: Sasaki, M.; Tachibana, K.; Nakanishi, H., *Tetrahedron Lett.,* **1991**, *32*, 6873-6876.

41. Thiophiles: Andersson, F.; Fugedi, P.; Garegg, P.J.; Nashed, M., *Tetrahedron Lett.*, **1986**, *27*, 3919-3922.

42. Fraser-Reid, B.; Udodong, U.E.; Wu, Z; Madsen, R., *Synlett,* **1992**, *12*, 927-942.

CHAPTER 5: *O*-GLYCOSYLATIONS USING THIOGLYCOSIDE DONORS

5.1 Research Significance

As mentioned earlier, chemical synthesis of oligosaccharides is necessary for a more profound understanding of glycobiology and the medical sciences. Oligosaccharides occur in all of the kingdoms and are important components of vaccines and therapeutics.[1,2,3] Methods for *O*-glycosylation are especially important in the synthesis of oligosaccharides. The development of efficient and stereoselective *O*-glycosylation methods is even more important if we want to be able to synthesize oligosaccharides with the same complexity as those found in nature.

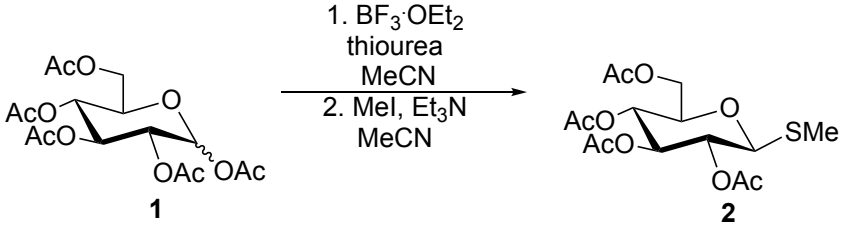

Scheme 5.1 Preparation of Thioglycosides from Acylated Sugars

Thioglycosides, although rarely found in nature, have become an essential tool for oligosaccharide synthesis.[4] Thioglycosides are one of the most common classes of glycosyl donor and have been used since seminal work was published by Ferrier and coworkers in 1973.[5] Prior to their use as glycosyl donors, thioglycosides were employed as an anomeric carbon protecting group on glycosyl acceptors due to their stability to many common glycosylation conditions.[6,7] This class of glycosyl donor can be conveniently synthesized, for example from acylated sugar derivatives via promotion with acid in the presence of thiourea and attack of the resulting nucleophile (-SH) on an alkyl halide (see Scheme 5.1.) The ease of synthesis, stability toward sugar backbone manipulations, and long shelf-life make thioglycosides a useful tool for the synthesis of oligosaccharides.[4,8]

The selective activation of the thio-aglycon is ideal for convergent, sequential, or "one pot"

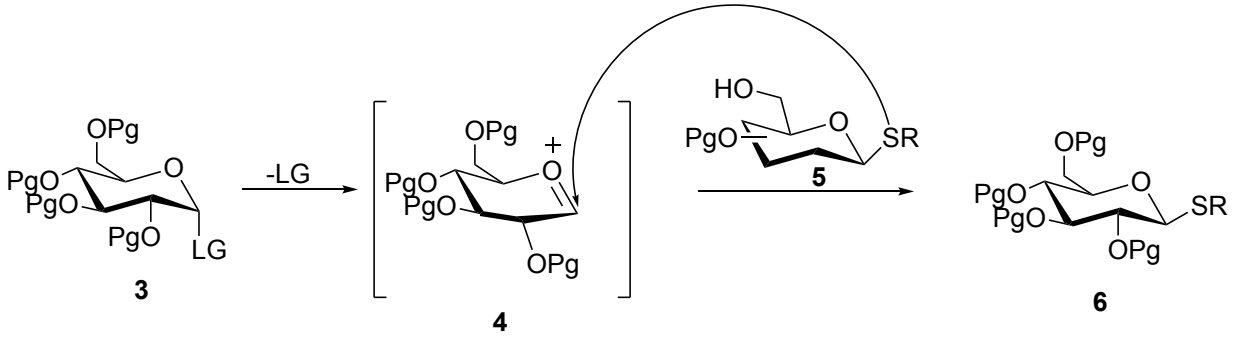

Scheme 5.2 Intermolecular Migration of Thio-aglycon under Glycosylation Conditions

syntheses; however, stoichiometric quantities of harsh electrophilic reagents such as heavy metals[5.8], halogenating agents[11], methylating agents[10], and other thiophilic promotors[12] are often required for the activation of thioglycosides. Additionally, *O*-glycosylation reactions using thioglycoside donors are sometimes plagued with side reactions. The thio-aglycon can undergo intra- and intermolecular migratory shifts.[13] An example of an intermolecular migratory shift is outlined in Scheme 5.2. The leaving group (Br or TCAI) of donor **3** leaves, forming oxocarbenium ion **4**. The thio-aglycon of acceptor **5** then attacks intermediate **4,** generating product **6.** Persistent glycosylation byproducts can also be generated by side reactions due to the excess thiophilic promotors utilized for thioglycoside activation and are often separated from the desired product with difficulty.[4]

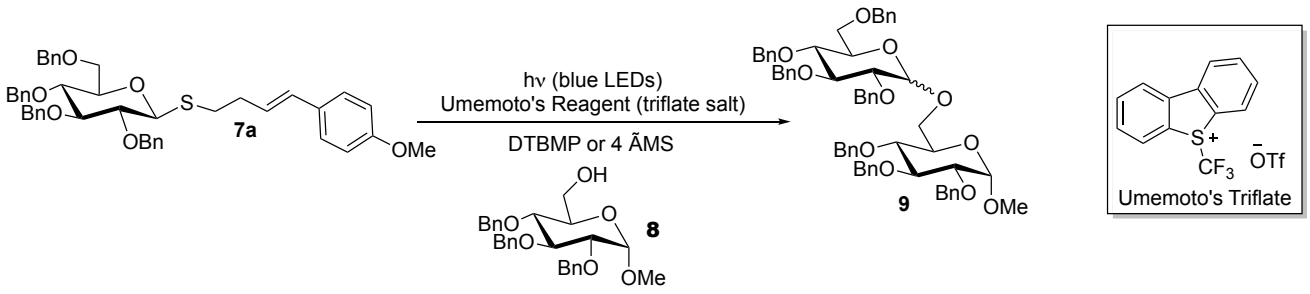

Scheme 5.3 Visible-Light Promoted *O*-Glycosylations with a Thioglycoside

Despite the vast number of glycosyl donors, a widely applicable method for *O*-glycosylation has not been established. Recently, the Ragains group began investigating 4-(4-methoxyphenyl)-3-butenylthioglycosides as a new class of donor for oligosaccharide synthesis.[14]

The glycosylation method (Scheme 5.3) reported by Ragains and coworkers is effective at producing disaccharides in moderate to high yields without the use of a photocatalyst, however, the method still required the use of an expensive CF_3 source: Umemoto's triflate. Moreover, the necessity of base or molecular sieves was intriguing as triflic acid is generated in their absence. The question then arose, could triflic acid alone be used to activate the 4-(4-methoxyphenyl)-3-butenylthioglycosides? If so, the use of a protic acid would provide an easy, inexpensive, and atom economical approach to the activation of 4-(4-methoxyphenyl)-3-butenylthioglycoside donors.

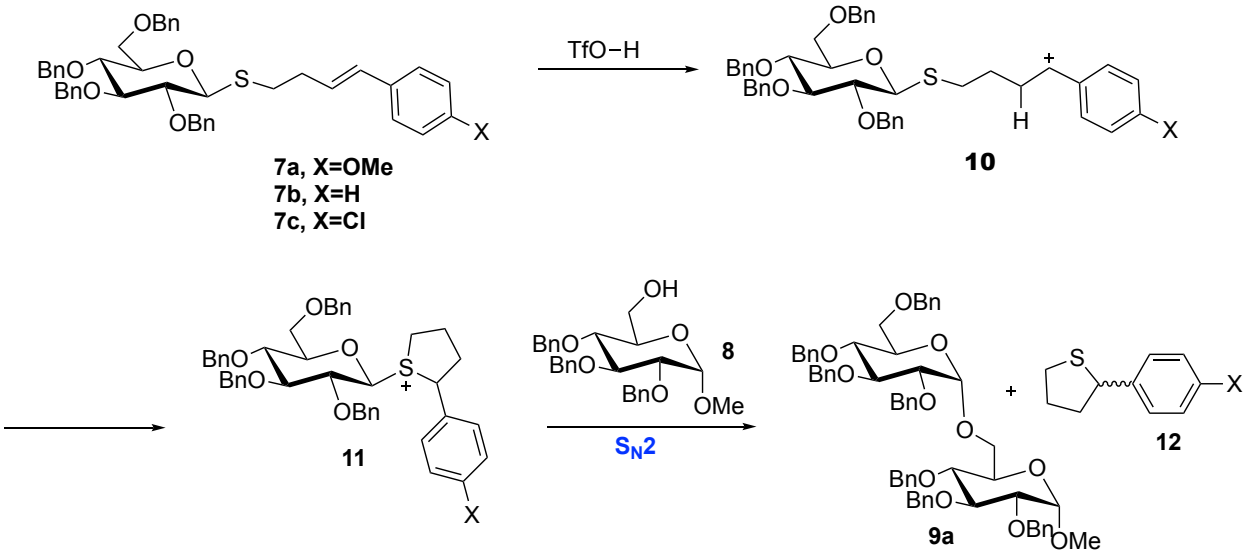

Scheme 5.4 Initial Hypothesis for *O*-Glycosylations with 4-Aryl-3-butenyl Thioglycosides

We proposed activation of a series of 4-aryl-3-butenylthioglycosides (**7a-7c**, Scheme 5.4) with triflic acid. While other glycosyl donors, namely trichloroacetimidates (TCAIs), are activated with the addition of catalytic Lewis or Bronsted acids, glycosyl TCAIs are not amenable to manipulation of the carbohydrate backbone (*e.g.,* protecting group manipulations), require immediate use, and are plagued by decomposition due to their instability.[6,15] We hypothesized that the 4-aryl-3-butenylthioglycoside donors would provide the combination of the stability of

thioglycosides with the reactivity of glycosyl TCAIs. In addition to enhancing atom economy, we hypothesized that the 4-aryl-3-butenylthioglycosides would react chemoselectively, diastereoselectively, and with high efficiency. We imagined the protonation of the styrene bond **7** (Scheme 5.4) would generate **10**, a benzylic carbocation. The benzylic carbocation **10** could then be stabilized or destabilized depending on substitution on the aromatic ring. Cyclization of the anomeric sulfur would generate **11**, a sulfonium ion intermediate. S_N2 displacement at the anomeric carbon would yield **9α** (bearing the1,2-*cis*-glycoside linkage) and heterocycle **12**.

5.2 Results and Discussion

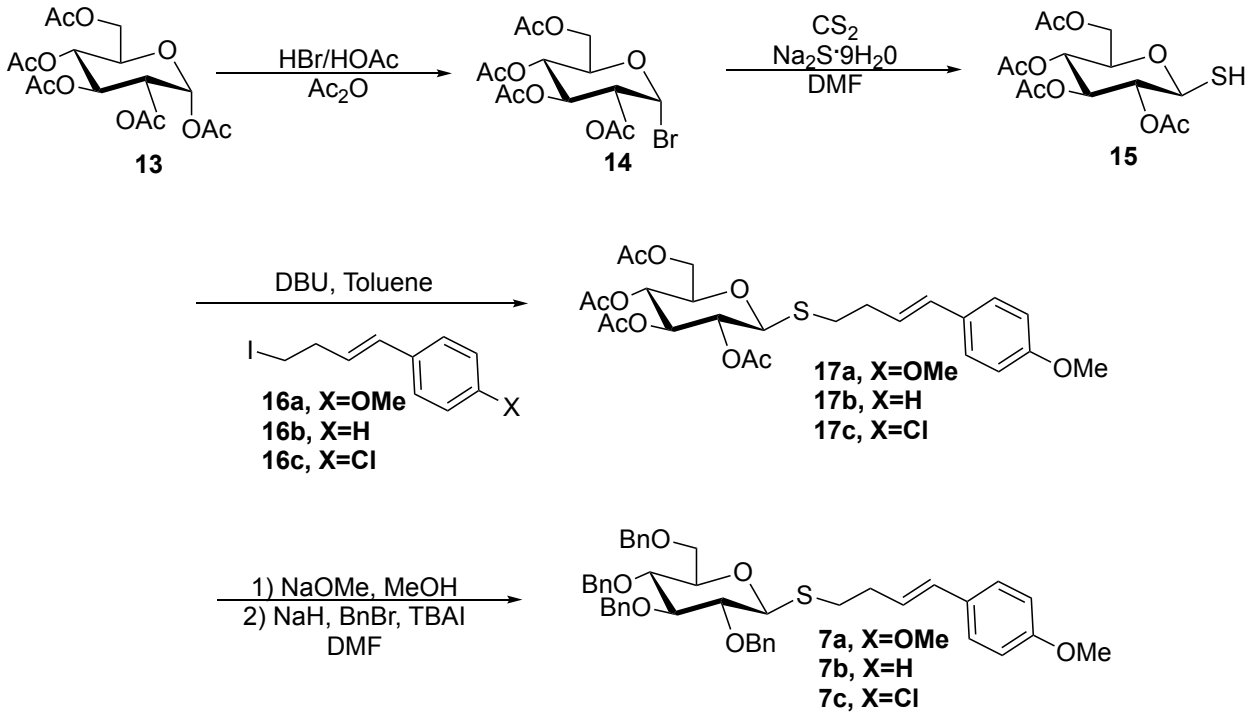

Scheme 5.5 Synthesis of 4-Aryl-3-butenyl Thioglycosides

Three 4-aryl-3-butenylthioglycosides (**7a- 7c**) were synthesized from α-D-(+)-glucose pentaacetate (Scheme 5.5). The acetylated sugar **13** is converted to the α-bromide **14**. Displacement of **14** with sulfur generates thiol **15**. Thiolate attack on the iodides **16** yield tetra-

acetates **17**. Deacetylation of **17** with NaOMe in MeOH followed by benzylation generate 4-aryl-3-butenylthioglycosides **7**.

Table 5.1 Evaluation of 4-Aryl-3-butenylthioglycosides

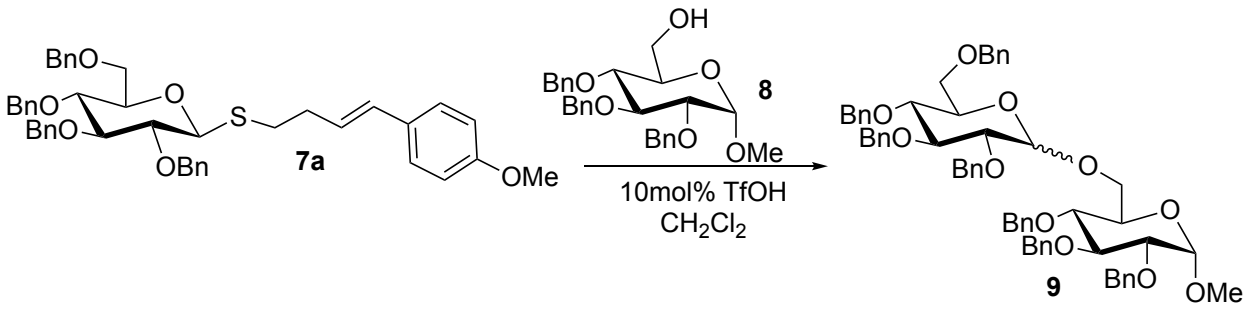

Entry	Donor	Yield	Selectivity
1	7a	87%	1.5α:β
2	7b	0%	-
3	7c	0%	-

Unless otherwise stated, 0.15mmol donor **7**, 10mol% TfOH, 0.5eq acceptor in 1mL CH_2Cl_2 were stirred for 1 hour at 25°C. All products were isolated by column chromatography and selectivity was determined using integration of the ^1H spectra.

Herein, I report the results of my optimization studies. To date, moderate to high yields have been achieved using catalytic Bronsted acid. Low anomeric selectively has been achieved in most cases. The series of 4-aryl-3-butenylthioglycosides **7** was subjected to the reaction conditions in Table 5.1. To our dismay, only the 4-(4-methoxyphenyl)-3-butenylthioglycoside donor **7a** could be activated by triflic acid. The electron-rich styrene of **7a** was able to react faster than styrenes without electron-donating groups (**7b**) or those with slightly deactivating groups (**7c**). My initial experiment with **7a** resulted in an 87% yield of the disaccharide **9** as a mixture of anomers. Attempts at further optimization were conducted. Although high-yielding, this transformation

requires an excess of donor. Studies were then conducted to determine the effect of concentration on this *O*-glycosylation.

Table 5.2 Concentration Studies

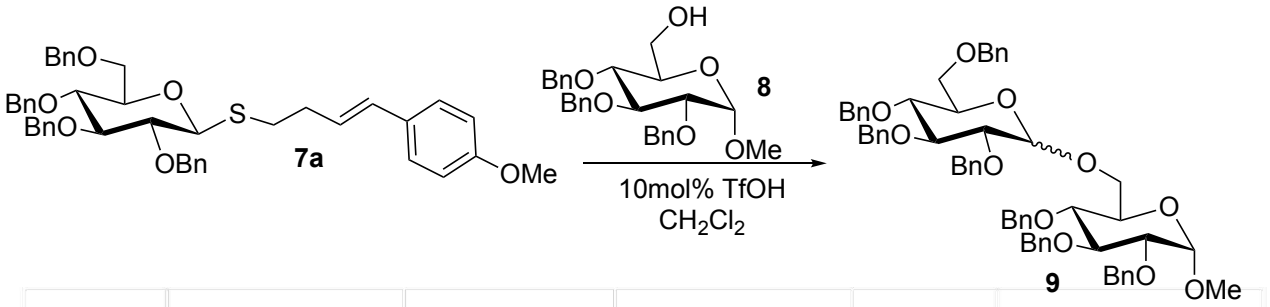

Entry	Donor	Acceptor	Time	Yield	Selectivity
1	0.150mmol	0.0752mmol	1h	87%	1.5α:β
2	0.0827mmol	0.0752mmol	1h	50%	1 α: β
3	0.0684mmol	0.0752mmol	1h	57%	1.5 α: β
4	0.150mmol	0.137mmol	1h	65%	1.3 α: β
5	0.150mmol	0.137mmol	4h	89%	1.6 α:β

All products were isolated by column chromatography and selectivity was determined using integration of the ^{1}H spectra.

Entries 2 and 3 (Table 5.2) correspond to decreases in reaction concentration due to reduction in the equivalents of donor **7a** relative to the hydroxyl acceptor **8**. More dilute concentrations of glycosyl donor correlated to significant decreases in the yield of **9** (50-57%). While increases (entries 4 and 5) in the concentration of the acceptor **8** relative to donor **7a** gave similar yields and selectivity seen with the initial conditions (entry 1), but required extended reaction time. These results suggested that excess donor **7a**, although not necessary, was beneficial in decreasing reaction time and increasing the yield of disaccharide **9**. These observations led us to investigate the role of temperature on the reaction.

Table 5.3 Temperature Profile

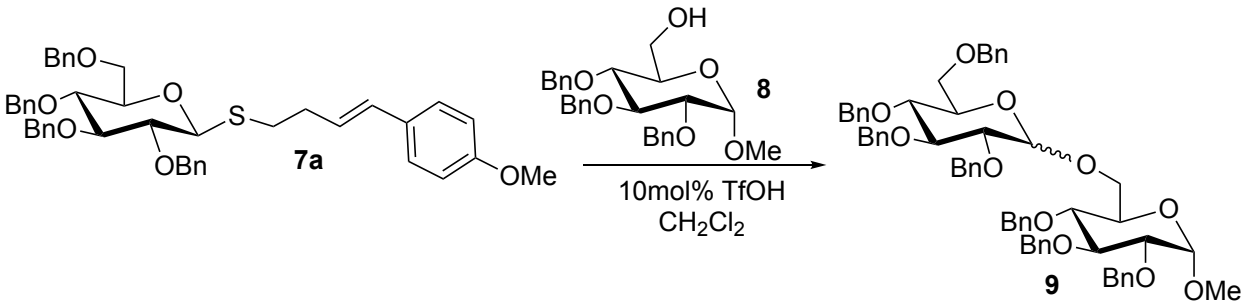

Entry	Acceptor	Temp	Time	Yield	Selectivity
1	0.137mmol	20°C	4h	89%	1.6α: β
2	0.137mmol	-20°C	18.5h	46%	1.1α: β
3	0.137mmol	0°C	7h	57%	1α: β
4[a]	0.137mmol	0°C	1.5h	44%	1.2α: β

Unless otherwise stated, 0.15mmol donor **7a**, 10mol% TfOH, 0.137mmol acceptor **8** in 1mL CH_2Cl_2 were stirred until the time noted. All products were isolated by column chromatography and selectivity was determined using integration of the ^1H spectra. [a] 1.0 equivalents of triflic acid.

I evaluated the temperature profile (Table 5.3) of the glycosylation reaction at the higher concentration ([**8**] = 0.137M). The glycosylation reaction at -20°C only gave a 46% yield of disaccharide **9** after 18.5 hours (entry 2). An increase in the reaction temperature to 0°C (seen in entry 3) resulted in a 57% yield of **9** after 7 hours. Using 1 equivalent of triflic acid, we investigated the reaction at 0°C (entry 4). After 1.5 hours, the donor was not consumed and both starting materials were still present. The use of a full equivalent of triflic acid (result not shown) with the entry 4 conditions resulted in complete consumption of donor **7a** within an hour at room temperature. The glycosylation reaction using standard conditions (0.150mmol **7a** and 0.075mmol of **8**) was evaluated at 0°C; however, the glycosyl acceptor was not consumed after 7 hours (results not shown). Although theses reactions were low-yielding, the entries provide great insight and suggest the potential utility of these reactions in oligosaccharide synthesis. Temperature plays an important role in our glycosylation method. At low temperature, the activation of the styrene

moiety on the 4- (4-methoxyphenol)-3-butenylthioglycoside **7a** is sluggish at best and results in substantially lower yields than observed at room temperature.

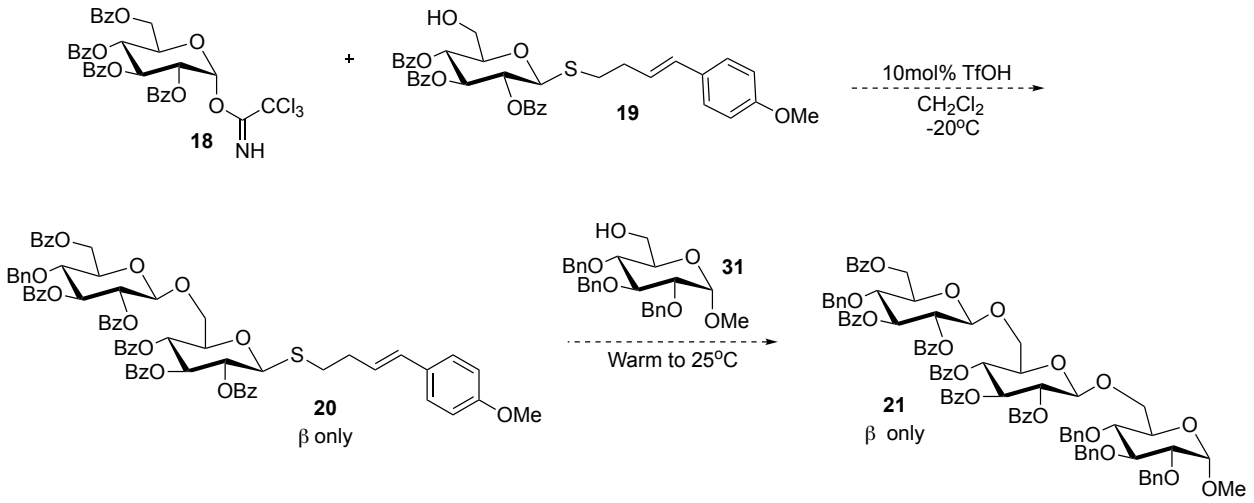

Scheme 5.6 Proposed Trisaccharide Synthesis Using a Thioglycoside Acceptor

These results illuminate the potential orthogonality of our thioglycoside with other glycosylation methods. I hypothesize that the use of glycosyl trichloroacetimidate **18**[16] (Scheme 5.6) and glycosyl acceptor **19**, a derivative of our 4-(4-methoxyphenyl)-3-butenylthioglycoside will form disaccharide **20** at -20ºC. After formation of the disaccharide, the reaction would then be warmed to room temperature to utilize **20** as a donor with hydroxyl acceptor **8**. The relative stability of our thioglycoside under acidic conditions at low temperature is encouraging and the one-pot synthesis of trisaccharides may now be an achievable goal.

The effect of solvent on glycosylation was also evaluated. Table 5.4, entry 2 showcases the use of ether as a cosolvent in an effort to enhance alpha selectivity (1,2-*cis*). A slight increase in α selectivity was observed; however, the reaction was inefficient as it was incomplete after 24 hours. The use of a polar aprotic solvent (entry 3) gave a slight increase in β selectivity. This is attributed to the formation of the nitrilium intermediate (mentioned previously in Chapter 4.2.3)**.** Unfortunately, the yield of disaccharide was moderate compared to results previously observed

with the use of dichloromethane. The use of toluene in entry 4 generated similar yields and selectivity seen with dichloromethane (entry1).

Table 5.4 Solvent Evaluation

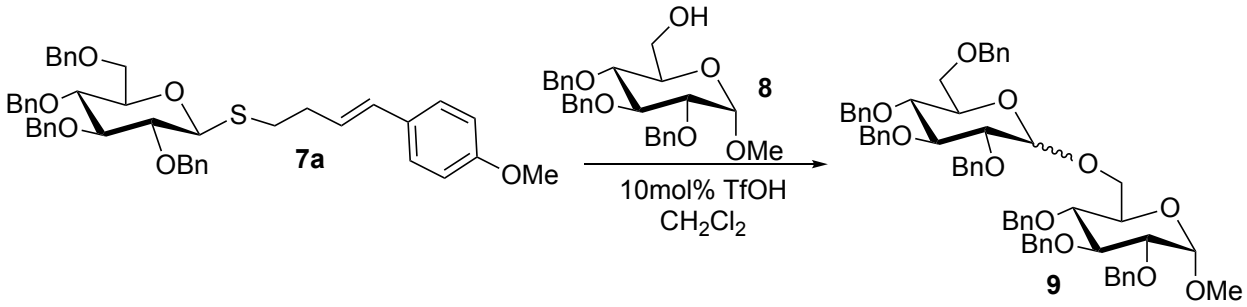

Entry	Solvent	Time	Yield	Selectivity
1	CH_2Cl_2	1h	87%	1.5 α:β
2	Et_2O/CH_2Cl_2	24h	27%	2.1 α:β
3	CH_3CN	2h	51%	3.2 β:α
4	Toluene	1h	88%	1.3 β:α

Unless otherwise stated, 0.15mmol donor **7a**, 10mol% TfOH, 0.5eq acceptor **8** in 1mL solvent were stirred for 1 hour at 25°C. All products were isolated by column chromatography and selectivity was determined using integration of the ^1H spectra.

I synthesized the tetraacetyl- and tetrabenzylgalactose derivatives of 4-(4-methoxyphenyl)-3-butenylthioglycoside. The use of acetate protecting groups in **22a** (entry 3) resulted in a 7% yield of disaccharide **24a**. The major product of entry 2 and 3 was the acetylation of hydroxyl acceptor **8** (see Table 5.5). A low yield of disaccharide **23** (26%) was also observed with the tetraacetate thioglucoside **17a** (entry 2). The results with the acetylated donors **17a** and **22a** were encouraging as **17a** was not activated by the visible-light promoted *O*-glycosylation with Umemoto's triflate.[14] Similar results (entry 4) were obtained for the tetrabenzylgalactose

thioglycoside **22b** (83%) as were observed with the tetrabenzylglucose derivative **7a** (87%, entry 1).

Table 5.5 Galactose Thioglycoside Donors

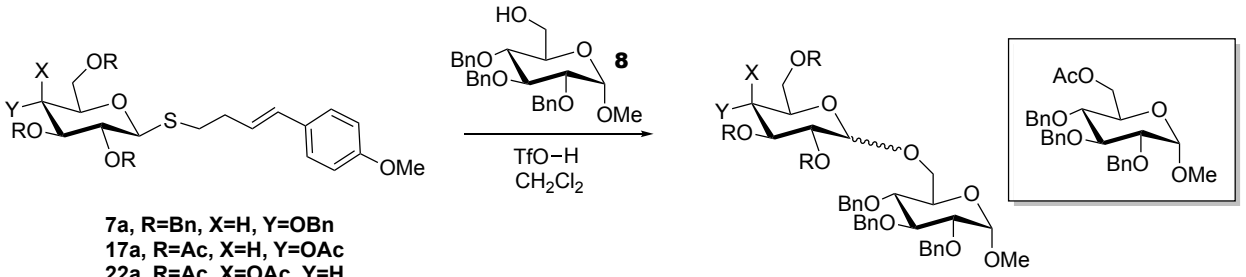

7a, R=Bn, X=H, Y=OBn
17a, R=Ac, X=H, Y=OAc
22a, R=Ac, X=OAc, Y=H
22b, R=Bn, X=OBn, Y=H

9, R=OBn, X=H, Y=OBn
23, R=OAc, X=H, Y=OAc
24a, R=Ac, X=OAc, Y=H
24b, R=Bn, X=OBn, Y=H

Entry	Donor	Yield	Selectivity
1	7a	87%	1.5 α:β
2	17a	26%	β
3	22a	7%	β
4	22b	83%	α

Unless otherwise stated, 0.15mmol donor **7**, 10mol% TfOH, 0.5eq acceptor **8** in 1mL CH_2Cl_2 were stirred for 1 hour at 25°C. All products were isolated by column chromatography and selectivity was determined using integration of the ^1H spectra.

Although 4-(4-methoxyphenyl)-3-butenylthioglycoside was explored with the goal of developing a diastereoselective method for oligosaccharide synthesis, the results do not support our original hypothesis. In Scheme 5.7, we now propose that the glycosylation is proceeding through an S_N1 type pathway rather than the S_N2-like pathway we proposed in Scheme 5.4. The protonation of the alkene in **7a** gives rise to the benzylic carbocation **10a** that is stabilized through resonance (**10a***). The cyclization of the anomeric sulfur results in the formation of **11a**. I assert that the formation of the oxocarbenium cation **25** releases the aglycon **12a**. Nucleophilic attack of

the oxocarbenium cation by the C_6-OH acceptor **8** can occur at the bottom or top face yielding a mixture of α (1,2-*cis*) and β (1,2-*trans*) anomers, respectively.

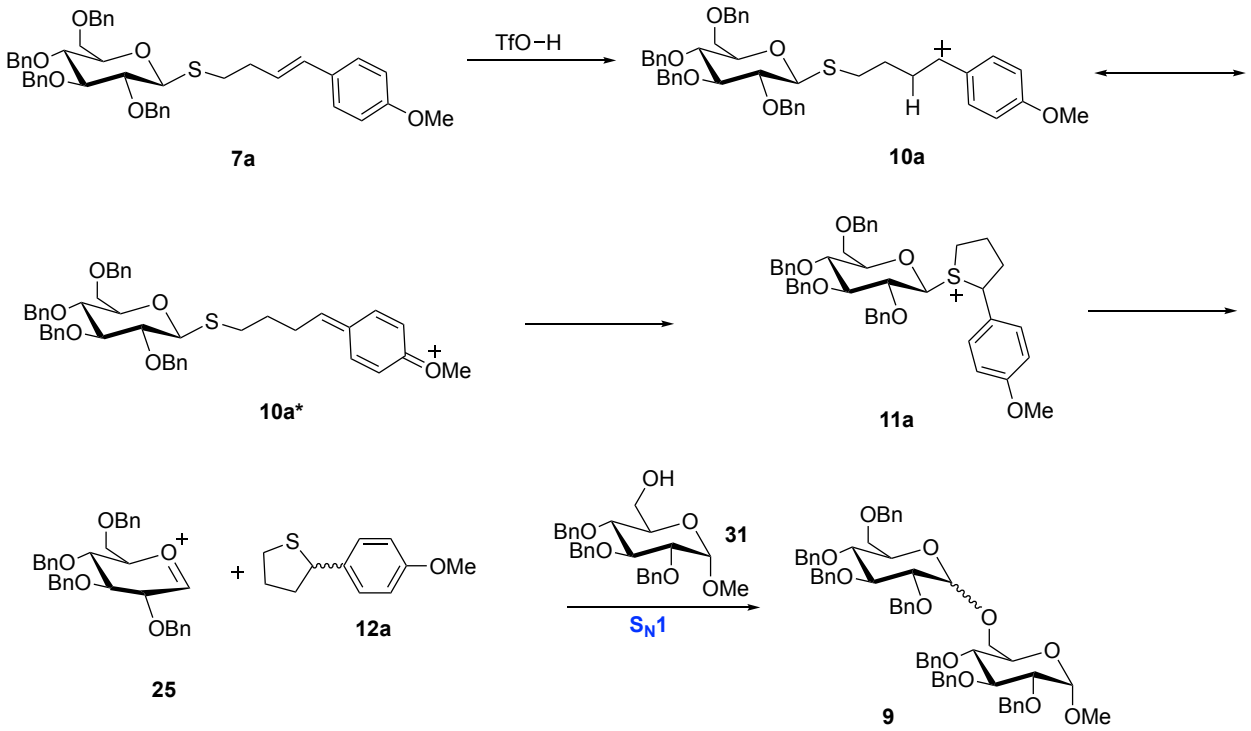

Scheme 5.7 Proposed Mechanism for Acid Promoted O-Glycosylation with 4-(4-methoxyphenyl)-3-butenylthioglycoside

Manipulations of the donor protecting groups are also underway in an effort to increase diastereoselectivity. Two additional glycosyl donors have been synthesized (Scheme 5.8). Preliminary results using the tetrabenzoyl-(4-(4-methoxyphenyl)-3-butenyl thioglycoside **26** have yielded moderate results (56-80%) with 1,2-*trans* glycosidic linkages as the only product due to neighboring group participation (**27**). Additionally, I synthesized **28** with the goal of achieving 1,2-*cis* glycosidic linkages diastereoselectively. The use of the 4,6-benzylidene protecting group has been shown to prevent ionization to the oxocarbenium through torsional deactivation.[19] I propose that cyclized sulfonium ion intermediate **29** will undergo an S_N2-like displacement to give the *alpha* anomer only.

5.3 Conclusion

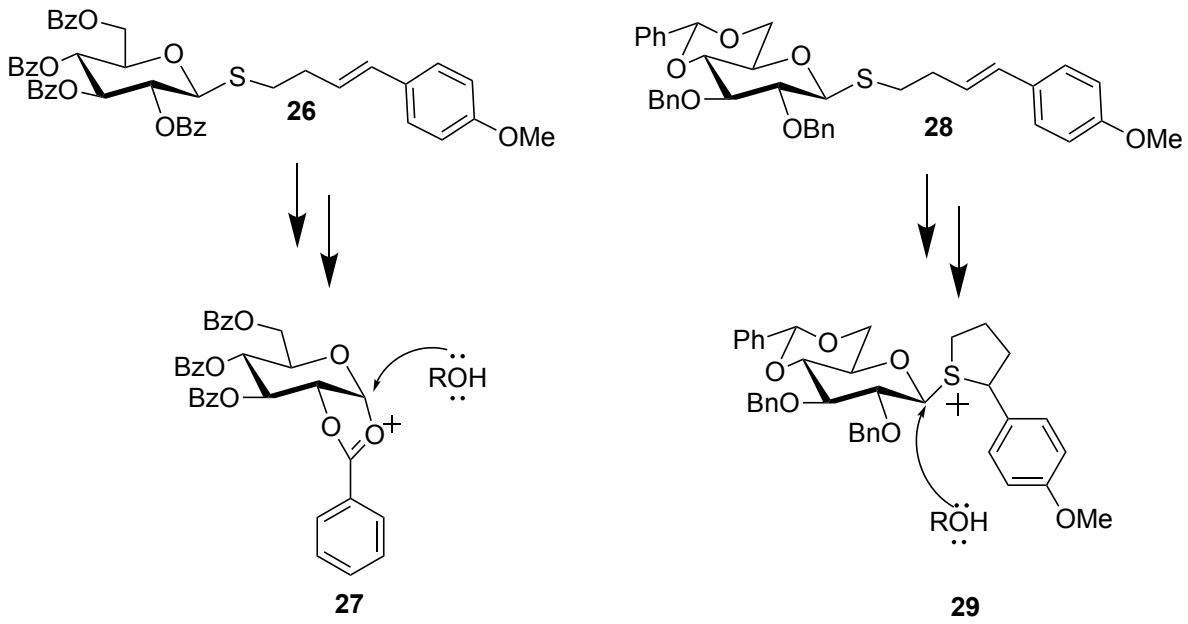

Scheme 5.8 Diatereoselective Donors

We have demonstrated that the remote activation of the 4-(4-methoxyphenyl)-3-butenyl thioglycoside donors is possible with the use of catalytic trifle acid. This method serves as a mild approach to *O*-glycosylation compared to others using thioglycoside donors. A mixture of anomers can be attained in high yield. Dilute concentrations of donor are inefficient for this *O*-glycosylation method and result in low yields of disaccharide. The conversion of the 4-(4-methoxyphenyl)-3-butenyl thioglycoside donor at low temperature is slow, resulting in low isolated yields. Benzoyloxy donor **26** has been shown to generate only 1,2-*trans*-glycosidic linkages. Efforts to obtain 1,2-*cis*-glycosidic linkages have culminated in the synthesis of **28**. Results of *O*-glycosylations with **28** are forthcoming. The pinnacle of this research will be the successful execution of the trisaccharide synthesis outlined in Scheme 5.6. Synthesis of donor **18** and acceptor **19** are in progress.

5.4 Experimental and Tabulated Data

5.4.1 General Methods

Reagents were purchased from Alfa Aesar, VWR, or Sigma-Aldrich and used without further purification. Flash column chromatography was performed using 60Å silica gel purchased from Sigma Aldrich. ^{1}H NMR and ^{13}C NMR spectroscopy were performed on a Bruker AV-400 or AV-500 spectrometer. Mass spectra were obtained using an Agilent 6210 electrospray time-of-flight mass spectrometer. Thin layer chromatography was conducted on aluminum sheets (Merck, silica gel 60, F254). Compounds were visualized by UV absorption (254 nm) and staining with anisaldehyde. Pyrex micro reaction vessels (5mL from Supelco) were used in the glycosylation reactions. All glassware was flame-dried under vacuum and backfilled with dry nitrogen prior to use. Deuterated solvents were obtained from Alfa Aesar. All solvents were purified according to the method of Grubbs.[20]

5.4.2 Procedures and Characterization

General Procedure for *O*-Glycosylation:

A flame-dried 5 mL Pyrex reactor vessel was charged with the glycosyl donor (1 equiv., 0.1504 mmol) and the glycosyl acceptor (0.5 equiv, 0.0752 mmol). The reaction was vacuum-purge-backfilled three times to remove moisture and left under nitrogen. Dry dichloromethane (1mL) was added under nitrogen atmosphere. Triflic acid (0.01equiv, 0.015mmol) was then added to the reaction vessel and the nitrogen line was removed. The reaction mixture was monitored by TLC and concentrated upon completion. The resulting residue was then purified by gradient silica gel chromatography to afford a mixture of anomeric products. The anomeric ratio (α/β) was determined based on the integration of key resonances in the ^{1}H NMR spectrum.

(*E*)-1-iodo-4-(4-methoxyphenyl)-3-butene:

16a

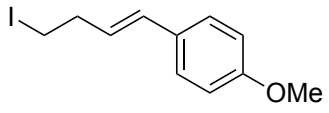

A solution of iodine (1.5equiv, 4.21mmol) and triphenylphosphine (1.5equiv, 4.21mmol) in 20mL of CH_2Cl_2 was prepared in a 100mL round-bottom flask charged with a stir bar and allowed to stir at 20°C.[21] After 10 minutes, imidazole (2.5equiv, 7.01mmol) was added and the reaction mixture allowed to stir for an additional ten minutes. A solution of (*E*)-4-(4-methoxyphenyl)-3-buten-1-ol (1.0equiv, 2.81mmol) in 6mL of CH_2Cl_2 was prepared and added dropwise to the reaction mixture. The reaction was monitored with TLC. Upon consumption of the alcohol (4 hrs), 20mL of saturated aqueous sodium metabisulfite were added to quench the reaction. The organic layer was separated and the aqueous layer was washed with 20mL diethyl ether three times. The combined organic layers were dried with magnesium sulfate, filtered and concentrated. The resulting residue was purified by column chromatography (10% EtOAc/Hexanes) to give 0.6524g (81 % yield) of a yellow solid. ^{1}H NMR (500 MHz, Chloroform-d) δ 7.30(d, *J*=8.5Hz, 2H), 6.85(d, *J*=8.6 Hz, 2H), 6.41 (d, *J*=15.8 Hz, 1H), 6.01(dt, *J*=15.8, 7.0 Hz, 1H), 3.81(s, 3H), 3.23 (t, *J* = 7.3 Hz, 2H), 2.76 (q, *J* = 7.2Hz, 2H). Spectral data matched that previously reported in literature.[14]

((*E*)-4-(4-methoxyphenyl)-3-butenyl β-D-1-thio-2,3,4,6-tetra-*O*-acetylglucopyranoside): 17a

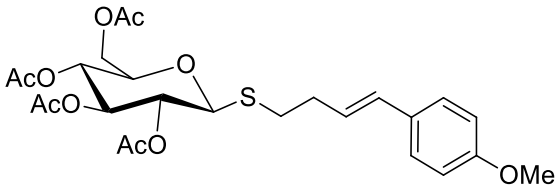

A solution of 2,3,4,6-Tetra-*O*-acetyl-1-mercapto-β-D-glucopyranoside[22] (1.0equiv, 2.26mmol) in 5mL of CH_2Cl_2 and cooled to -10°C in a dry ice 20% MeOH-H_2O bath. 1,8-Diazabicycloundec-7-ene (1.0equiv, 2.26mmol) was added to the solution at -10°C. After fifteen minutes, solution of (*E*)-1-iodo-4-(4-methoxyphenyl)-3-butene (1.0equiv, 2.26mmol) in 2mL of CH_2Cl_2 was prepared and added to the reaction mixture. After consumption of 2,3,4,6-Tetra-*O*-acetyl-1-mercapto-β-D-glucopyranoside as observed by TLC, the reaction was quenched with 10mL of H_2O and the layers were separated. The aqueous layer was then extracted with 3 × 20 mL of CH_2Cl_2 followed by dilution with 50 mL of CH_2Cl_2. The organic layer was then washed with 20mL of 1M H_2SO_4 and 20mL of saturated $NaHCO_3$. The combined organic layer were dried over Na_2SO_4, filtered and concentrated to give the crude material. Purified by gradient silica gel chromatography 20% → 40% ethyl acetate in hexanes to give 1.04 g (88% yield) a white solid. ^{1}H NMR (500 MHz, $CDCl_3$) δ 7.27 (d, *J* = 8.8 Hz, 2H), 6.84 (d, *J* = 8.6 Hz, 2H), 6.38 (d, *J* = 15.8 Hz, 1H), 6.05 (dt, *J* = 15.8, 6.9 Hz, 1H), 5.26 – 5.20 (m, 1H) , 5.07 (dt, *J* = 17.4, 9.7 Hz, 2H), 4.52 (d, *J* = 10.0 Hz, 1H), 4.25 (dd, *J* = 12.4, 5.0 Hz, 1H), 4.14 (dd, *J* = 12.4, 2.4 Hz, 1H), 3.80 (s, 3H), 3.71 (ddd, *J* = 10.0, 4.9, 2.3 Hz, 1H), 2.80 (tdd, *J* = 20.1, 9.7, 6.0 Hz, 2H), 2.57 – 2.40 (m, 2H), 2.07 (s, 3H), 2.04 (s, 3H), 2.03 (s, 3H), 2.01 (s, 3H). Spectral data matched that previously reported in literature. [14]

((*E*)-4-(4-methoxyphenyl)-3-butenyl β-D-1-thio-2,3,4,6-tetra-*O*-benzylglucopyranoside):

7a

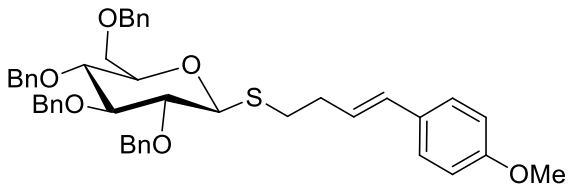

A 250 mL round bottom flask was charged with (*E*)-4-(4-methoxyphenyl)-3-butenyl-D-1-thio-2,3,4,6-tetra-*O*-acetylglucopyranoside (1equiv, 4.00 mmol) and 22mL of methanol under a nitrogen atmosphere. 1M NaOMe (0.55equiv, 2.20mmol) was prepared and added dropwise to the reaction solution. The resulting mixture was stirred for three hours. The solvent was then removed yielding the tetra-ol. The residue was then diluted with 40mL of DMF, followed by the addition of tetrabutylammonium iodide (0.2equiv, 0.801mmol) and placed under a stream of nitrogen. The solution was cooled to 0°C in an ice-water bath. 60% Sodium hydride (5.0equiv, 20.0mmol) was added to the solution at 0°C and the suspension was stirred for 30 minutes. Benzyl bromide (5.5equiv, 22.0mmol) was then added dropwise to the suspension at 0°C. The suspension was then allowed to warm to room temperature and stir for 16 hrs. The reaction was then quenched with 40 mL of saturated NH_4Cl at 0°C followed by extraction with 2 × 40mL Et_2O. The combined organic layers were washed with 2 x 40mL cold H_2O, dried over Na_2SO_4, filtered and concentrated.The residue was purified by gradient silica gel chromatography 10% → 20% EtOAc/Hexanes to give 1.42g. (49% yield over 2 steps) white solid. ^{1}H NMR (500 MHz, $CDCl_3$) δ 7.40 – 7.20 (m, 20H), 7.17 (d, *J* = 7.5 Hz, 2H), 6.82 (d, *J* = 8.6 Hz, 2H), 6.37 (d, *J* = 15.8 Hz, 1H), 6.09 (dt, *J* = 15.7, 6.9 Hz, 1H), 4.92 (d, *J* = 10.6 Hz, 2H), 4.88 – 4.78 (m, 2H), 4.74 (d, *J* = 10.2 Hz, 1H), 4.64 – 4.52 (m, 3H), 4.49 (d, *J* = 9.7 Hz, 1H), 3.80 (s, 3H), 3.75 (dd, *J* = 10.9, 1.9

Hz, 1H), 3.71 – 3.65 (m, 2H), 3.65 – 3.59 (m, 1H), 3.51 – 3.39 (m, 2H), 2.95 – 2.76 (m, 2H), 2.56 (qd, *J* = 7.3, 1.4 Hz, 2H). Spectral data matched that previously reported in literature.[14]

(*E*)-4-(4-methoxyphenyl)-3-butenyl-β-D-1-thio-2,3,4,6-tetra-*O*-acetylgalactopyranoside:

22a

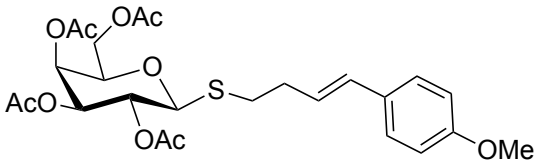

A solution of 2,3,4,6-Tetra-*O*-acetyl-1-mercapto-β-D-galactopyranoside[23] (1.0equiv, 2.26 mmol) in 5mL of CH_2Cl_2 was cooled to -10°C in a dry ice MeOH/water bath.[14] 1,8-Diazabicycloundec-7-ene (1.0equiv, 2.26mmol) was added to the solution at -10°C dropwise over five minutes. After fifteen minutes, a solution of (*E*)-1-iodo-4-(4-methoxyphenyl)-3-butene (1equiv, 2.26mmol) in 2mL of CH_2Cl_2 was prepared and added dropwise to the reaction mixture. After consumption of 2,3,4,6-Tetra-*O*-acetyl-1-mercapto-β-D-galactopyranoside as observed by TLC, the reaction was quenched with 10 mL of H_2O and the layers were separated. The aqueous layer was then extracted with 3 × 20 mL of CH_2Cl_2 followed by dilution of all organic extracts with 50 mL of CH_2Cl_2. The organic layer was then washed with 20mL of 1M H_2SO_4 and 20mL of saturated $NaHCO_3$. The combined organic layer was dried over Na_2SO_4, filtered, and concentrated to give the crude material. Purification by gradient silica gel chromatography (20% → 40% ethyl acetate in hexanes) gave 1.11 g (61% yield) a yellow oil. ^{1}H NMR (400 MHz, $CDCl_3$) 7.27 (d, *J* = 8.6 Hz, 2H), 6.84 (d, *J* = 8.8Hz, 2H), 6.39 (d, *J* = 16.0 Hz, 1H), 6.06 (dt, *J* = 15.7, 7.0 Hz, 1H) 5.44 (d, *J* = 2.5 Hz, 1H), 5.27 (dd, *J* = 18.8, 8.8Hz, 1H), 5.05 (dd, *J* = 10.0, 3.4 Hz, 1H), 4.52 (d, *J* = 10.0 Hz, 1H), 4.17-4.10 (m, 2H), 3.94 (t, *J* = 6.5Hz, 1H), 3.80 (s, 3H), 2.84-2.79 (m, 2H), 2.51 (q, *J* = 7.3 Hz,

2H), 2.16-1.99 (m,12H).δ ^{13}C NMR(126 MHz, $CDCl_3$) δ 170.5, 170.3, 170.2 169.7, 159.1, 131.1, 130.2, 127.3, 125.8, 114.1, 84.2, 74.6, 72.0, 67.4, 67.3, 61.6, 55.4, 33.4, 30.1, 20.9, 20.8(2), 20.7. HRMS m/z Calcd for $C_{25}H_{32}O_{10}SK$ $(M+K)^+$ 563.1348, found 563.134

(*E*)-4-(4-methoxyphenyl)-3-butenyl β-D-1-thio-2,3,4,6-tetra-*O*-benzylgalactopyranoside:

22b

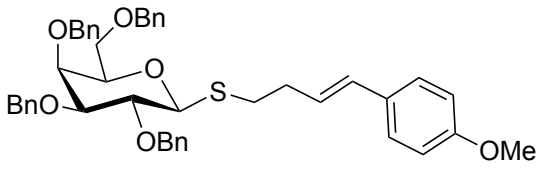

A 250 mL round bottom flask was charged with (*E*)-4-(4-methoxyphenyl)-3-butenyl-β-D-1-thio-2,3,4,6-tetra-*O*-acetylgalactopyranoside (1equiv, 4.00mmol) and 22mL of methanol under a nitrogen atmosphere. 1M NaOMe (0.55equiv, 2.20mmol) was prepared and added dropwise to the reaction solution.[14] The resulting mixture was stirred for three hours. The solvent was then removed yielding the tetra-ol. The residue was then diluted with 40mL of DMF, followed by the addition of tetrabutylammonium iodide (0.2equiv, 0.801mmol), and placed under a stream of nitrogen. The solution was cooled to 0°C in an ice-water bath. 60% Sodium hydride (5equiv, 20.0mmol, in mineral oil) was added to the solution at 0°C and the suspension was stirred for 30 minutes. Benzyl bromide (5.5 equiv, 22.0mmol) was then added dropwise to the suspension at 0°C. The suspension was then allowed to warm to room temperature and stir for 16 hrs. The reaction was then quenched with 40 mL of saturated NH_4Cl at 0°C followed by extraction with 2 × 40mL Et_2O. The combined organic layers were washed with 2 x 40mL cold H_2O, dried over Na_2SO_4, filtered and concentrated. The residue was purified by gradient silica gel chromatography (10% → 15% EtOAc/Hexanes) to give 1.26g. (83% yield over 2 steps) white solid. ^{1}H NMR (500

MHz, $CDCl_3$) δ 7.38-7.22 (m, 22H), 6.82 (d, *J*=8.8Hz, 2H), 6.35 (d, *J*=15.9Hz, 1H), 6.08 (dt, *J*=15.8Hz, 1H), 4.95 (d, *J*=11.7Hz, 1H), 4.88(d, *J*=10.2Hz, 1H), 4.79 (d, *J*=10.2Hz, 1H), 4.73(m, 2H), 4.61 (d, *J*=11.7Hz, 1H), 4.46-4.39 (m, 3H), 3.95 (d, *J*=2.7Hz, 1H), 3.82 (t, *J*=9.3Hz, 1H), 3.80 (s, 3H), 3.57 (m, 4H), 2.85(m, 2H), 2.80 (m, 2H). ^{13}C NMR (126 MHz, $CDCl_3$) δ 159.0, 138.9, 138.6, 138.5, 138.1, 130.8, 130.5, 128.8, 128.7 (6), 128.5 (2), 128.4 (2), 128.2 (2), 128.1 (2), 128.0, 127.94, 127.86 , 127.8 (2), 127.7, 127.4 (2), 126.6, 114.1(2), 85.7, 84.3, 78.7, 76.0, 74.7, 73.8 (2), 72.9, 69.1, 55.5, 33.8, 30.8. HRMS m/z Calcd for $C_{45}H_{48}O_6SK$ $(M+K)^+$ 755.2803, found 755.2823.

Preparation of (*E*)-4-(4-methoxyphenyl)-3-butenyl β-D-1-thio-2,3- *O*-benzyl-4,6-*O*-benzylidene acetalglucopyranoside):

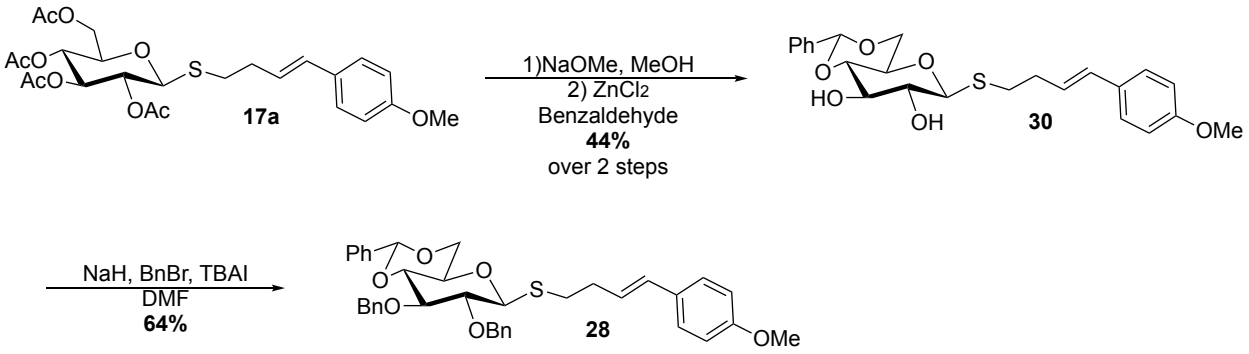

(*E*)-4-(4-methoxyphenyl)-3-butenyl β-D-1-thio-4,6-*O*-benzylidene acetalglucopyranoside):

30

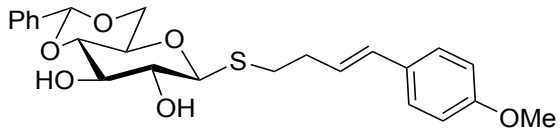

A 250 mL round bottom flask was charged with (*E*)-4-(4-methoxyphenyl)-3-butenyl-D-1-thio-2,3,4,6-tetra-*O*-acetylglucopyranoside[14](1.0equiv, 4.80mmol) and 25mL of methanol under a

nitrogen atmosphere. 2.64mL (0.55equiv, 2.64 mmol) of a 1M NaOMe solution was added at once and the reaction was stirred for 3 hrs. The resulting mixture was concentrated to remove solvent yielding the tetra-ol. The residue was placed on high vacuum to remove any additional solvent. Benzaldehyde (21equiv, 101mmol) was then added to the crude residue, followed by the addition of $ZnCl_2$ (2.1equiv, 10.1mmol). The reaction was allowed to stir at room temperature until complete via TLC analysis. Purified by gradient silica gel chromatography (10% → 20% ethyl acetate in hexanes) to give 0.939g (44% yield over 2 steps) white solid. ^{1}H NMR (400 MHz, $CDCl_3$) δ 7.48(m, 2H), 7.36 (m, 3H) 7.27 (t, *J*=5.7Hz, 2H), 6.84 (d, *J*=8.6Hz, 2H), 6.40 (d, *J*=15.8Hz, 1H), 6.06 (dt, *J*=15.6Hz, 6.9Hz, 1H), 5.52 (s, 1H), 4.45(d, *J*=9.7Hz, 1H), 4.33 (dd, *J*= 10.5, 4.9Hz, 2H), 3.70 (s, 3H), 3.76 (q, *J*=22.1, 6.4Hz, 2H), 3.57-3.43 (m, 3H), 3.19 (bs, 1H), 2.92 (bs, 1H), 2.87-2.80 (m, 2H), 2.54 (q, *J*=14.6, 7.2Hz, 1H). ^{13}C NMR (100 MHz, $CDCl_3$) δ 159.2, 137.1, 131.4, 130.1, 129.5, 128.5, 127.4, 126.5, 125.6, 114.2, 102.1, 86.9, 80.5, 74.7, 73.5, 70.8, 68.8, 55.5, 33.9, 30.6. HRMS m/z Calcd for $C_{24}H_{28}O_6SNa$ $(M+Na)^+$ 467.1499, found 467.1495.

Synthesis of (*E*)-4-(4-methoxyphenyl)-3-butenyl β-D-1-thio-2,3- *O*-benzyl-4,6-*O*-benzylidene acetalglucopyranoside):

28

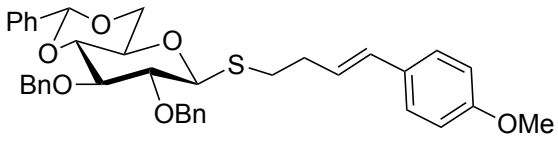

The diol (1.0eq, 1.11mmol) was added to a flame-dried 250 mL round bottom flask, followed by the addition of tetrabutylammonium iodide (0.2equiv, 0.221mmol), and 11 mL of DMF under an atmosphere of nitrogen. The solution was cooled to 0°C in an ice-water bath. Sodium hydride (4.0eq, uiv4.42mmol, 60% in mineral oil) was added to the solution at 0°C and the suspension was stirred for 30 minutes. Benzyl bromide (4.0equiv, 4.42mmol) was then added dropwise to the

suspension at 0°C. The suspension was then allowed to warm to room temperature and stir for 16 hrs. The reaction was then quenched with 15 mL of saturated NH_4Cl at 0°C followed by extraction with 3 × 15mL Et_2O. The combined organic layer was washed with cold water, dried over Na_2SO_4, filtered, and concentrated. The crude mixture was purified by gradient silica gel chromatography (100% Hexanes → 20% EtOAc/Hexanes) to give 0.442g (64%) of a white solid. NMR (400 MHz, $CDCl_3$) δ 7.49(dd, *J*= 7.5, 2.4Hz, 2H), 7.40-7.33(m, 7H) 7.32-7.24(m, 8H), 6.83(d, *J*=8.7Hz, 2H), 6.39(d, *J*=15.8Hz, 1H), 6.09 (dt, *J*=13.8Hz, 6.9Hz, 1H), 5.58 (s, 1H), 4.95(d, *J*=14.1Hz, 1H), 4.89(d, *J*=12.6Hz, 1H), 4.82(d, *J*=6.7Hz, 1H), 4.80(d, *J*=6.7Hz, 1H), 4.59(d, *J*=9.8Hz, 1H), 4.36(dd, *J*= 10.5, 5.1Hz, 2H), 3.80(s, 3H), 3.83-3.69(m, 3H), 3.50-3.45(m, 2H), 2.87-2.82(m, 2H), 2.54(q, *J*=14.3, 7.0Hz, 1H). ^{13}C NMR (126 MHz, $CDCl_3$) δ159.0, 138.4, 137.9, 137.3, 130.9, 130.1, 129.0, 128.4 (3), 128.34 (2), 128.27 (2), 128.1 (2), 127.9, 127.7, 127.2 (2), 126.0, 125.8, 114.0 (2), 101.1, 86.1, 82.8, 81.6, 81.3, 77.2, 76.0, 75.3, 70.3, 68.7, 55.3, 33.5, 31.0. HRMS m/z Calcd for $C_{38}H_{40}O_6SNa$ $(M+Na)^+$ 647.2438, found 647.2469.

methyl-*O*-(2,3,4,6-tetra-*O*-benzyl-α-D-glucopyranosyl)-(1→6)-2,3,4-tri-*O*-benzyl-α-D-glucopyranoside: 9

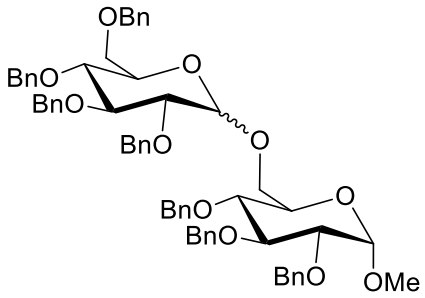

Started with 107.8mg (0.150mmol) of glycosyl donor **7a**, 34.9mg (0.0754mmol) of methyl 2,3,4-tri-O-benzyl-α-D-glucopyranoside **8**, 1.3μL of triflic acid in 1 mL of CH_2Cl_2.

Purified by column chromatography to obtain 63.1mg (87%) colorless oil in a 1.5:1 (α:β) mixture. Spectral data matched that previously reported in literature.[24]

methyl-*O*-(2,3,4,6-tetra-*O*-acetyl-α-D-galactopyranosyl)-(1→6)-2,3,4-tri-*O*-benzyl-α-D-glucopyranoside:

24a

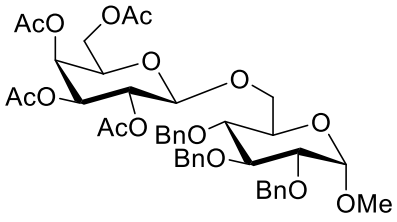

Started with 78.9mg (0.150mmol) of glycosyl donor **22a**, 34.9mg (0.0754mmol) of methyl 2,3,4-tri-O-benzyl-α-D-glucopyranoside **8**, 1.3μL of triflic acid in 1 mL of CH_2Cl_2. Purified to obtain 4.1mg (7%) as a colorless oil with β only selectivity. Spectral data matched that previously reported in literature.[25]

methyl-*O*-(2,3,4,6-tetra-*O*-benzyl-α-D-galactopyranosyl)-(1→6)-2,3,4-tri-*O*-benzyl-α-D-glucopyranoside:

24b

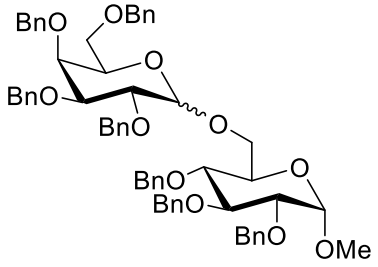

Started with 107.8mg (0.150mmol) of glycosyl donor **22b**, 34.9mg (0.0754mmol) of methyl 2,3,4-tri-O-benzyl-α-D-glucopyranoside **8**, 1.3μL of triflic acid in 1 mL of CH_2Cl_2. Purified via column chromatography to obtain 61.8mg (83%) colorless oil a 1:1 (α:β) mixture of anomers. Spectral data matched that previously reported in literature.[26]

5.5 References

1. Fungi: (a) Bittencourt, V.C.B.; Figueiredo, R.T.; da Silva, R.B., Mourão-Sá, D.S., Fernandez, P.L., Sassaki, G.L.; Mulloy, B., Bozza, M.T.; Barreto-Bergter, E. J., *Biol. Chem*. **2006**, 281, 22614–22623
2. Bacteria: *Bacteroides fragilis* (a) Tzianabos AO, Pantosti A, Baumann H, Brisson JR, Jennings HJ, Kasper DL., *J. Biol. Chem.,* **1992**, 267, 18230-18235; *Staphylococcus aureus* (b) Jones C., *Carbohydr. Res*. **2005**, 340, 1097-1106
3. Vancomycin: (a) Evans, D. A.; Wood, M. R.; Trotter, B. W.; Richardson, T. I.; Barrow, J. C.; Katz, J.L.; *Angew. Chem. Chem. Int. Ed.,* **1998**, 37, 2700- 2704; (b) Evans, D. A.; Wood, M. R.; Trotter, B. W.; Richardson, T. I.; Barrow, J. C.; Katz, J.L.; *Angew. Chem. Int. Ed* **1998**, 110, 2864-2868; Angew. (c) Boger, D. L.; Miyazaki, S.; Kim, S. H.; Wu, J. H.; Loiseleur, O.; Castle, S. L.; *J. Am. Chem. Soc*. **1999**, 121, 3226-3227.
4. Lian, G.; Zhang, X.; Yu, B., *Carbohydr. Res.,* **2015**, 403, 13-22
5. Mercury: Ferrier, R.J.; Hay, R.W.; Vethaviayasar, N.A.; *Carbohydr. Res.,* **1973**, 27, 55-61
6. Levy, D.E. and Fügedi, P. *The Organic Chemistry of Sugars*. CRC Press, Boca Raton, 2005.
7. Hanaya, T.; Baba, H.; Toyota, H.; Yamamoto, H., *Tetrahedron*, **2009**, 65, 38, 7989-7997
8. Swati S. Nigudkar and Alexei V. Demchenko, *Chem Sci*. 2015, 6, 5, 2687–2704

9. Lead: Takeda, K.; Tsuboyama, K.; Torii, K.; Furuhata, K.; Sato, N.; Ogura, H., *Carbohydr. Res.,* 1990, 203, 57-63

10. Methylating agents: Lonn, H., J *Carbohydr. Chem.,* **1987**, 6, 301-306

11. Halogenation: Sasaki, M.; Tachibana, K.; Nakanishi, H., Tetrahedron Lett., 1991, 32, 6873-6876

12. Thiophiles: Andersson, F.; Fugedi, P.; Garegg, P.J.; Nashed, M., *Tetrahedron Lett.,* **1986**, 27, 3919-3922

13. Leigh, D. A.; Smart, J.P.; Truscello, A.M., *Carbobydr.Res.,* **1995**, 27, 417-42

14. Spell, M.L.; Deveaux, K.; Bresnahan, C.G.; Bernard, B.L.; Sheffield, W.; Kumar, R.; Ragains, J.R., *Angew. Chem. Int. Ed.* **2016**, 55, 6515-6519.

15. TCAI: Zhu, X., Schmidt, R. R., *Angew. Chem., Int. Ed.,* **2009**, 48, 1900–1934

16. Thioglycosides: Zhong W, Boons G-J. In: Handbook of Chemical Glycosylation. Demchenko AV, editor. Wiley-VCH, Weinheim; Germany: 2008. pp. 261–303.

17. Liu, C.-Y. I.; Mulani, S.; Mong, K.-K. T., *Adv. Synth. Catal.*, **2012**, 354, 3299–3310

18. Mootoo, D.R.; Konradsson, P.; Fraser-Reid, B.; *J. Am. Chem. Soc.*, **1988**, 110, 55883-85584

19. Fraser-Reid, B.; Radatus, B., ***J. Chem. Soc. D***, 1970, 779-780

20. Pangborn, A. B.; Giardello, M. A.; Grubbs, R. H.; Rosen, R. K.; Timmers, F. J. *Organometallics* **1996**, *15*, 1518.

21. Lanni Jr., T.B.; Greene, K.L.; Kolz, C.N.; Para, K.S.; Visnick, M.; Mobley, J. L.; Dudley, D.T.; Baginski, T. J.; Liimatta, M. B., *Bioorg. Med. Chem.,* **2007**, 17, 3, 756-760

22. Jana, M.; Misra, A. K. *J. Org. Chem.* **2013**, *78*, 2680–2686.

23. Floyd, N.; Vijayakrishnan, B.; Koeppe, J.R.; Davis, B.G., *Angew. Chem. Int. Ed.,* **2009**, 48, 7798-7802

24. Nokami, T.; Shibuya, A.; Tsuyama, H.; Suga, S.; Bowers, A. A.; Crich, D.; Yoshida, J. *J. Am. Chem. Soc***. 2007**, *129*, 10922–10928.

25. Vibhute, A.M.; Dhaka, A.; Athiyarath, V.; Sureshan, K.M., *Chem. Sci.,* **2016**, 7, 4259-4263

26. Bennett, Clay S., and An-Hsiang A. Chu. Stereoselective Glycosylation Reactions. Trustees of Tufts College Boston, MA, assignee. Patent US 2014/0303359 A1. 9 Oct. 2014. Print.

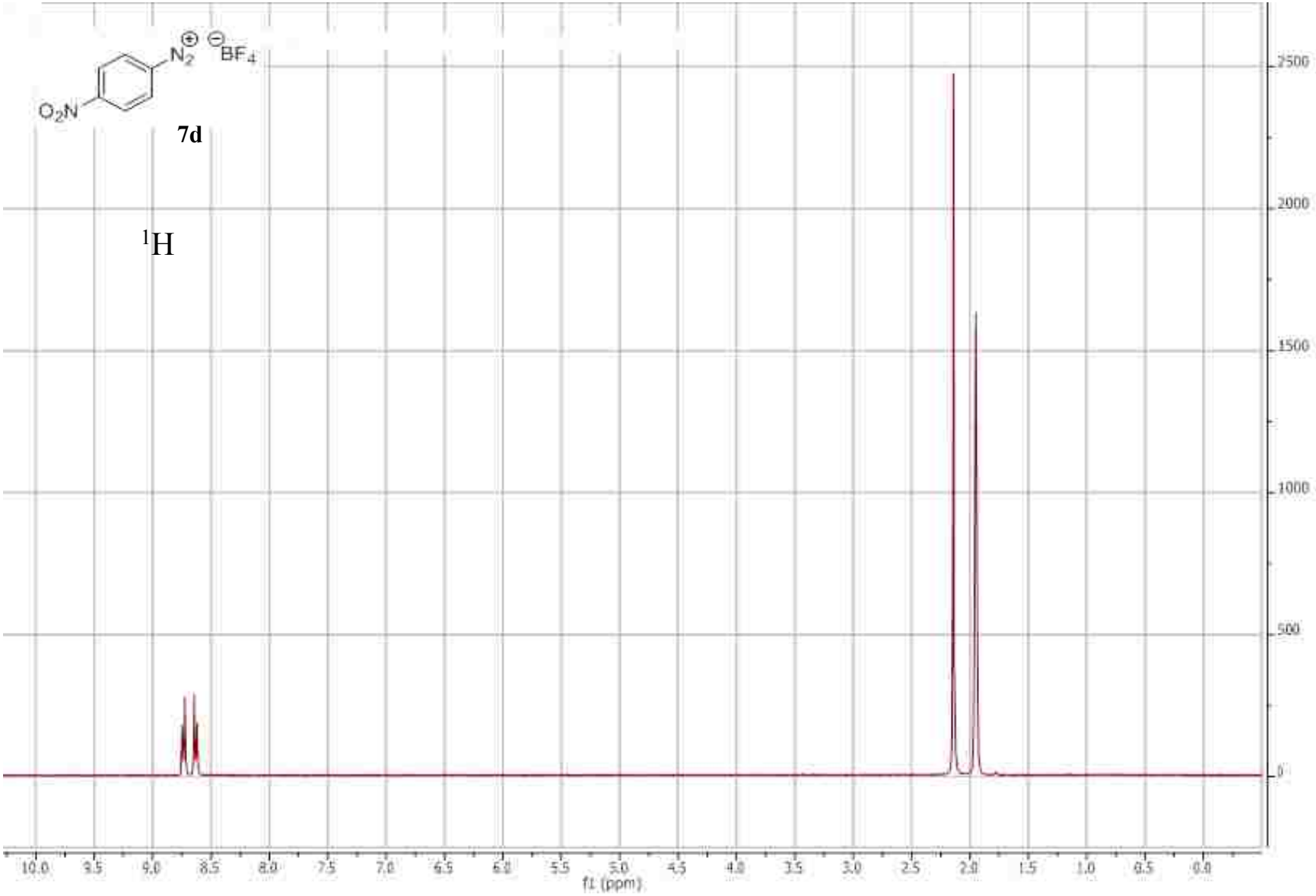
$N_2^{\oplus}$ $^{\ominus}BF_4$
O_2N
7d
^1H
2500
2000
1500
1000
500
0
10.0 9.5 9.0 8.5 8.0 7.5 7.0 6.5 6.0 5.5 5.0 4.5 4.0 3.5 3.0 2.5 2.0 1.5 1.0 0.5 0.0
f1 (ppm)

I. Water Contact Angle.

A water contact angle of 86 $^{o}\pm$ 2 ^{o} was observed for the organic thin film formed after 30 minutes of irradiation at 0.1M NBDT.

II. Experimental Setup.

Figure 2. Photograph of the apparatus used for immersion of gold substrates. The substrate is located at the center bottom area of the flask. The stir bar rotates at the side of the flask.

III. Control Experiments.

Figure 3. Control experiment for a sample prepared on Au(111) with 4-nitrobenzenediazonium tetrafluoroborate (NBDT) with no catalyst present. The spontaneous grafting of the diazonium salt was evaluated using 0.1 M NBDT for 30 min reaction time. (a) Topography (5×5 μm^2) and (b) concurrently acquired lateral force image obtained in air using contact mode AFM. (c) Cursor profile for the line drawn across three nanorings in a. For these conditions, the sample prepared without catalyst shows evidence of spontaneous grafting of polyphenylene at areas near the meniscus sites of the mesosphere masks to form ring nanostructures, with thicknesses ranging from 1 to 3 nm.

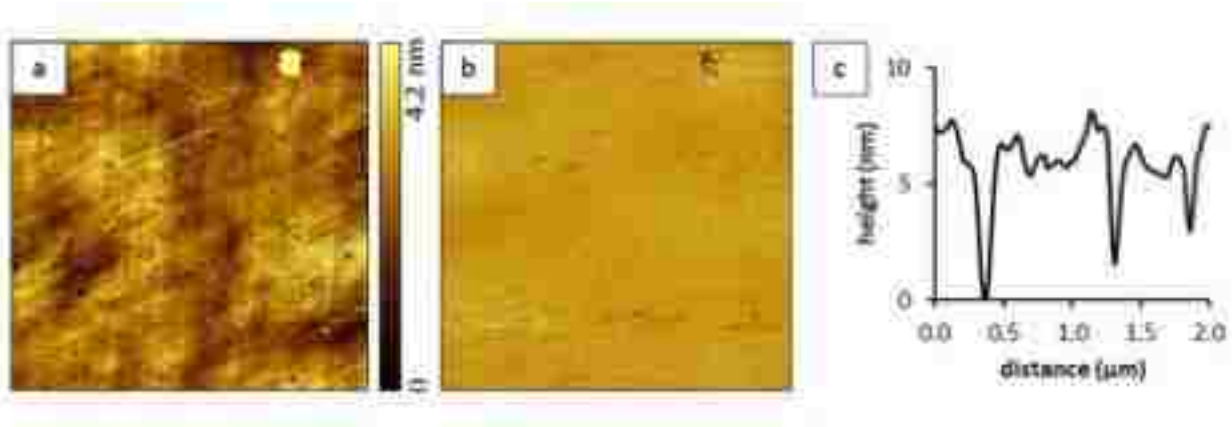

Figure 4. Control experiment for a sample prepared without visible light irradiation of $Ru(bpy)_3(PF_6)_2$ in the presence of 0.1 M *p*-nitrobenzenediazonium tetrafluoroborate (NBDT). (a) Topography (6×6 μm^2) image acquired in air after 30 min immersion in NBDT; (b) corresponding lateral force frame; (c) Cursor profile for the white line in a. The sample prepared without visible light illumination reveals evidence of the spontaneous grafting of polyphenylene at areas throughout the sample, measuring 7 ± 2 nm in thickness. A periodic arrangement of nanopores is visible in the topography frame, however the resolution in the lateral force image was not sufficient to reveal the locations of nanopores.

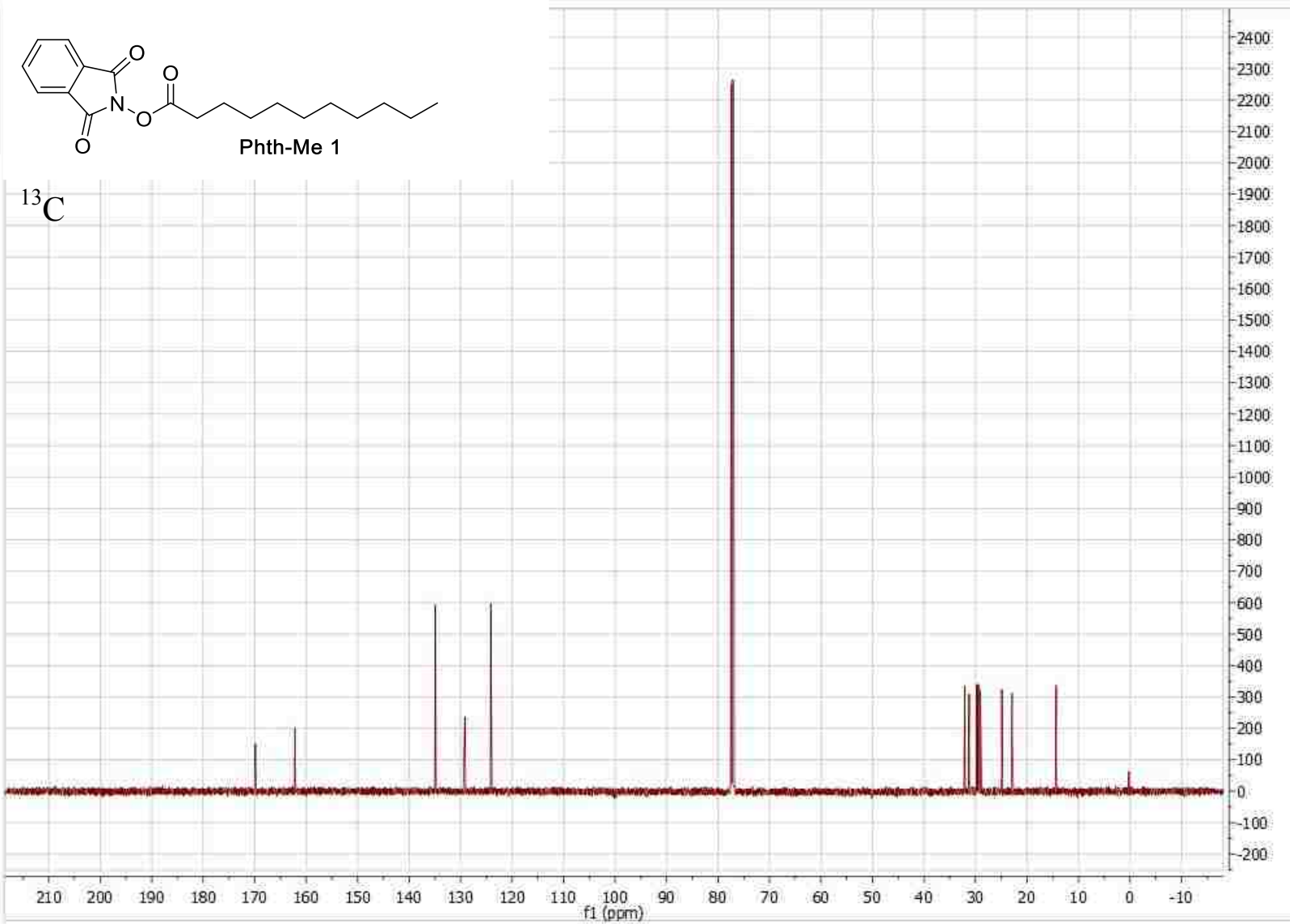
Phth-Me 1
13C
f1 (ppm)

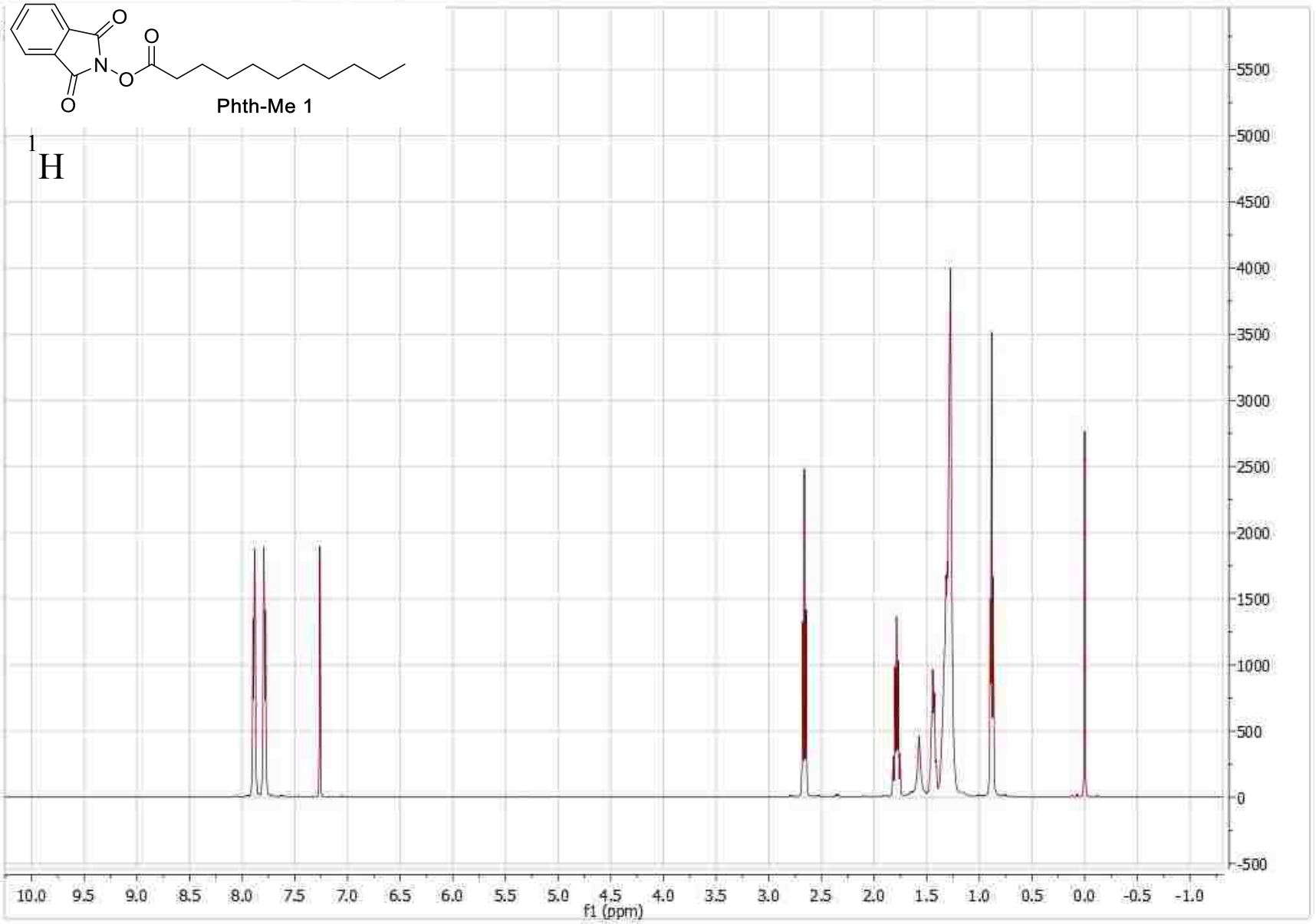
Phth-Me 1
1H
5500
5000
4500
4000
3500
3000
2500
2000
1500
1000
500
0
-500
10.0 9.5 9.0 8.5 8.0 7.5 7.0 6.5 6.0 5.5 5.0 4.5 4.0 3.5 3.0 2.5 2.0 1.5 1.0 0.5 0.0 -0.5 -1.0
f1 (ppm)

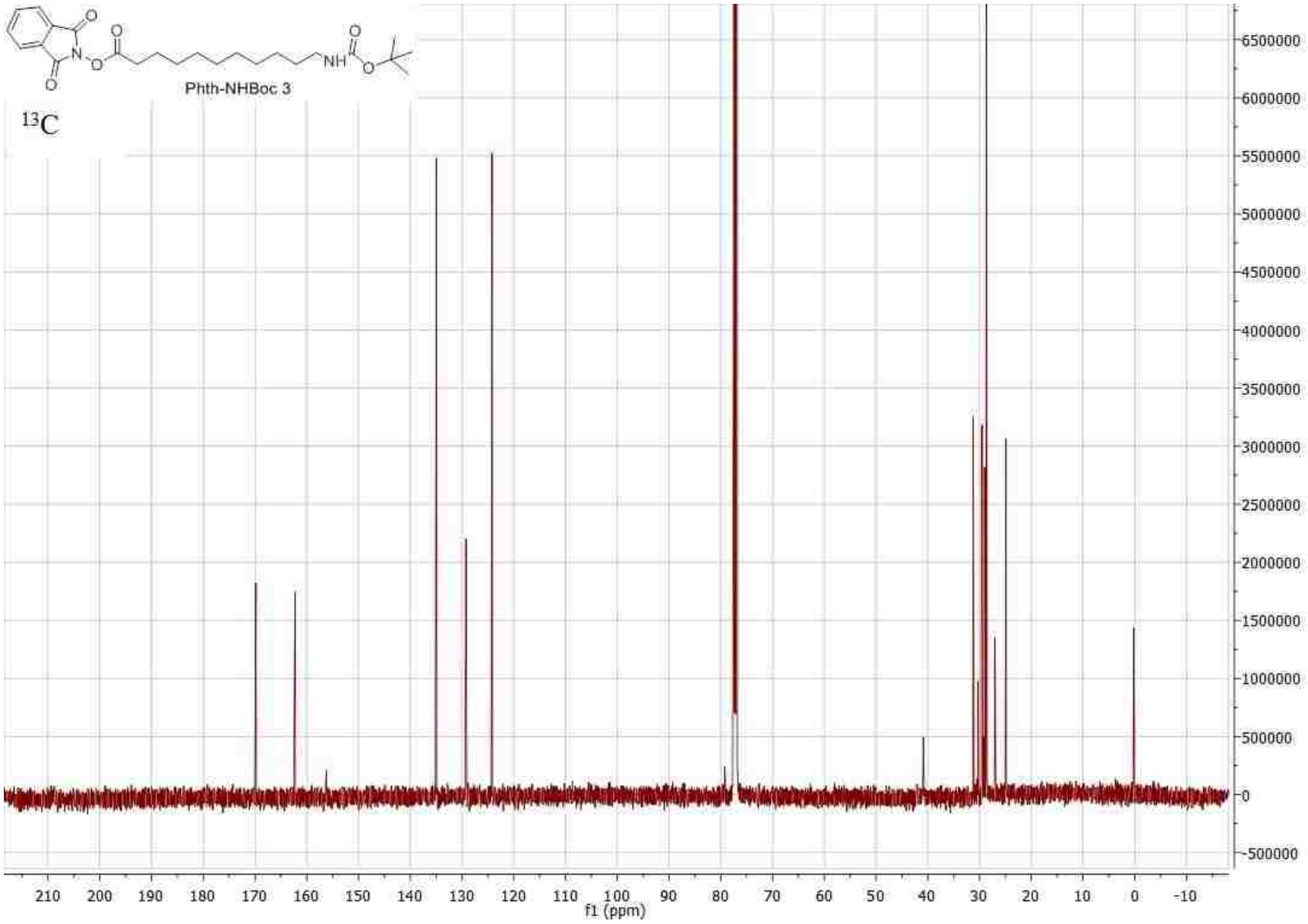
Phth-NHBoc 3
13C
6500000
6000000
5500000
5000000
4500000
4000000
3500000
3000000
2500000
2000000
1500000
1000000
500000
0
-500000
210 200 190 180 170 160 150 140 130 120 110 100 90 80 70 60 50 40 30 20 10 0 -10
f1 (ppm)

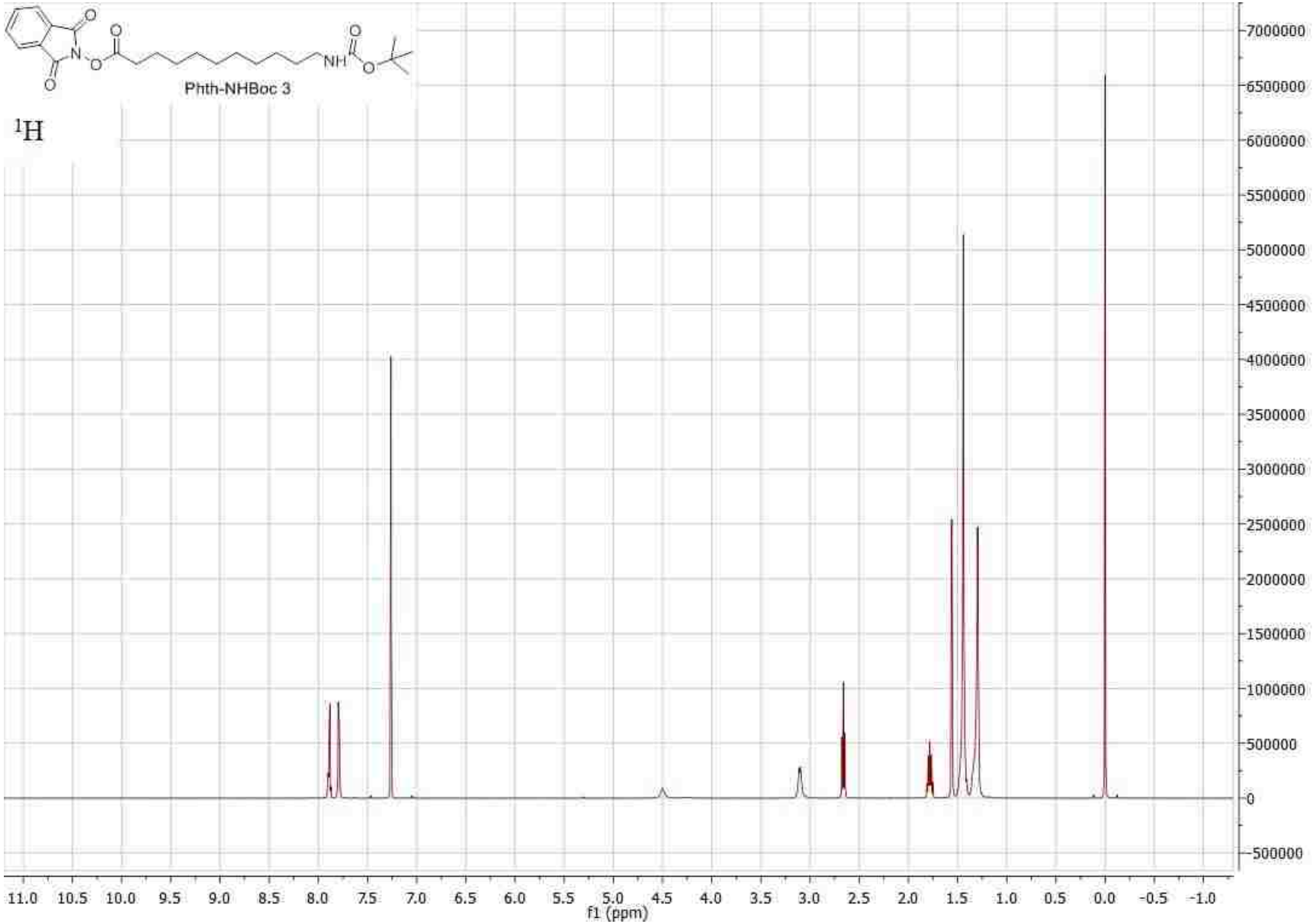
Phth-NHBoc 3
^{1}H
7000000
6500000
6000000
5500000
5000000
4500000
4000000
3500000
3000000
2500000
2000000
1500000
1000000
500000
0
-500000
11.0 10.5 10.0 9.5 9.0 8.5 8.0 7.5 7.0 6.5 6.0 5.5 5.0 4.5 4.0 3.5 3.0 2.5 2.0 1.5 1.0 0.5 0.0 -0.5 -1.0
f1 (ppm)

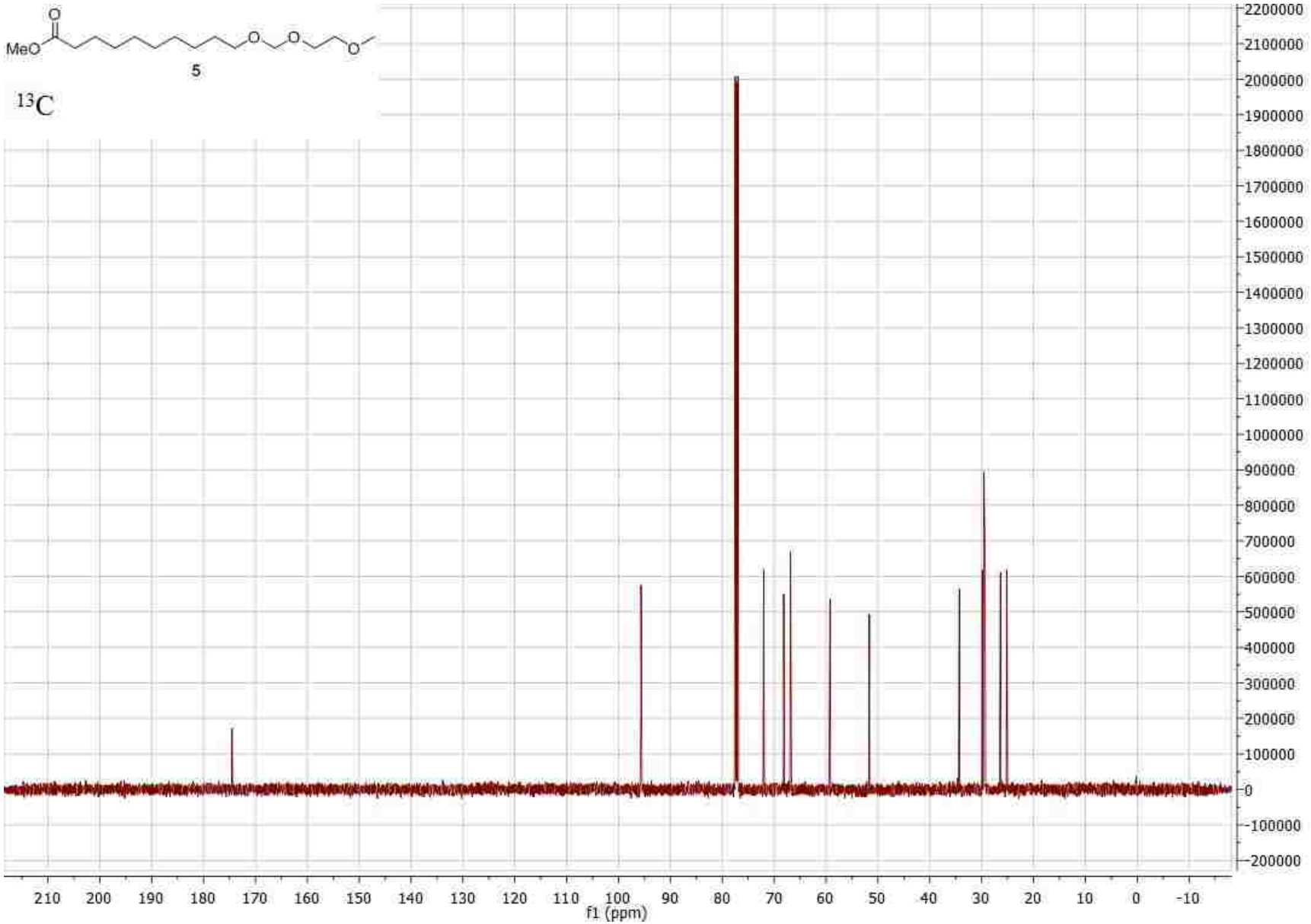
MeO
O
O
O
O
5
13C
2200000
2100000
2000000
1900000
1800000
1700000
1600000
1500000
1400000
1300000
1200000
1100000
1000000
900000
800000
700000
600000
500000
400000
300000
200000
100000
0
-100000
-200000
210 200 190 180 170 160 150 140 130 120 110 100 90 80 70 60 50 40 30 20 10 0 -10
f1 (ppm)

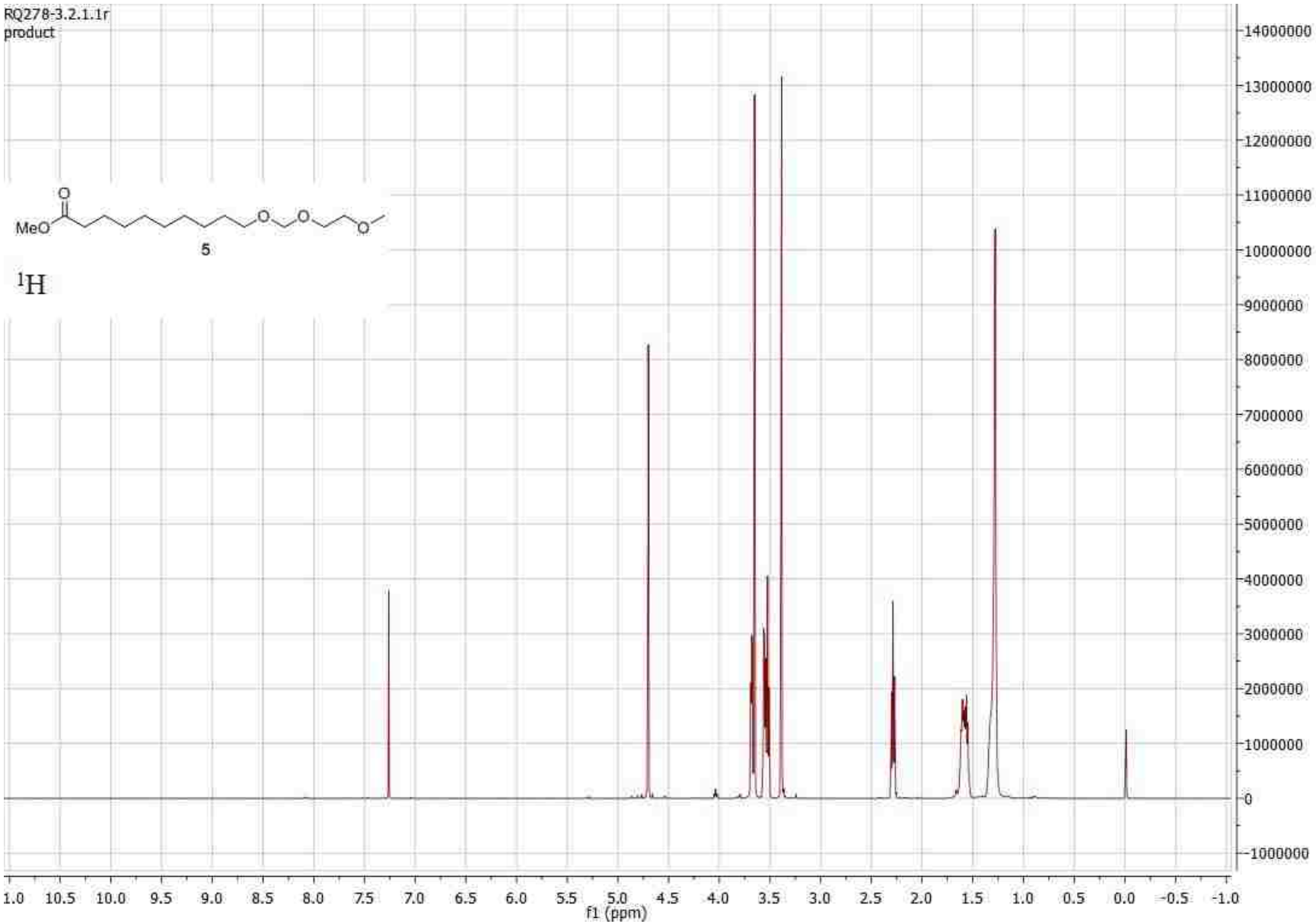
RQ278-3.2.1.1r
product
MeO
O
O
O
O
5
^{1}H
14000000
13000000
12000000
11000000
10000000
9000000
8000000
7000000
6000000
5000000
4000000
3000000
2000000
1000000
0
-1000000
1.0 10.5 10.0 9.5 9.0 8.5 8.0 7.5 7.0 6.5 6.0 5.5 5.0 4.5 4.0 3.5 3.0 2.5 2.0 1.5 1.0 0.5 0.0 -0.5 -1.0
f1 (ppm)

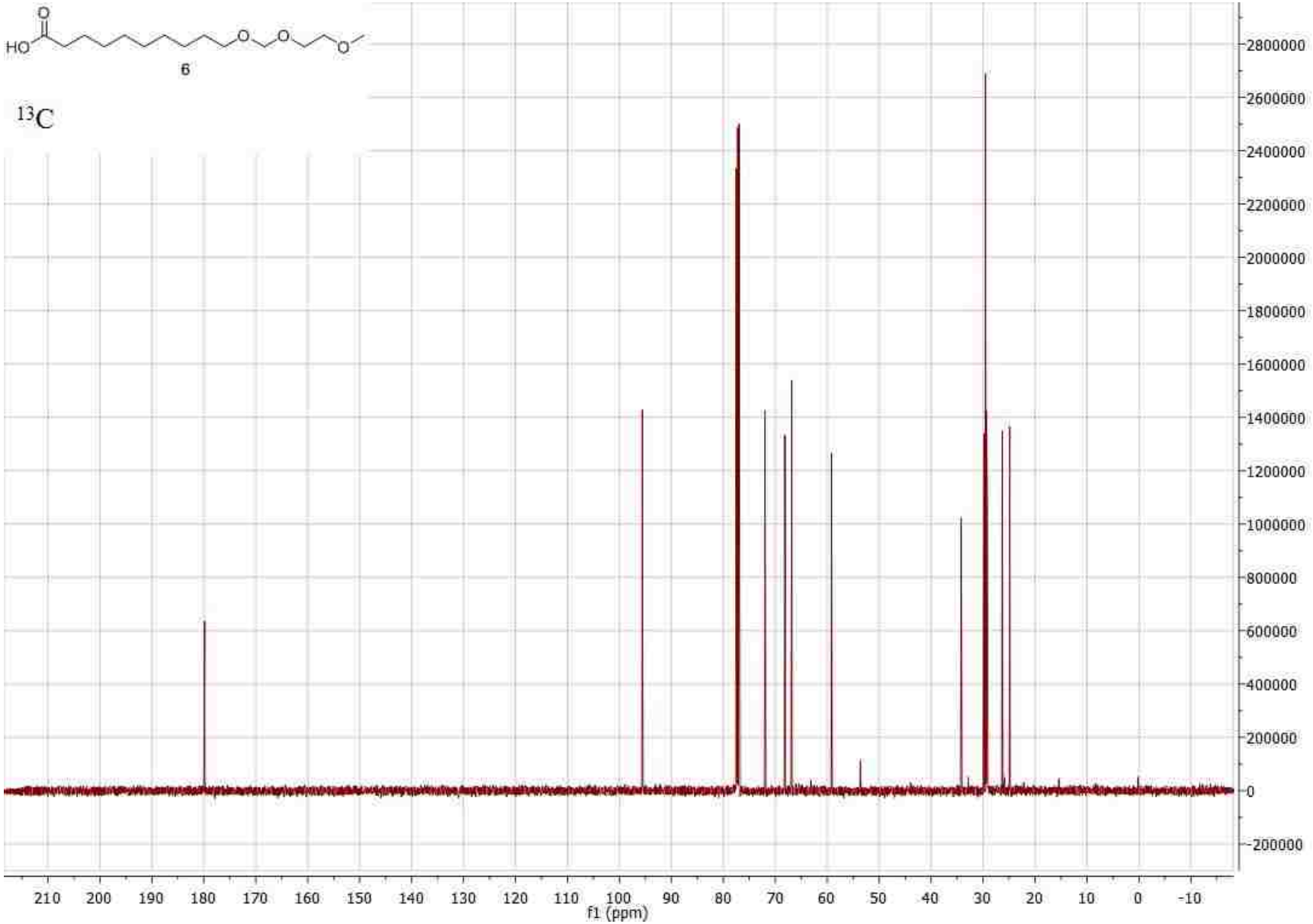
HO
O
O
O
O
6
^{13}C
2800000
2600000
2400000
2200000
2000000
1800000
1600000
1400000
1200000
1000000
800000
600000
400000
200000
0
-200000
210 200 190 180 170 160 150 140 130 120 110 100 90 80 70 60 50 40 30 20 10 0 -10
f1 (ppm)

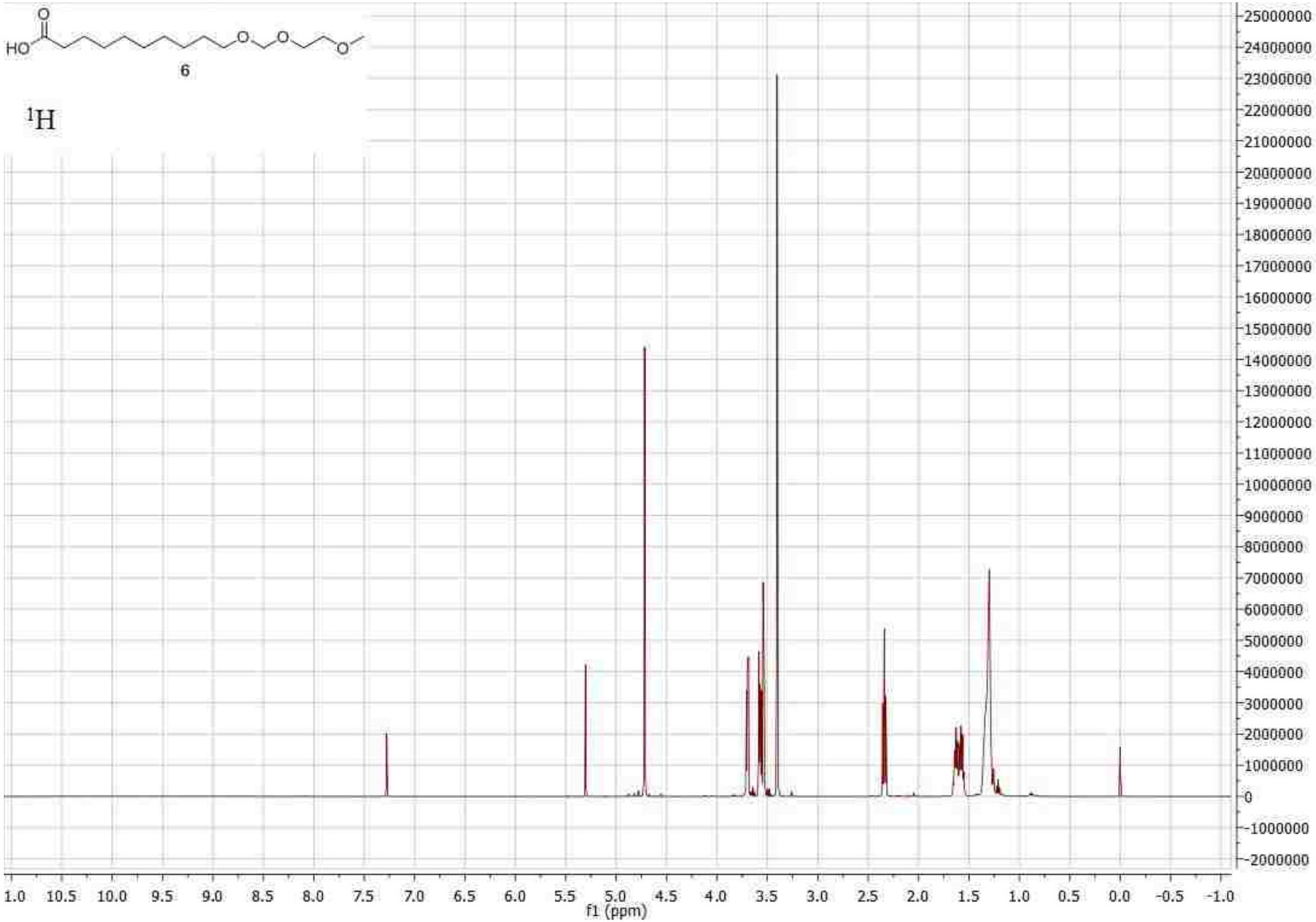
HO
O
O
O
O
6
^{1}H
25000000
24000000
23000000
22000000
21000000
20000000
19000000
18000000
17000000
16000000
15000000
14000000
13000000
12000000
11000000
10000000
9000000
8000000
7000000
6000000
5000000
4000000
3000000
2000000
1000000
0
-1000000
-2000000
1.0 10.5 10.0 9.5 9.0 8.5 8.0 7.5 7.0 6.5 6.0 5.5 5.0 4.5 4.0 3.5 3.0 2.5 2.0 1.5 1.0 0.5 0.0 -0.5 -1.0
f1 (ppm)

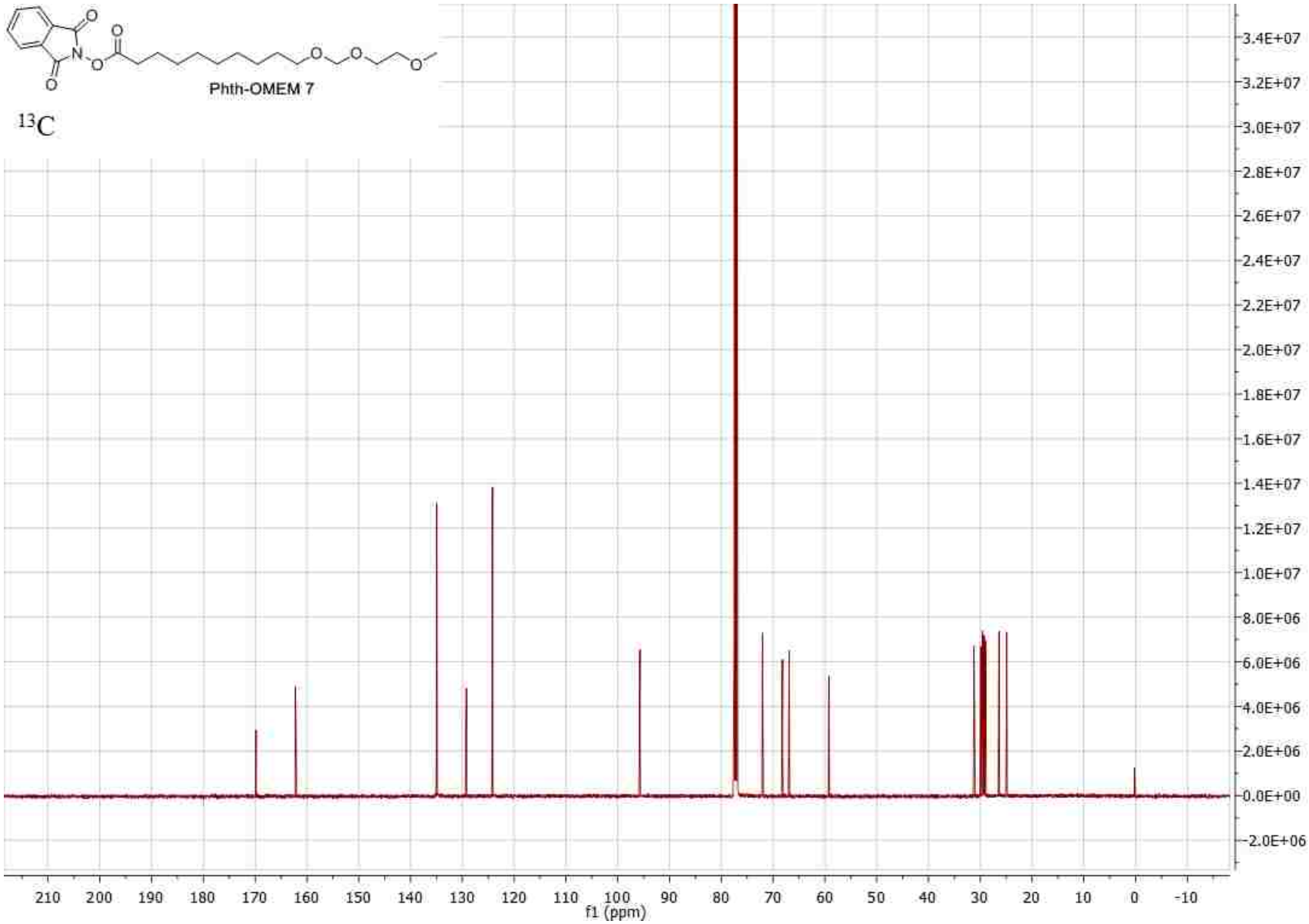
Phth-OMEM 7
13C
3.4E+07
3.2E+07
3.0E+07
2.8E+07
2.6E+07
2.4E+07
2.2E+07
2.0E+07
1.8E+07
1.6E+07
1.4E+07
1.2E+07
1.0E+07
8.0E+06
6.0E+06
4.0E+06
2.0E+06
0.0E+00
-2.0E+06
210 200 190 180 170 160 150 140 130 120 110 100 90 80 70 60 50 40 30 20 10 0 -10
f1 (ppm)

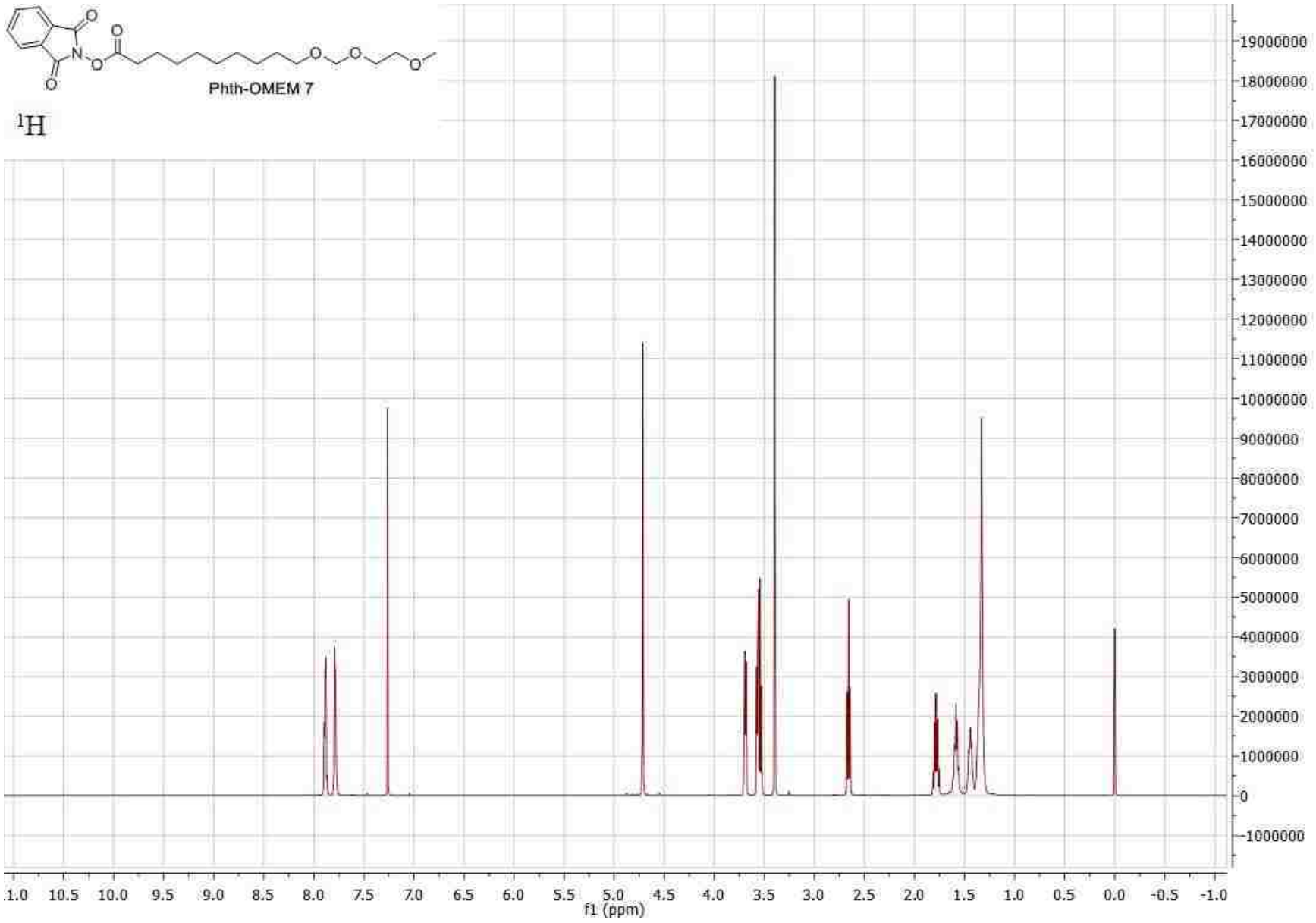
Phth-OMEM 7
^{1}H
19000000
18000000
17000000
16000000
15000000
14000000
13000000
12000000
11000000
10000000
9000000
8000000
7000000
6000000
5000000
4000000
3000000
2000000
1000000
0
-1000000
10.5 10.0 9.5 9.0 8.5 8.0 7.5 7.0 6.5 6.0 5.5 5.0 4.5 4.0 3.5 3.0 2.5 2.0 1.5 1.0 0.5 0.0 -0.5 -1.0
f1 (ppm)

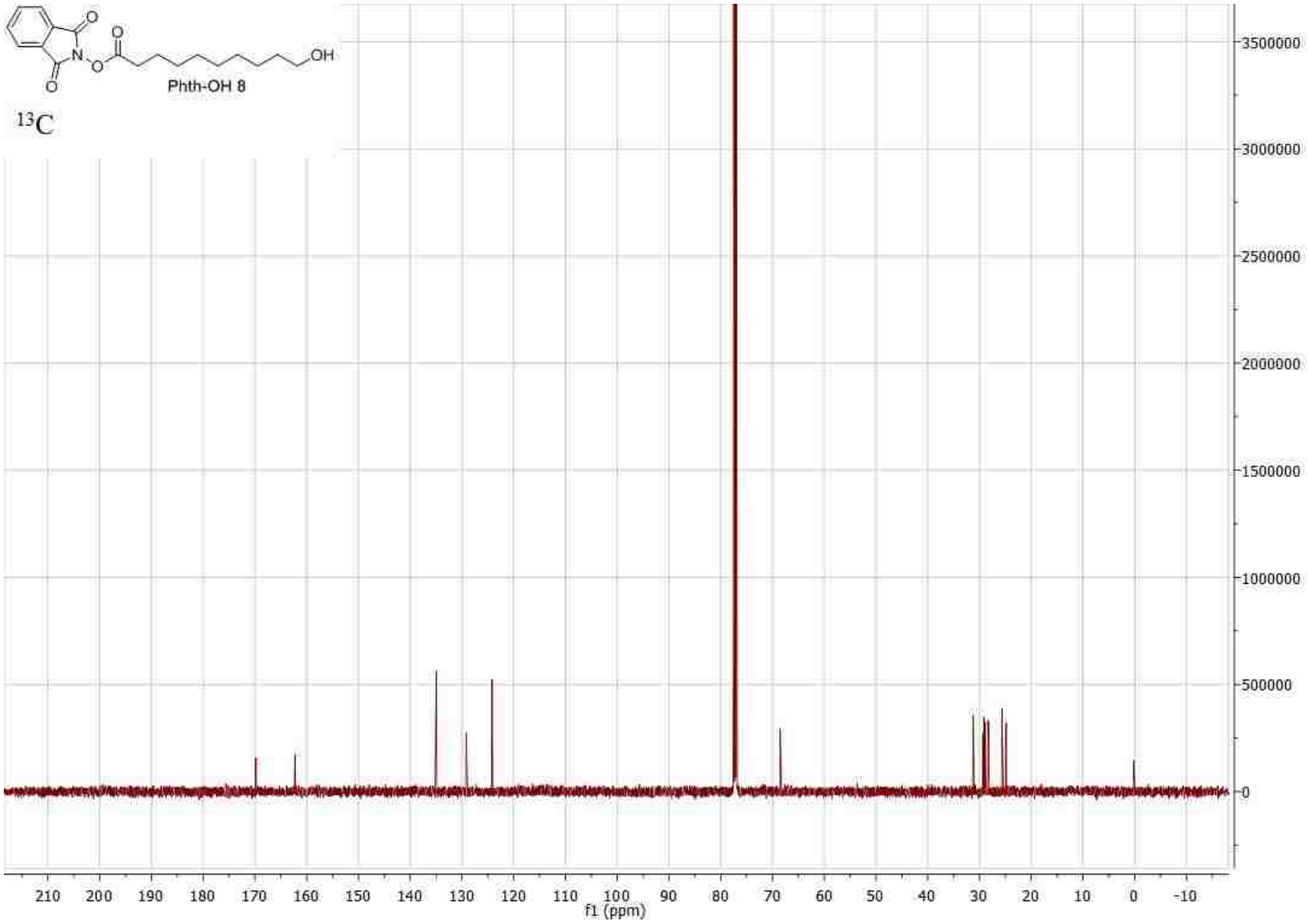
Phth-OH 8
13C
3500000
3000000
2500000
2000000
1500000
1000000
500000
0
210 200 190 180 170 160 150 140 130 120 110 100 90 80 70 60 50 40 30 20 10 0 -10
f1 (ppm)

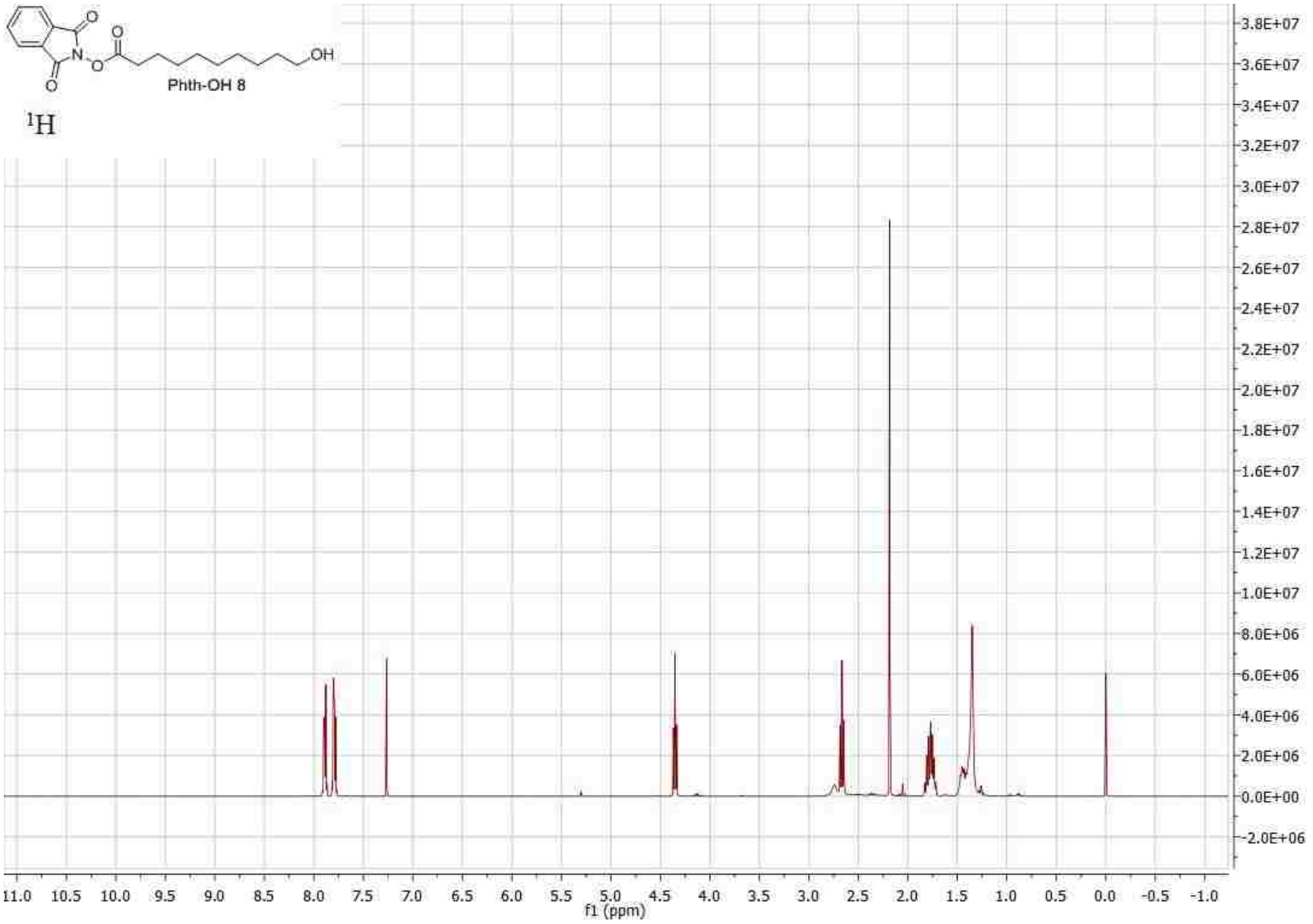
Phth-OH 8
^{1}H
3.8E+07
3.6E+07
3.4E+07
3.2E+07
3.0E+07
2.8E+07
2.6E+07
2.4E+07
2.2E+07
2.0E+07
1.8E+07
1.6E+07
1.4E+07
1.2E+07
1.0E+07
8.0E+06
6.0E+06
4.0E+06
2.0E+06
0.0E+00
-2.0E+06
11.0 10.5 10.0 9.5 9.0 8.5 8.0 7.5 7.0 6.5 6.0 5.5 5.0 4.5 4.0 3.5 3.0 2.5 2.0 1.5 1.0 0.5 0.0 -0.5 -1.0
f1 (ppm)

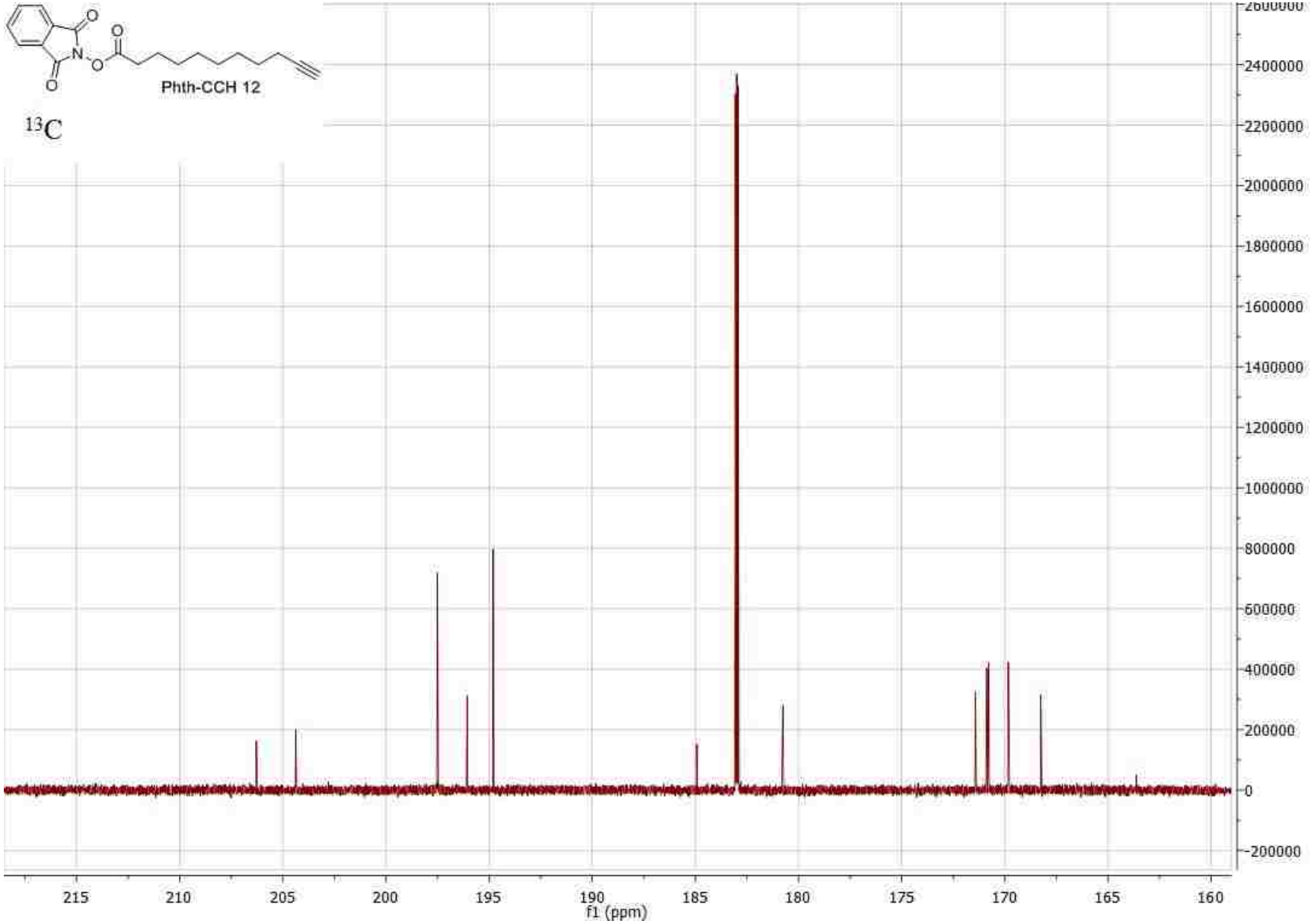
Phth-CCH 12
13C
2600000
2400000
2200000
2000000
1800000
1600000
1400000
1200000
1000000
800000
600000
400000
200000
0
-200000
215
210
205
200
195
190
185
180
175
170
165
160
f1 (ppm)

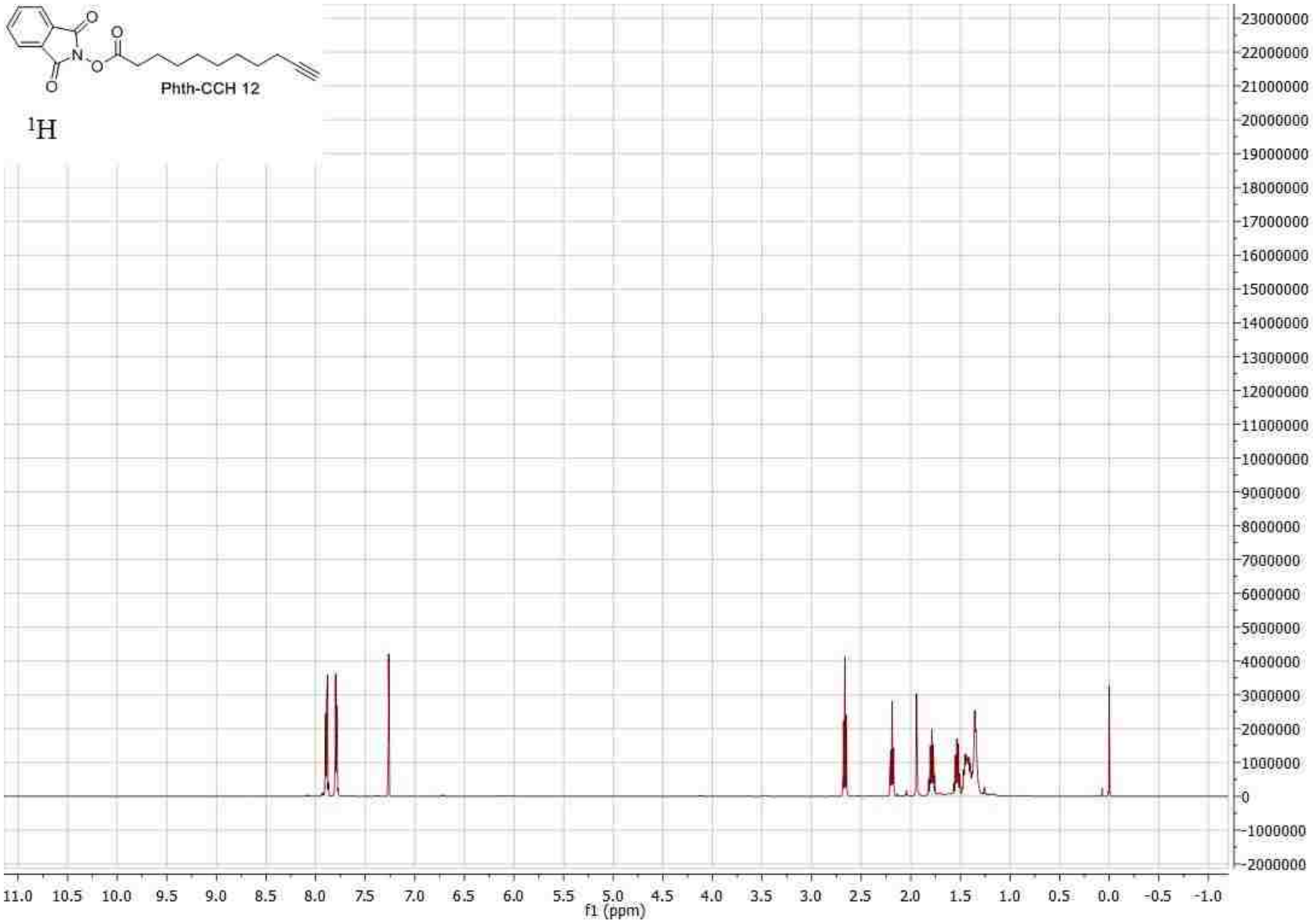
Phth-CCH 12
^{1}H
23000000
22000000
21000000
20000000
19000000
18000000
17000000
16000000
15000000
14000000
13000000
12000000
11000000
10000000
9000000
8000000
7000000
6000000
5000000
4000000
3000000
2000000
1000000
0
-1000000
-2000000
11.0 10.5 10.0 9.5 9.0 8.5 8.0 7.5 7.0 6.5 6.0 5.5 5.0 4.5 4.0 3.5 3.0 2.5 2.0 1.5 1.0 0.5 0.0 -0.5 -1.0
f1 (ppm)

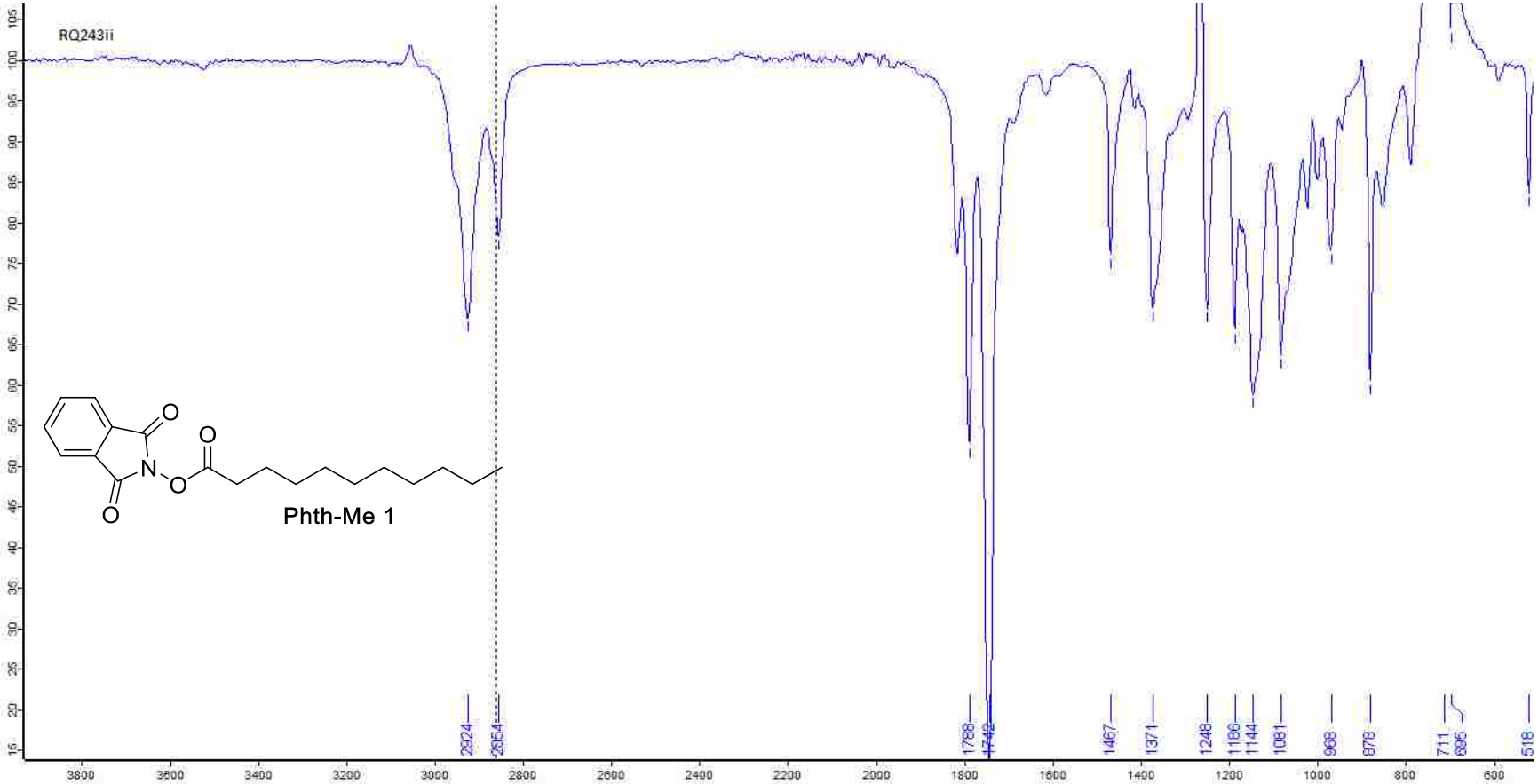

Figure 1. IR Spectra for Phth-Me **1**

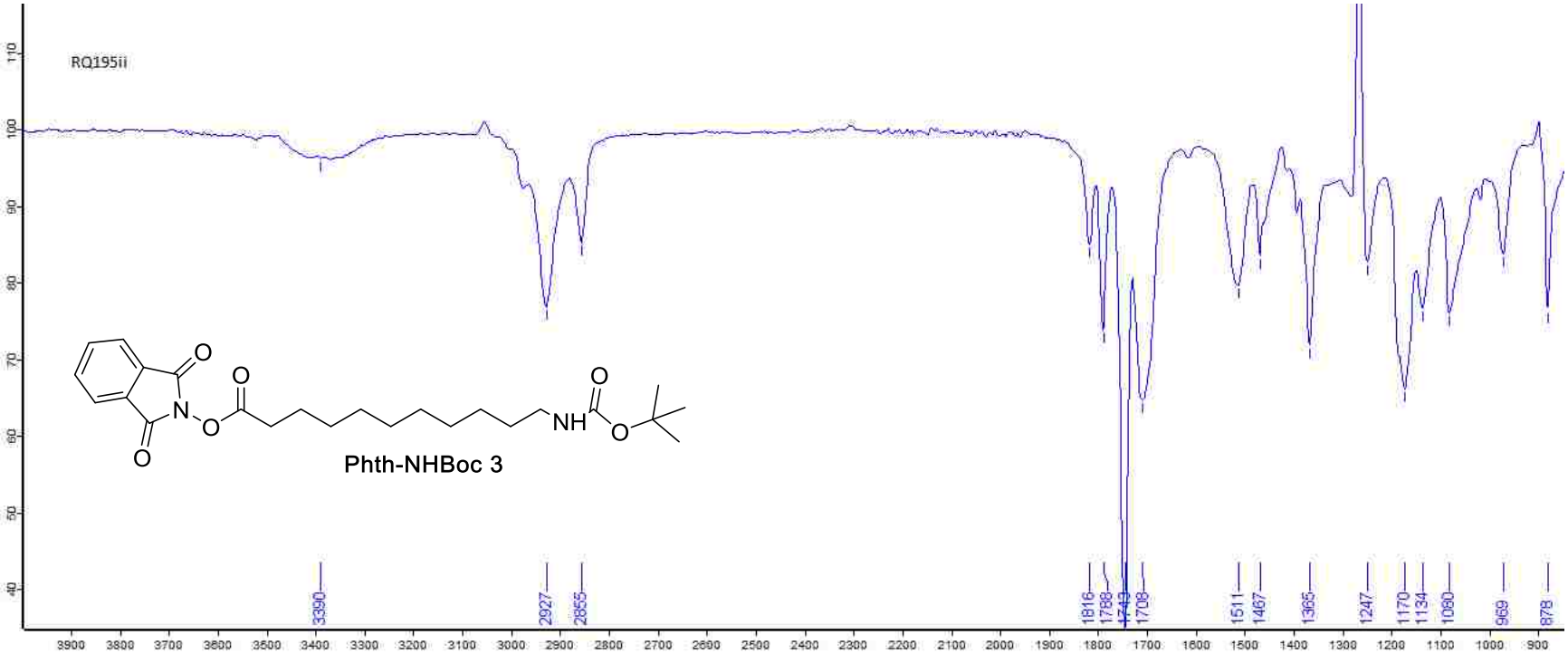

Figure 2. Phth-NHBoc **3** IR Spectraum

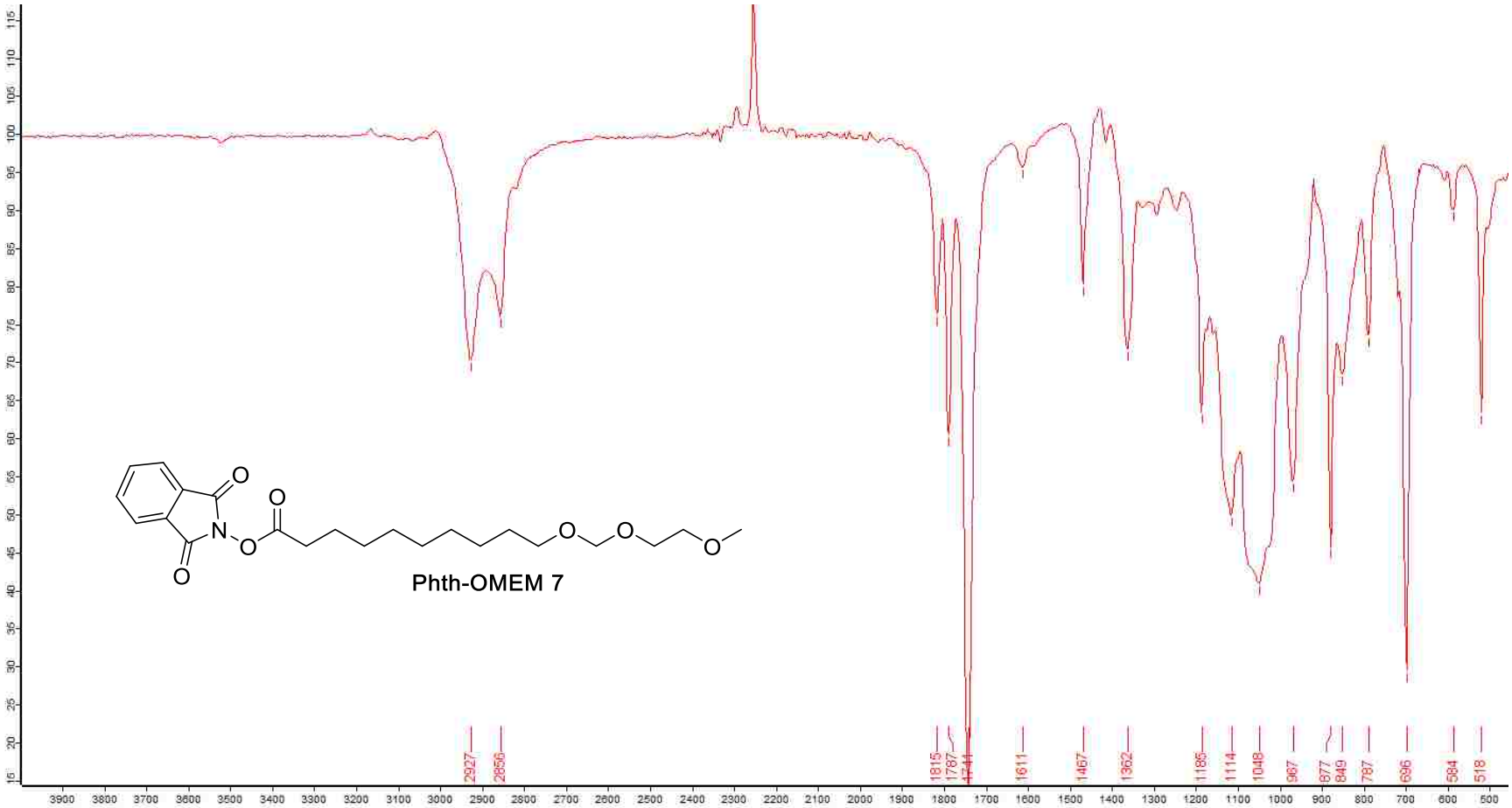

Figure 3. Phth-OMEM **7** IR spectrum

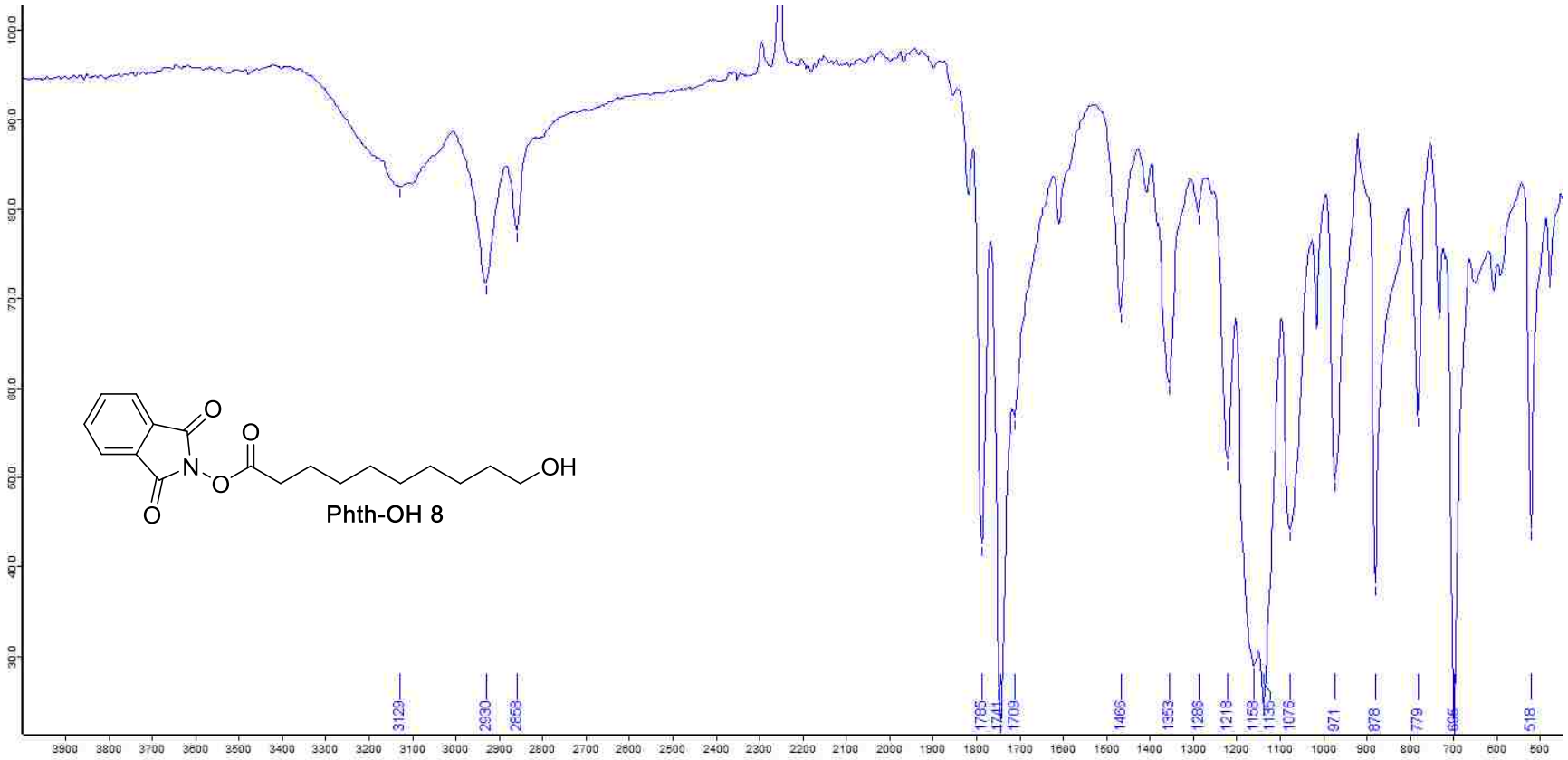

Figure 4. Phth-OH **8** IR Spectra

Experimental Setup

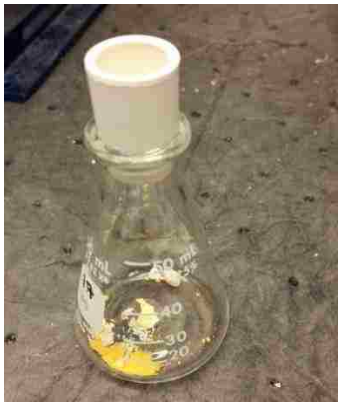

Figure 5. Grafting Setup with Stirbar, BNAH, and Template-Stripped Gold Substrate in Preparation. This setup was used for particle lithography experiments.

Figure 6. Grafting Experiment in Progress. This setup was used for particle lithography experiments. Note that the stirbar (at bottom of the image) has been physically separated from the Au substrate (near the LED strip on the other side of the Erlenmeyer flask) to prevent perturbation of the substrate.

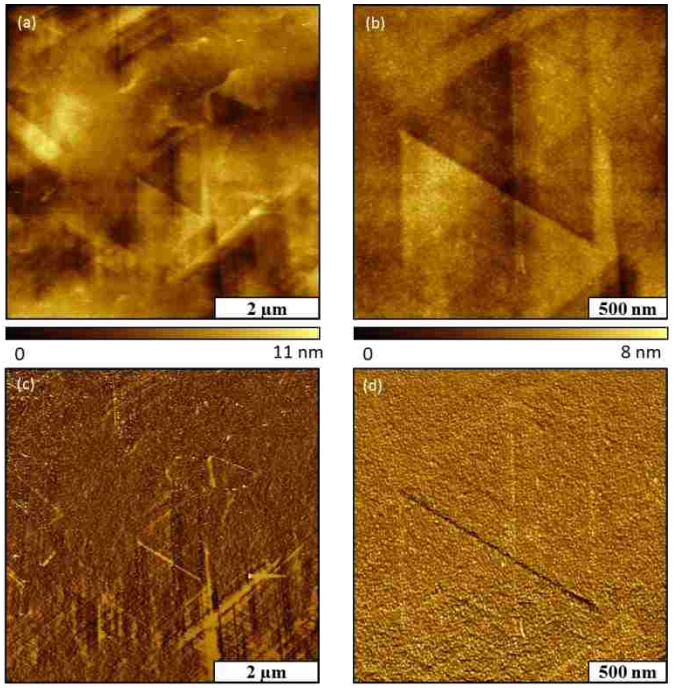

Figure 7. Control Sample Prepared without Adding Phthalimide Ester. The irradiation of BNAH and $Ru(bpy)_3Cl_2$ in MeCN was conducted for 30 min in the presence of a mask of silicon dioxide mesospheres (500 nm) on Au(111). Tapping mode images were acquired after the removal of the particle mask. (a) Topography image; (b) zoom-in view; (c) corresponding phase image of *a* (d) phase image of *b*. No nanostructures were detected, indicating the absence of a thin film. Without phthalimide ester, a thin film is not produced on Au(111).

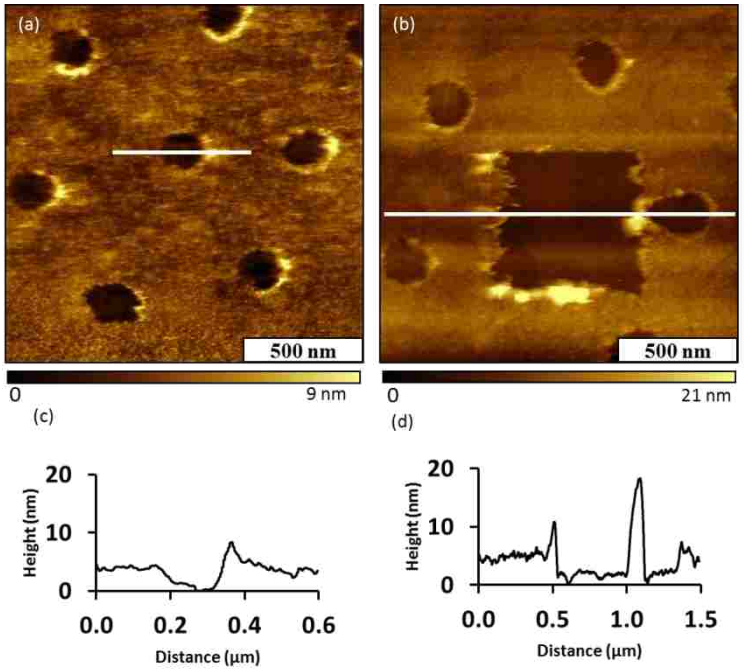

Figure 8. Control Sample of Au-Me Prepared without Applying Visible Light Irradiation. (a) Topograph; (b) nanoshaved area within the Au-Me film; (c) cursor profile for line in *a*; (d) cursor profile for line in *b*. The sample acquired without visible light irradiation reveals spontaneous grafting on Au(111), with a film measuring 4.0 ± 0.5 nm in thickness. Nanoshaving was conducted using contact mode in an ethanolic solution with 10 nN of applied force. The film prepared without the presence of applied visible light irradiation was easily removed with nanoshaving.

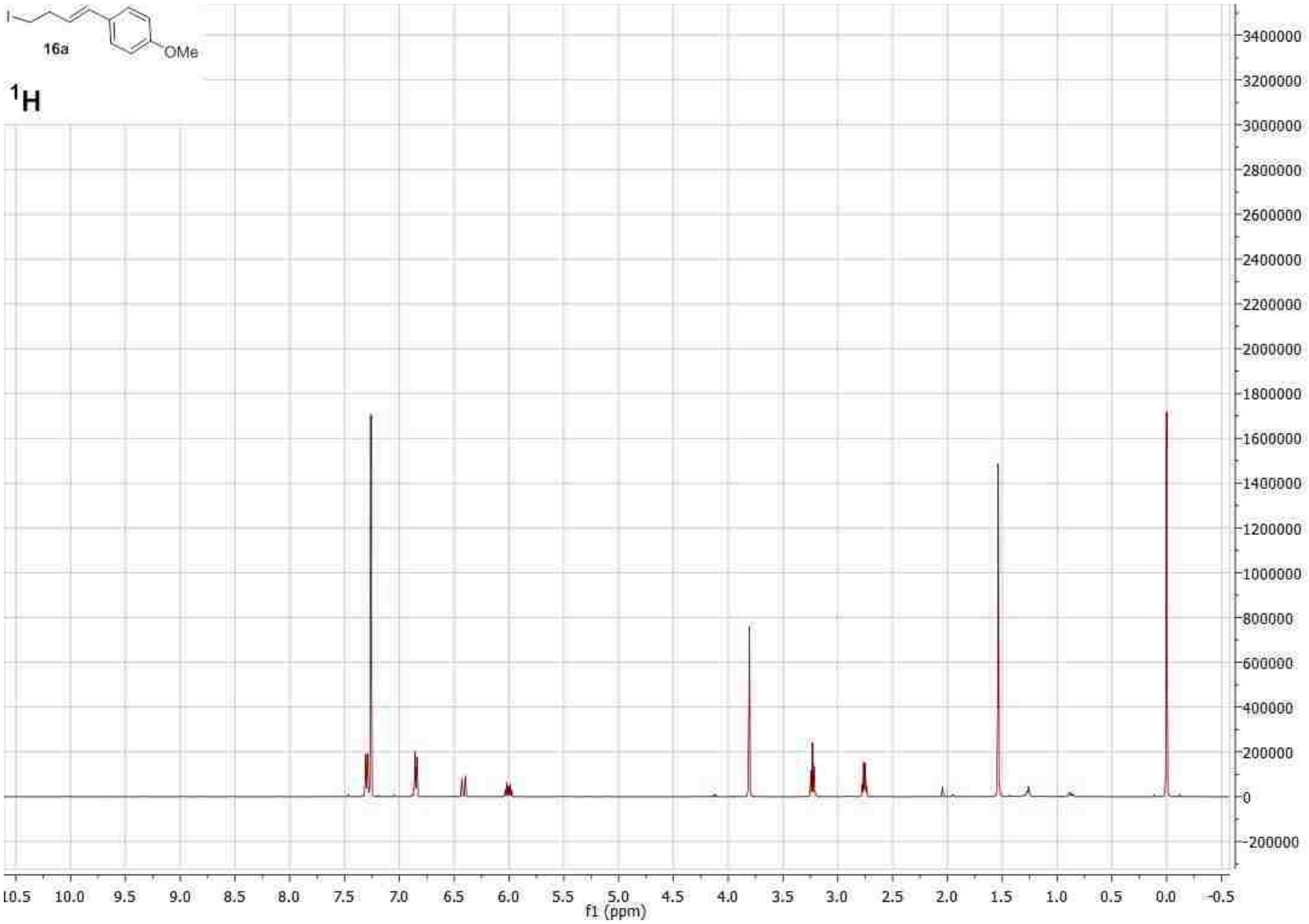
16a
OMe
1H
3400000
3200000
3000000
2800000
2600000
2400000
2200000
2000000
1800000
1600000
1400000
1200000
1000000
800000
600000
400000
200000
0
-200000
10.5 10.0 9.5 9.0 8.5 8.0 7.5 7.0 6.5 6.0 5.5 5.0 4.5 4.0 3.5 3.0 2.5 2.0 1.5 1.0 0.5 0.0 -0.5
f1 (ppm)

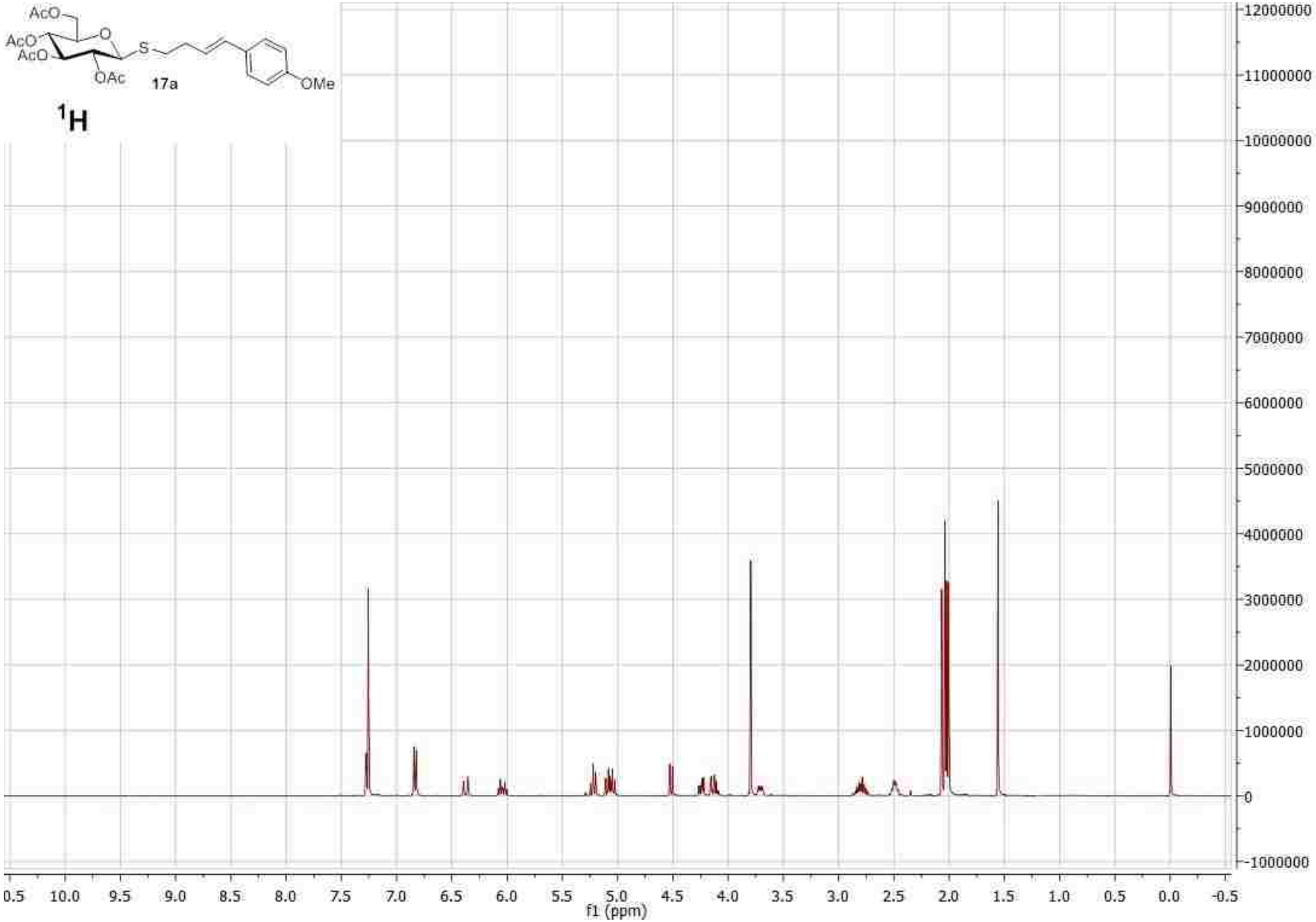
AcO
AcO
AcO
OAc
O
S
OMe
17a
1H
12000000
11000000
10000000
9000000
8000000
7000000
6000000
5000000
4000000
3000000
2000000
1000000
0
-1000000
10.5
10.0
9.5
9.0
8.5
8.0
7.5
7.0
6.5
6.0
5.5
5.0
4.5
4.0
3.5
3.0
2.5
2.0
1.5
1.0
0.5
0.0
-0.5
f1 (ppm)

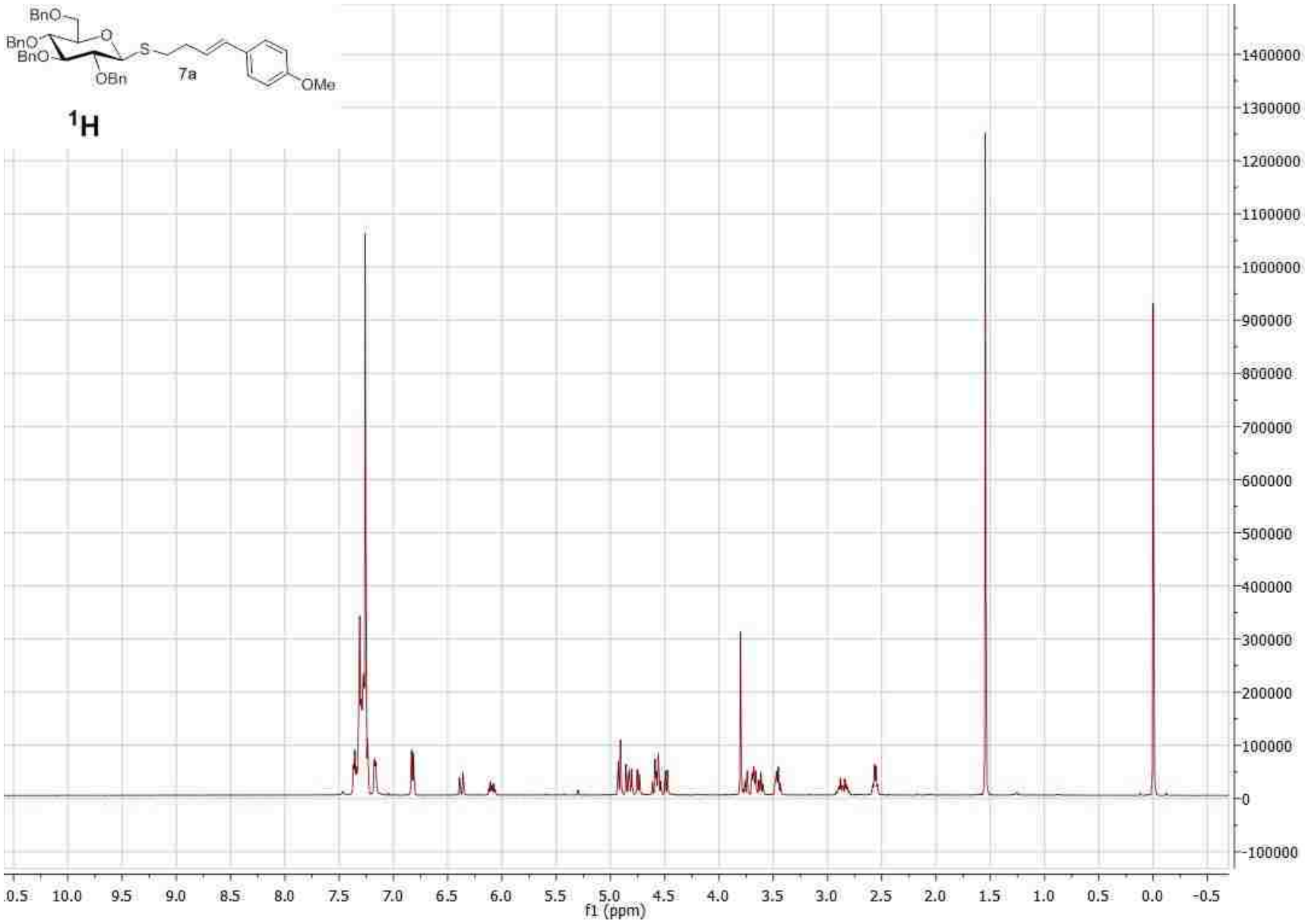
BnO
BnO
BnO
OBn
S
7a
OMe
1H
1400000
1300000
1200000
1100000
1000000
900000
800000
700000
600000
500000
400000
300000
200000
100000
0
-100000
10.0
9.5
9.0
8.5
8.0
7.5
7.0
6.5
6.0
5.5
5.0
4.5
4.0
3.5
3.0
2.5
2.0
1.5
1.0
0.5
0.0
-0.5
f1 (ppm)

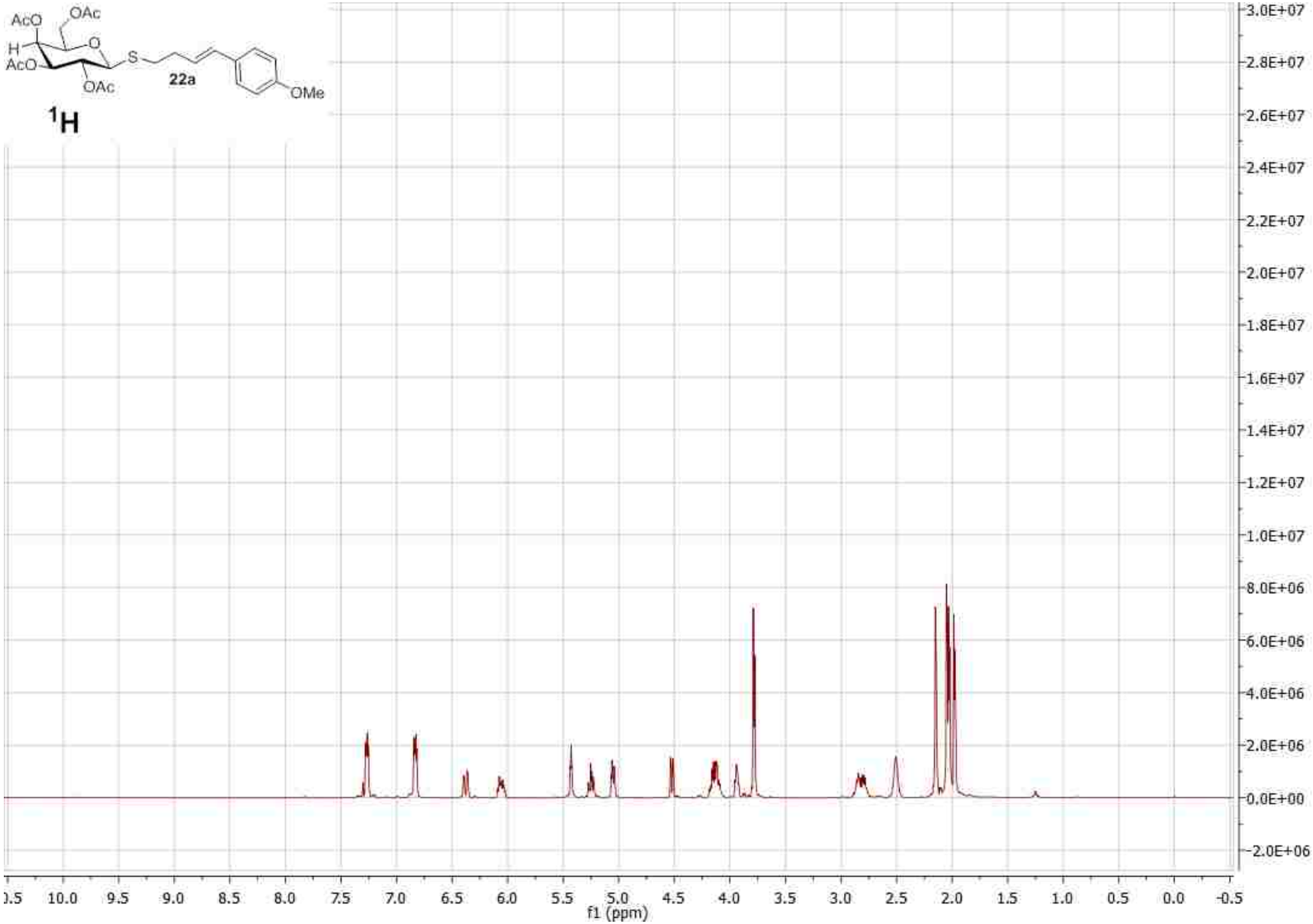
AcO
OAc
H
AcO
O
S
OAc
22a
OMe
1H
3.0E+07
2.8E+07
2.6E+07
2.4E+07
2.2E+07
2.0E+07
1.8E+07
1.6E+07
1.4E+07
1.2E+07
1.0E+07
8.0E+06
6.0E+06
4.0E+06
2.0E+06
0.0E+00
-2.0E+06
10.0
9.5
9.0
8.5
8.0
7.5
7.0
6.5
6.0
5.5
5.0
4.5
4.0
3.5
3.0
2.5
2.0
1.5
1.0
0.5
0.0
-0.5
f1 (ppm)

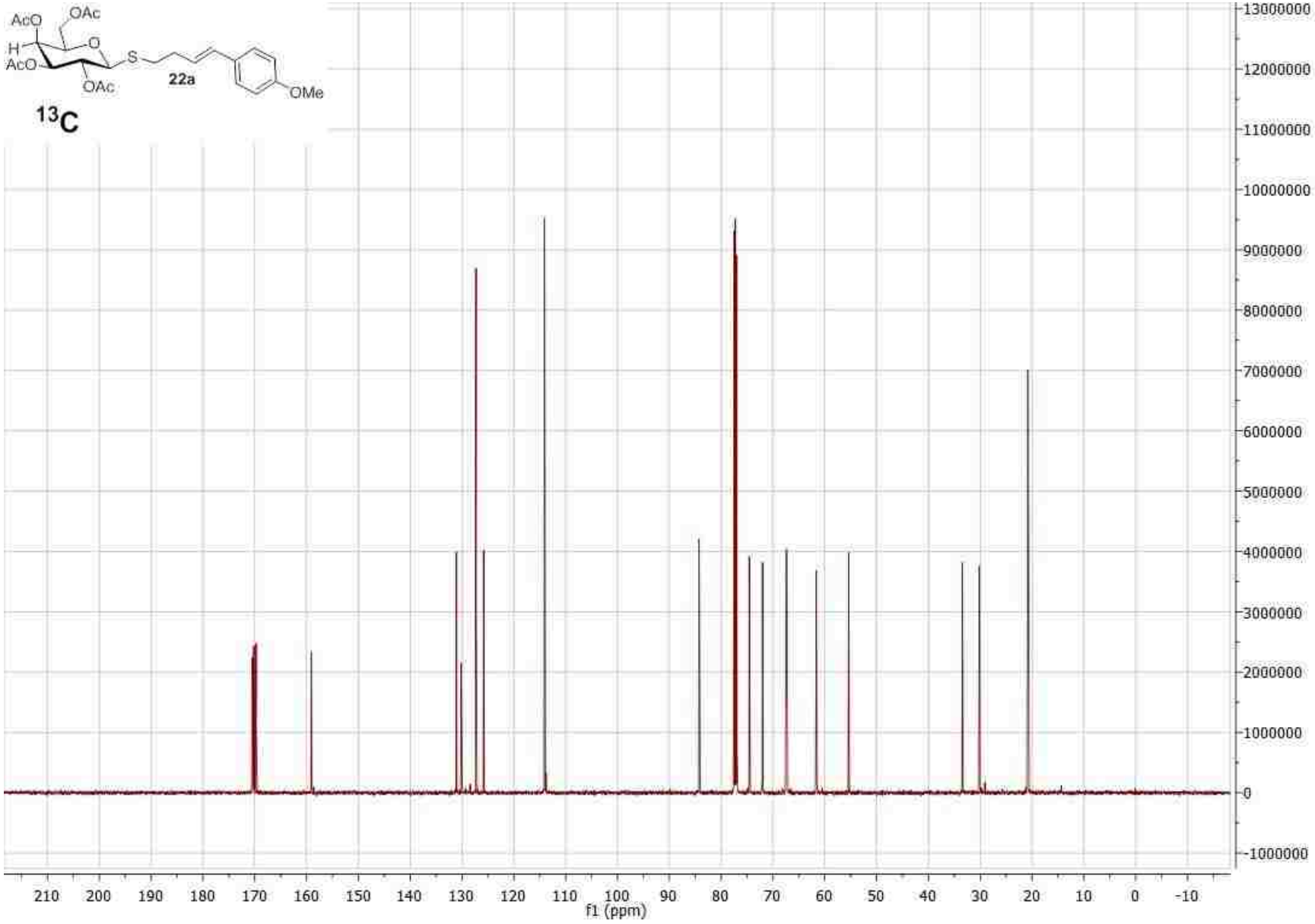
AcO
OAc
H
AcO
O
S
OAc
22a
OMe
13C
13000000
12000000
11000000
10000000
9000000
8000000
7000000
6000000
5000000
4000000
3000000
2000000
1000000
0
-1000000
210 200 190 180 170 160 150 140 130 120 110 100 90 80 70 60 50 40 30 20 10 0 -10
f1 (ppm)

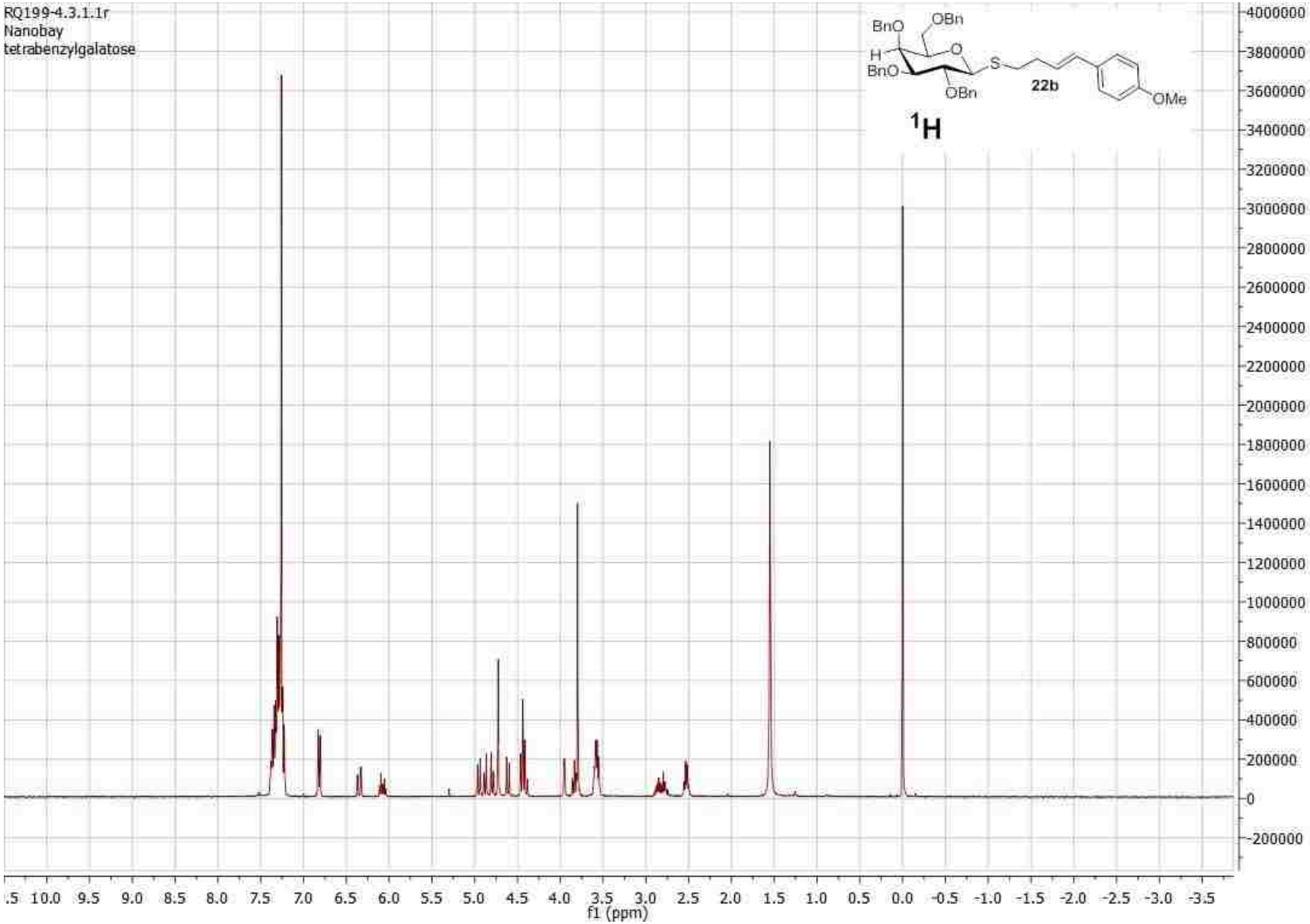
RQ199-4.3.1.1r
Nanobay
tetrabenzylgalatose
BnO
OBn
H
O
S
BnO
OBn
22b
OMe
1H
4000000
3800000
3600000
3400000
3200000
3000000
2800000
2600000
2400000
2200000
2000000
1800000
1600000
1400000
1200000
1000000
800000
600000
400000
200000
0
-200000
10.0 9.5 9.0 8.5 8.0 7.5 7.0 6.5 6.0 5.5 5.0 4.5 4.0 3.5 3.0 2.5 2.0 1.5 1.0 0.5 0.0 -0.5 -1.0 -1.5 -2.0 -2.5 -3.0 -3.5
f1 (ppm)

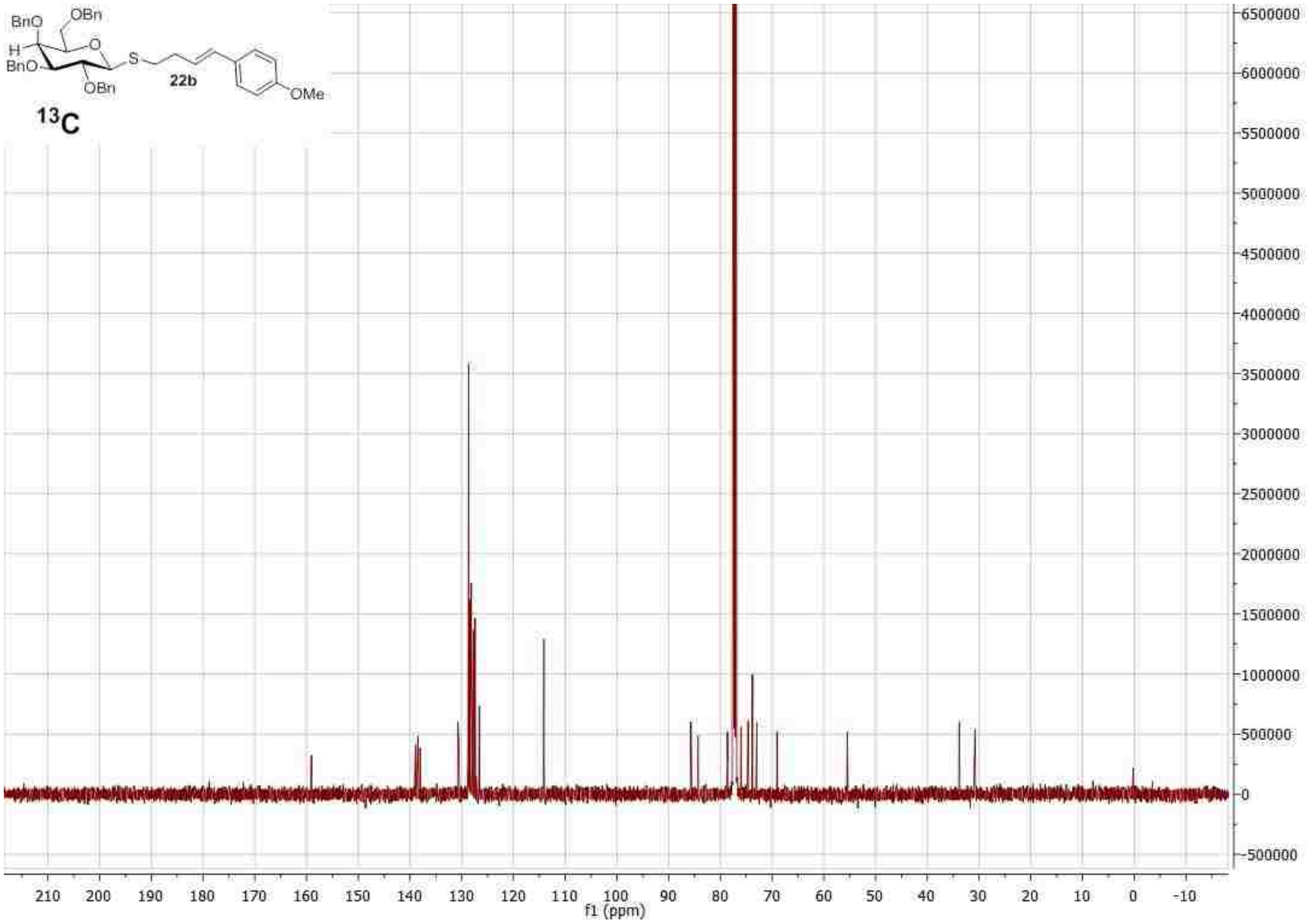
BnO
OBn
H
BnO
O
S
OBn
22b
OMe
13C
6500000
6000000
5500000
5000000
4500000
4000000
3500000
3000000
2500000
2000000
1500000
1000000
500000
0
-500000
210 200 190 180 170 160 150 140 130 120 110 100 90 80 70 60 50 40 30 20 10 0 -10
f1 (ppm)

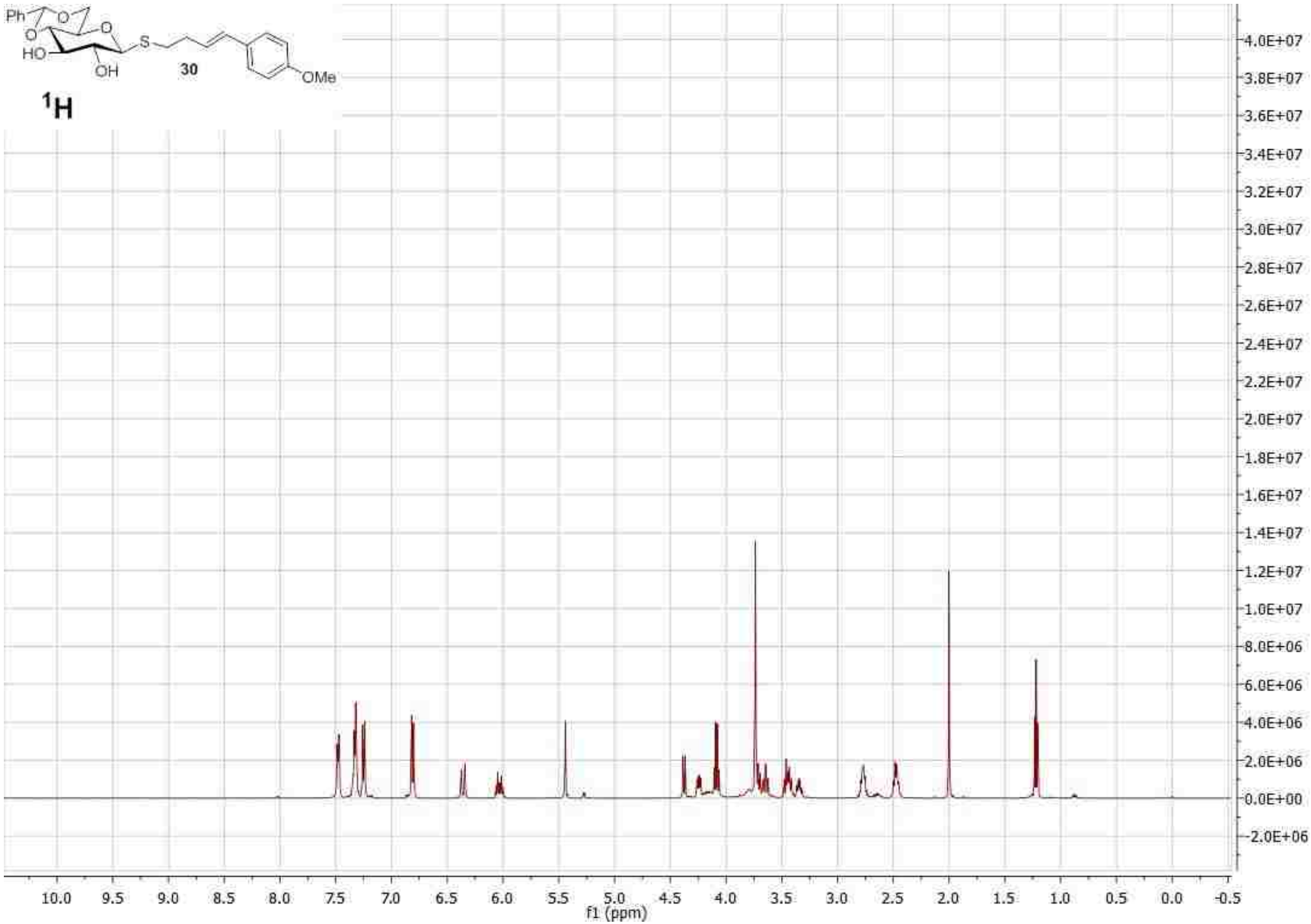
Ph
O
O
O
HO
OH
S
30
OMe
1H
4.0E+07
3.8E+07
3.6E+07
3.4E+07
3.2E+07
3.0E+07
2.8E+07
2.6E+07
2.4E+07
2.2E+07
2.0E+07
1.8E+07
1.6E+07
1.4E+07
1.2E+07
1.0E+07
8.0E+06
6.0E+06
4.0E+06
2.0E+06
0.0E+00
-2.0E+06
10.0 9.5 9.0 8.5 8.0 7.5 7.0 6.5 6.0 5.5 5.0 4.5 4.0 3.5 3.0 2.5 2.0 1.5 1.0 0.5 0.0 -0.5
f1 (ppm)

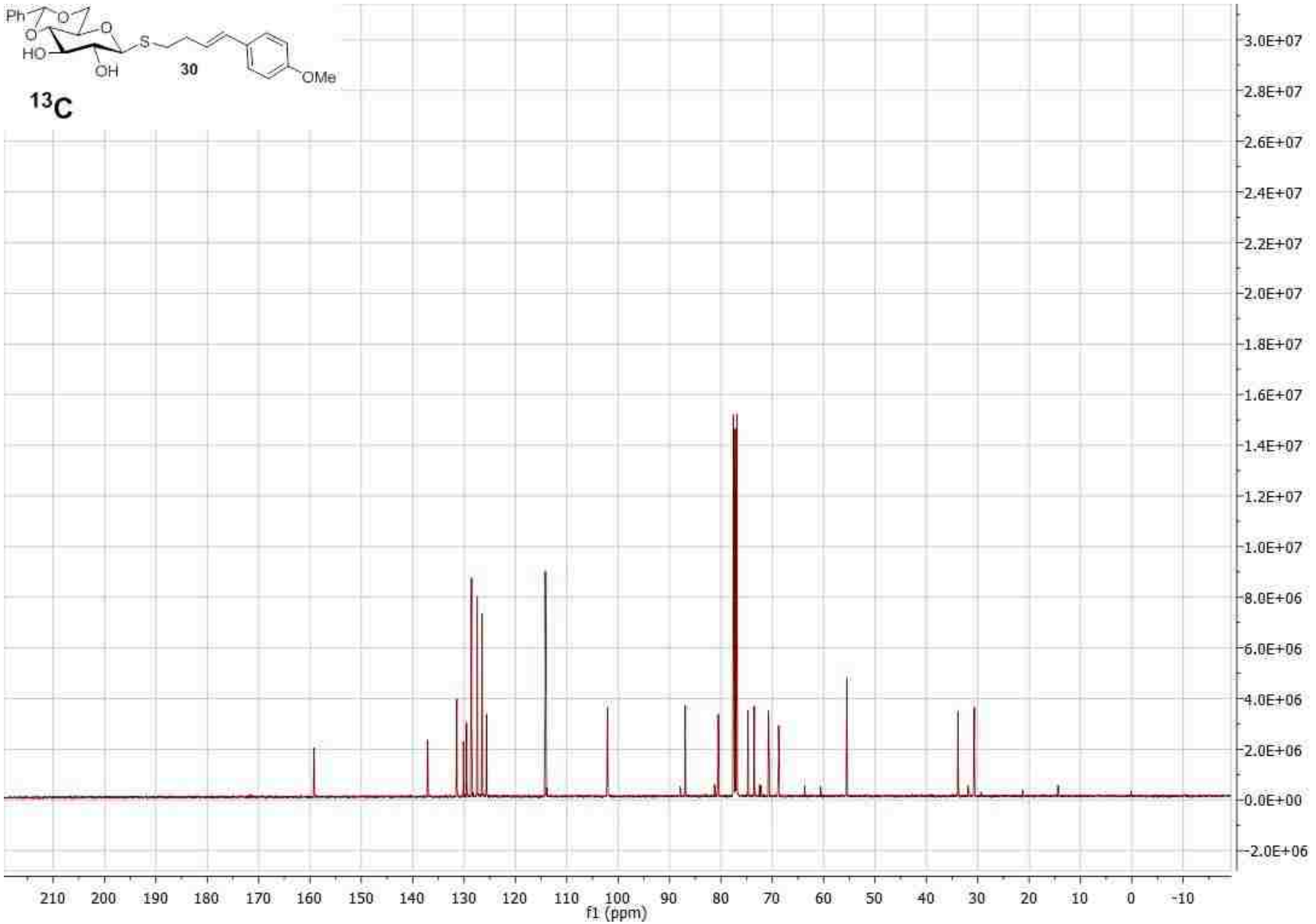
Ph
O
O
O
HO
OH
S
30
OMe
13C
3.0E+07
2.8E+07
2.6E+07
2.4E+07
2.2E+07
2.0E+07
1.8E+07
1.6E+07
1.4E+07
1.2E+07
1.0E+07
8.0E+06
6.0E+06
4.0E+06
2.0E+06
0.0E+00
-2.0E+06
210 200 190 180 170 160 150 140 130 120 110 100 90 80 70 60 50 40 30 20 10 0 -10
f1 (ppm)

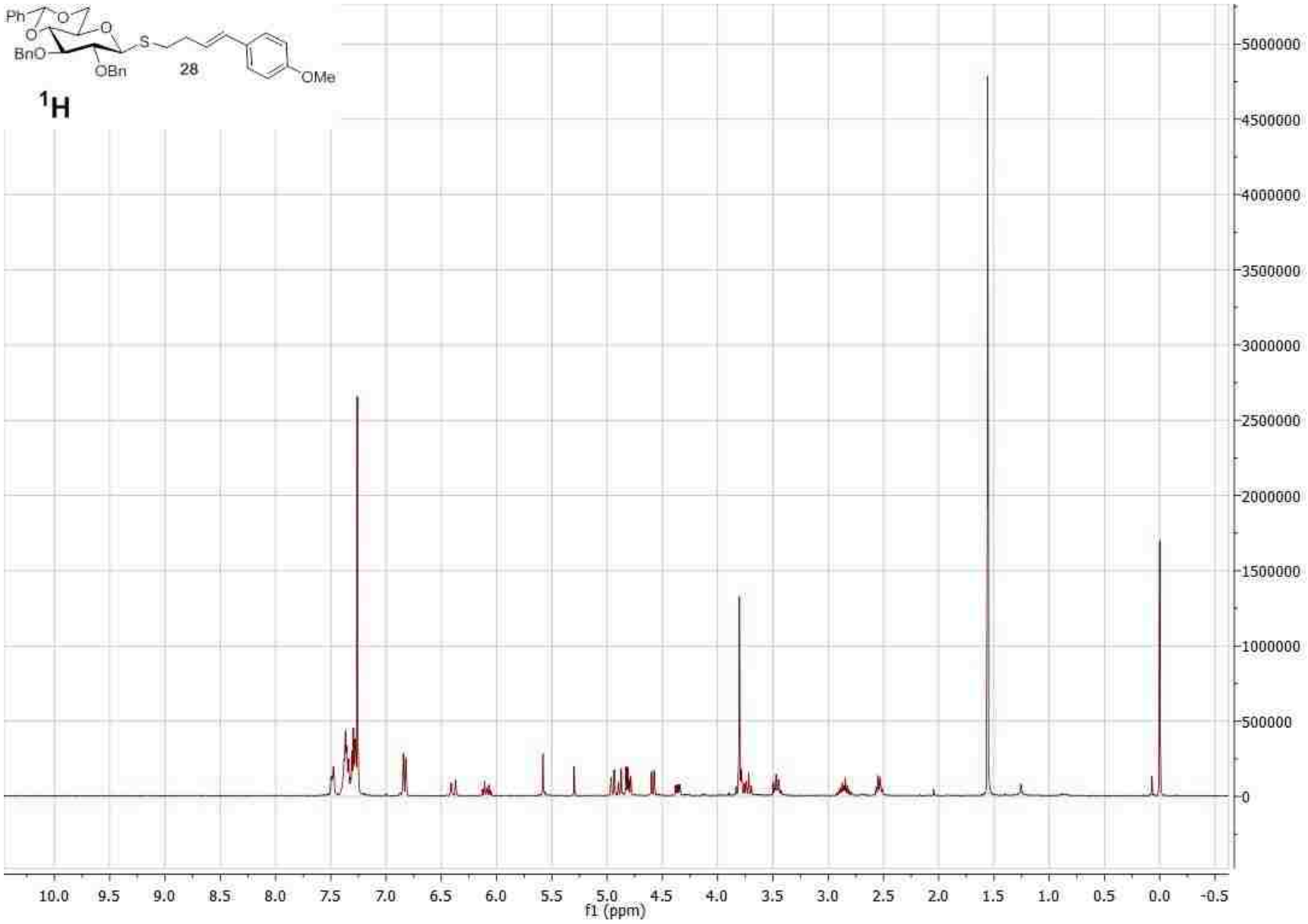
Ph
O
O
O
BnO
OBn
S
28
OMe
1H
5000000
4500000
4000000
3500000
3000000
2500000
2000000
1500000
1000000
500000
0
10.0
9.5
9.0
8.5
8.0
7.5
7.0
6.5
6.0
5.5
5.0
4.5
4.0
3.5
3.0
2.5
2.0
1.5
1.0
0.5
0.0
-0.5
f1 (ppm)

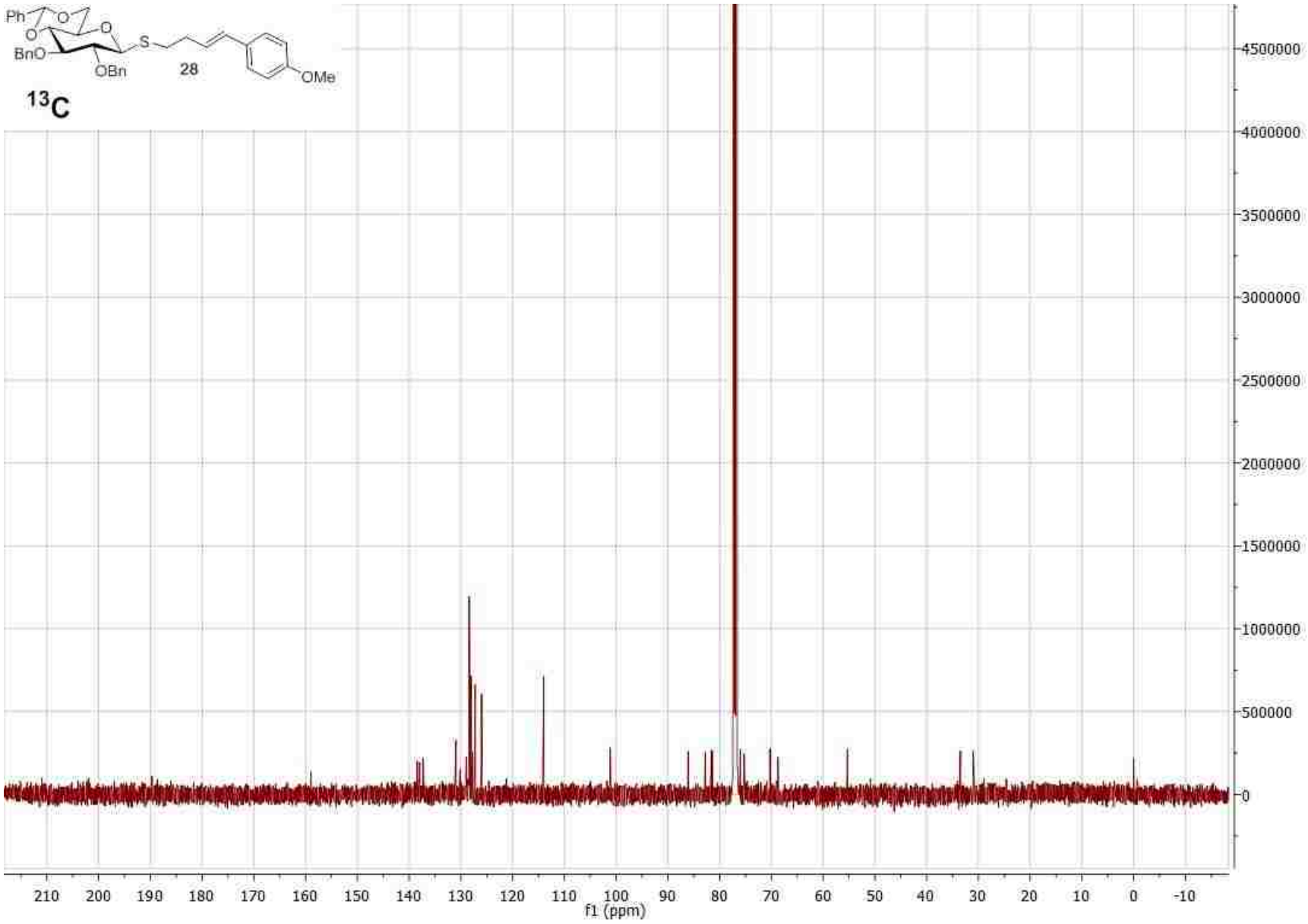
Ph
O
O
O
BnO
OBn
S
28
OMe
13C
4500000
4000000
3500000
3000000
2500000
2000000
1500000
1000000
500000
0
210
200
190
180
170
160
150
140
130
120
110
100
90
80
70
60
50
40
30
20
10
0
-10
f1 (ppm)

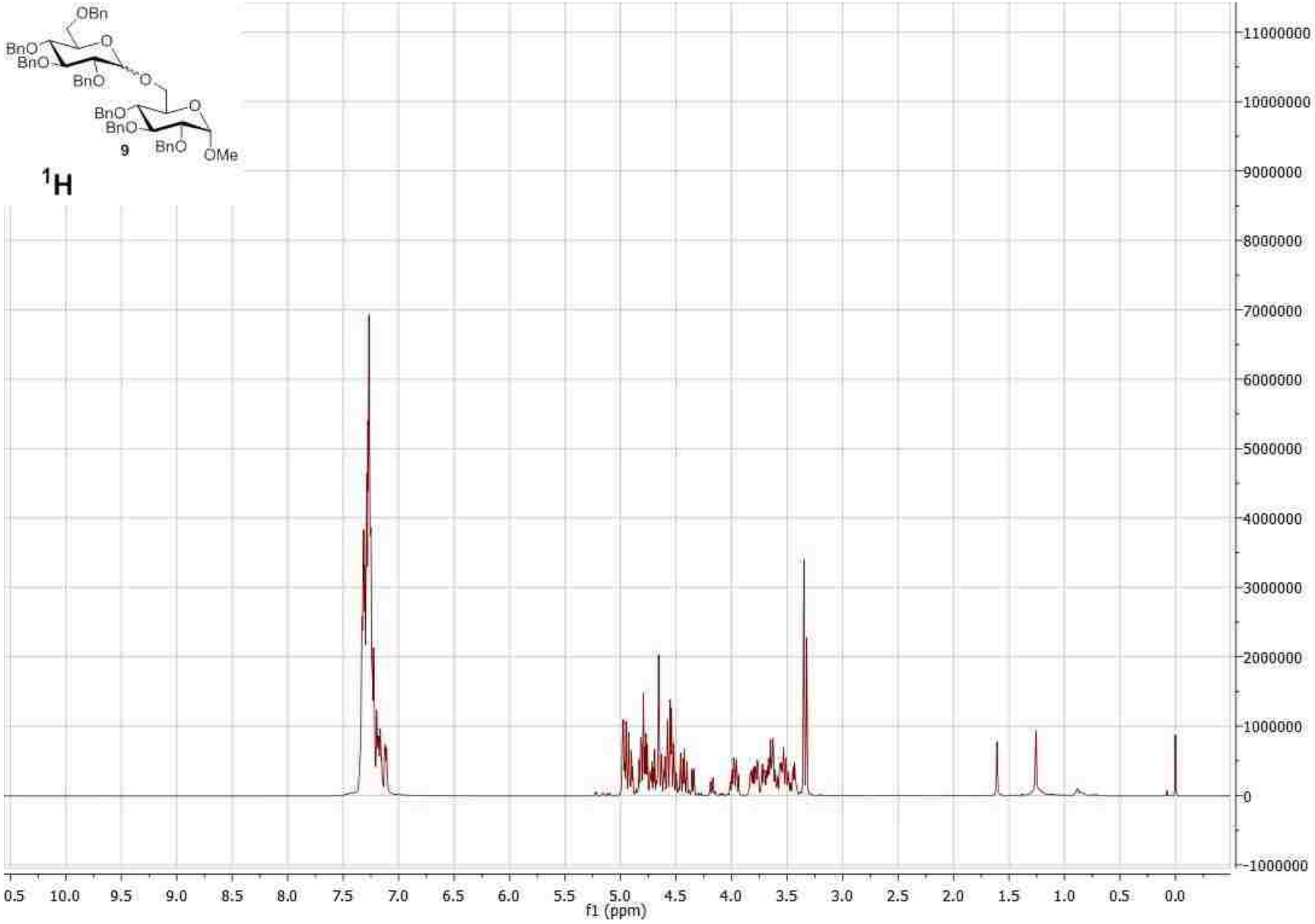
OBn
BnO
BnO
BnO
O
O
BnO
BnO
BnO
OMe
9
1H
11000000
10000000
9000000
8000000
7000000
6000000
5000000
4000000
3000000
2000000
1000000
0
-1000000
0.5 10.0 9.5 9.0 8.5 8.0 7.5 7.0 6.5 6.0 5.5 5.0 4.5 4.0 3.5 3.0 2.5 2.0 1.5 1.0 0.5 0.0
f1 (ppm)

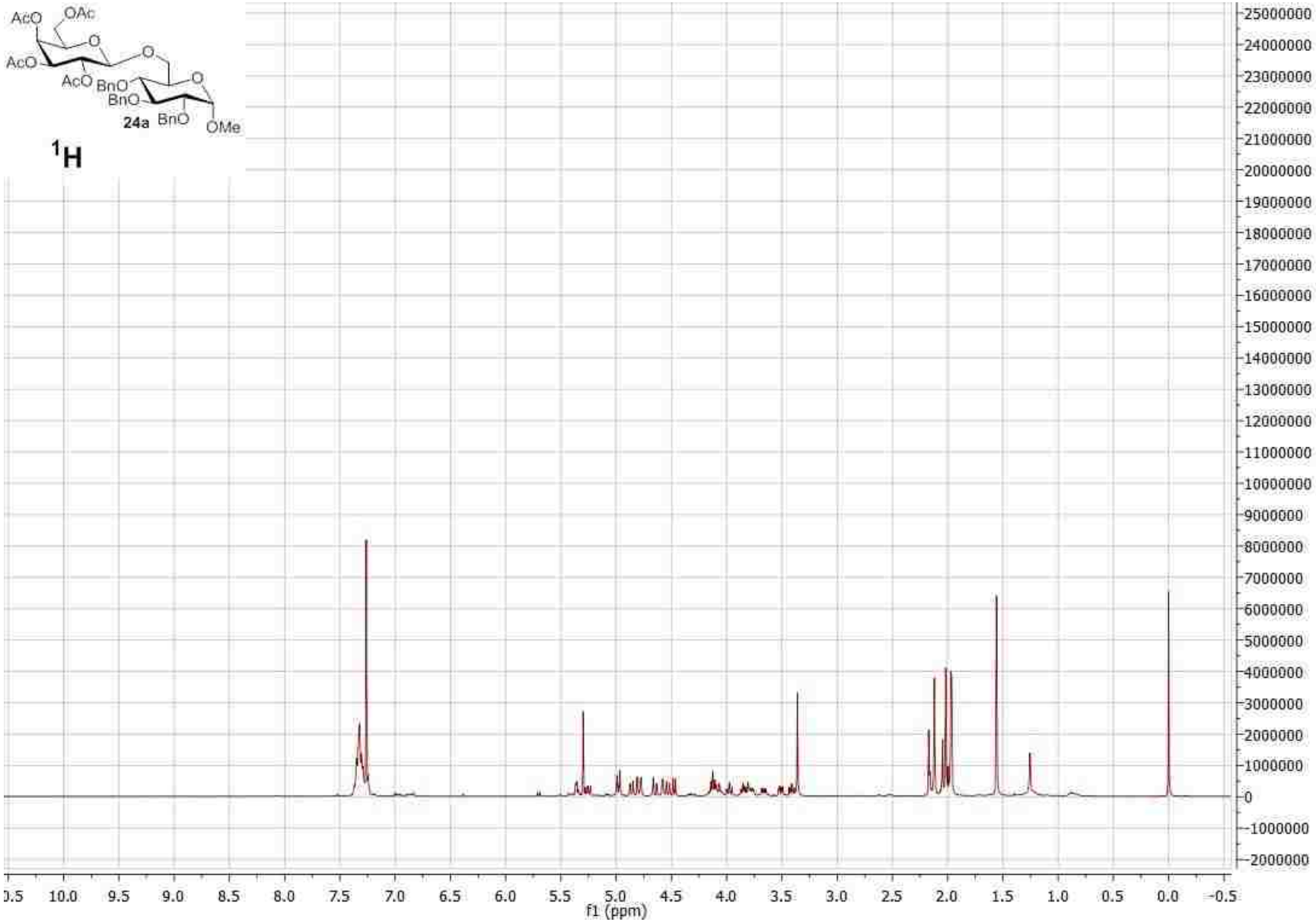
AcO
OAc
AcO
AcO
BnO
BnO
BnO
OMe
24a
1H
25000000
24000000
23000000
22000000
21000000
20000000
19000000
18000000
17000000
16000000
15000000
14000000
13000000
12000000
11000000
10000000
9000000
8000000
7000000
6000000
5000000
4000000
3000000
2000000
1000000
0
-1000000
-2000000
10.0
9.5
9.0
8.5
8.0
7.5
7.0
6.5
6.0
5.5
5.0
4.5
4.0
3.5
3.0
2.5
2.0
1.5
1.0
0.5
0.0
-0.5
f1 (ppm)

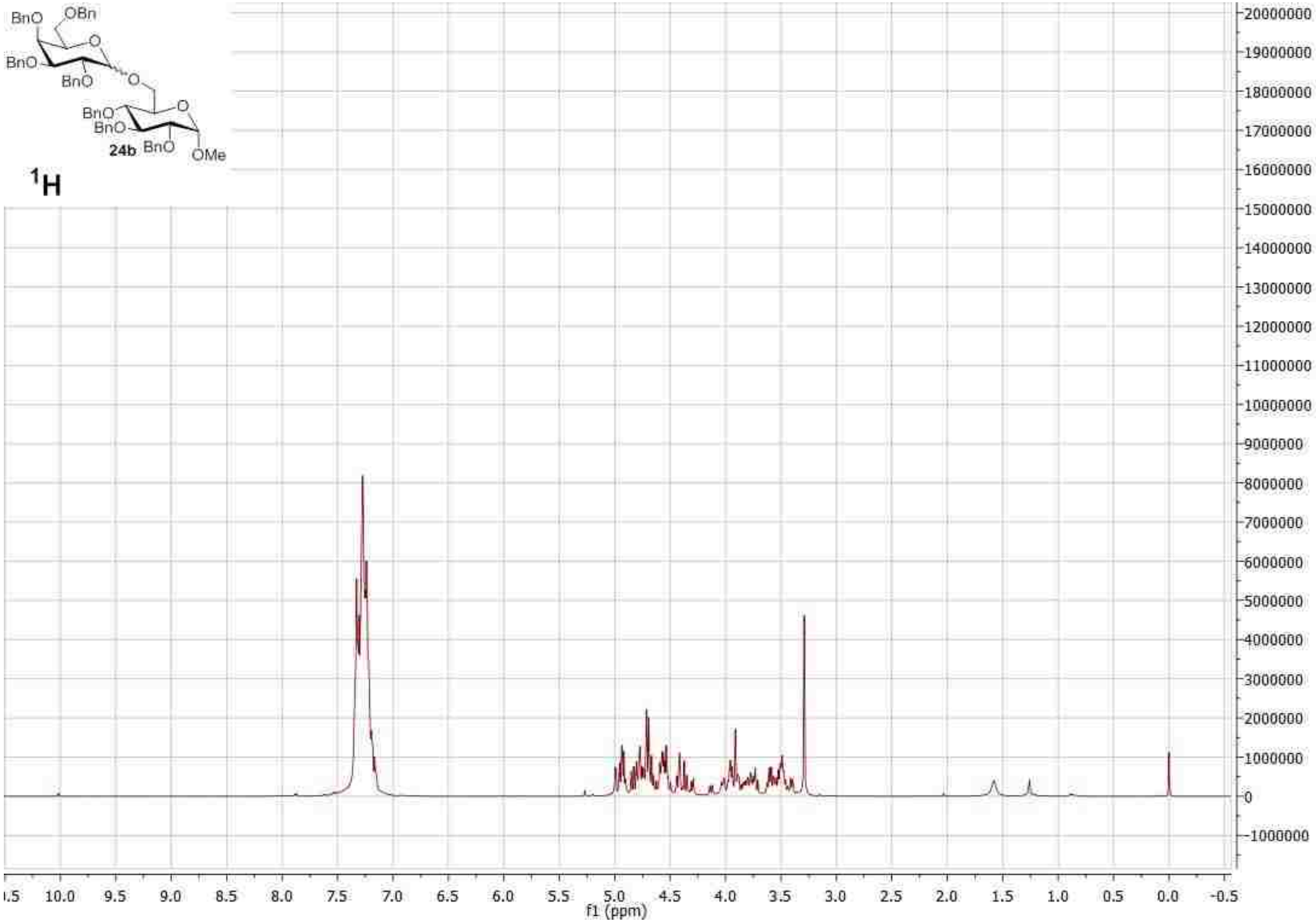
BnO
OBn
BnO
BnO
BnO
BnO
BnO
OMe
24b
1H
20000000
19000000
18000000
17000000
16000000
15000000
14000000
13000000
12000000
11000000
10000000
9000000
8000000
7000000
6000000
5000000
4000000
3000000
2000000
1000000
0
-1000000
10.0
9.5
9.0
8.5
8.0
7.5
7.0
6.5
6.0
5.5
5.0
4.5
4.0
3.5
3.0
2.5
2.0
1.5
1.0
0.5
0.0
-0.5
f1 (ppm)

ACS Publications
Most Trusted. Most Cited. Most Read.

Title: Application of Visible Light Photocatalysis with Particle Lithography To Generate Polynitrophenylene Nanostructures

Author: Susan D. Verberne-Sutton, Rashanique D. Quarels, Xianglin Zhai, et al

Publication: Journal of the American Chemical Society

Publisher: American Chemical Society

Date: Oct 1, 2014

Copyright © 2014, American Chemical Society

LOGIN

If you're a copyright.com user, you can login to RightsLink using your copyright.com credentials. Already a **RightsLink user** or want to learn more?

PERMISSION/LICENSE IS GRANTED FOR YOUR ORDER AT NO CHARGE

This type of permission/license, instead of the standard Terms & Conditions, is sent to you because no fee is being charged for your order. Please note the following:

- Permission is granted for your request in both print and electronic formats, and translations.
- If figures and/or tables were requested, they may be adapted or used in part.
- Please print this page for your records and send a copy of it to your publisher/graduate school.
- Appropriate credit for the requested material should be given as follows: "Reprinted (adapted) with permission from (COMPLETE REFERENCE CITATION). Copyright (YEAR) American Chemical Society." Insert appropriate information in place of the capitalized words.
- One-time permission is granted only for the use specified in your request. No additional uses are granted (such as derivative works or other editions). For any other uses, please submit a new request.

BACK CLOSE WINDOW

VITA

Rashanique Deondria Quarels is a native of New Orleans, LA and was born to Danielle Quarels-Ruffin and Richard Jackson. She attended Baton Rouge Magnet High School where she graduated summa cum laude in 2008. Rashanique attended Southern University and A&M College in Baton Rouge where she received several academic scholarships. A few of those awards included the Dolores Margaret Richards-Spikes Honors College scholarship, the Timbuktu Academy scholarship, the Hewlett- Packard Department of Chemistry scholarship, an American Chemical Society Scholars Fellowship, the 1890s Monsanto Fellowship, and the UNCF/Merck Fellowship. At Southern, Rashanique found her love for chemistry. Although Rashanique was originally interested in pursuing a health sciences professional degrees, Dr. Ella Kelley convinced her to apply to graduate school. In May 2012, Rashanique graduated from Southern University and A&M College magna cum laude and as a Research Honors graduate. She began her doctoral studies at Louisiana State University in the Fall of 2012. In the spring of 2013, she joined the research group of Dr. Justin Ragains. Rashanique published her first paper in the summer of 2014. Her doctoral research is focused on the formation of organic thin film and the development of new glycosylation methods. Rashanique is currently a candidate for a Doctor of Philosophy in Chemistry. This degree is anticipated to be conferred upon her at the Spring 2017 commencement.